



## Long & low; or short & high; photoperiods and light differentially influence growth and potential niches of PhycoCyanin and PhycoErythrin-rich picocyanobacteria

Journal:	<i>Limnology and Oceanography</i>
Manuscript ID	LO-24-0249.R1
Wiley - Manuscript type:	Research Article
Date Submitted by the Author:	n/a
Complete List of Authors:	Śliwińska-Wilczewska, Sylwia; Mount Allison University Department of Biology; University of Gdańsk, Department of Marine Ecosystems Functioning, Faculty of Oceanography and Geography Konik, Marta; University of Victoria, Department of Geography; Polish Academy of Sciences, Institute of Oceanology Savoie, Mireille; Mount Allison University Department of Biology Aguilera, Anabella; Linnaeus University, Department of Biology and Environmental Science, Centre for Ecology and Evolution in Microbial Model Systems (EEMiS); Swedish University of Agricultural Sciences, Department of Aquatic Sciences and Assessment Omar, Naaman M; Mount Allison University Department of Biology Campbell, Douglas; Mount Allison University Department of Biology
Keywords:	Cumulative diel photon dose, Light-capture, PAR, Photic regime, Phase of growth, Photoperiod, Picocyanobacteria, PUR
Abstract:	Strains from the picocyanobacteria genus <i>Synechococcus</i> are currently found across a wide range of photoperiods and photosynthetically active radiation. Future scenarios now forecast range expansions of marine <i>Synechococcus</i> into new photic regimes. We found that temperate coastal PhycoCyanin(PC)-rich and PhycoErythrin(PE)-rich <i>Synechococcus</i> strains grew fastest under moderate photosynthetically active radiation, and a 24-hour photoperiod, despite a cumulative diel photon dose equivalent to conditions where growth was slower, under higher light and shorter photoperiods. Under optimal conditions, a PE-rich <i>Synechococcus</i> sp. achieved a highest recorded cyanobacterial chlorophyll-specific exponential growth rate ( $\mu$ ) of $4.5 \text{ d}^{-1}$ . Two PE-rich strains demonstrated wider ability to modulate light capture capacity, whereas the two PC-rich strains showed less change in light capture across increasing cumulative diel photon dose. We found that all four coastal strains showed consistent patterns of an exponential decay of effective absorption cross section for PSII photochemistry, versus increasing cumulative diel PAR doses, although this pattern damped out under stationary phase. Within each strain, $\mu$ showed saturating responses to increasing cumulative diel PSII electron flux. As photoperiod opportunists, coastal picocyanobacteria show potential to expand into longer photic regimes as higher latitudes warm.



SCHOLARONE™  
Manuscripts

### Scientific Significance Statement Topic

In PhycoCyanin(PC)-rich, and particularly in PhycoErythrin(PE)-rich phenotypes of *Synechococcus*, photoperiod alters the responses of growth rates to cumulative diel photons, with both 8 and 24 h photoperiods provoking increased photoinhibition of growth. In contrast, growth rates show simpler saturating responses to cumulative diel reductant generation, accessed through a chlorophyll fluorescence measure of electron flux, across a matrix of photoperiods and photosynthetically active radiation levels.

Under optimal conditions of 24 h photoperiod and moderate photosynthetically active radiation, a PE-rich *Synechococcus* sp. reached a chlorophyll-specific exponential growth rate of  $4.5 \text{ d}^{-1}$ , a record for cyanobacteria, comparable with genetically-modified industrial strains.

As photoperiod opportunitists, with capacity to grow rapidly under 24 h photoperiod, coastal *Synechococcus* sp. show potential to emerge as phytoplankton components during summer in future, warmed, polar regions.

### Scientific Significance Statement Outlet

Dear Editor-in-Chief

K. David Hambright,

Our work indicating that picocyanobacteria have the potential to expand into new photic regimes while PE-rich picocyanobacteria may emerge as the dominant phytoplankton.

The findings of this study are helpful for further research on picocyanobacteria ecophysiology, and should be of interest to readers of Limnology and Oceanography, which has previously published articles on similar topics.

On behalf of all the authors of this paper, we would like to express our sincere gratitude to the two Editors, Ilana Berman-Frank and Elisa Schaum, and two Reviewers for their efforts reviewing and improving this manuscript.

## COMMENTS TO THE AUTHORS

Associate Editor:

Deputy Editor: 1

Comments to the Authors:

Dear authors,

your manuscript has been assessed by two expert reviewers and the editorial panel. All agree that this is an interesting, well written manuscript. Both reviewers have been very thorough and as a result, there are now a fair few points to address during the revision process.

Additionally, I was wondering whether a more process-based title might work better, e.g. a title highlighting the differences between PhycoCyanin and PhycoErythrin-rich picocyanobacteria more explicitly.

Response: Thank you for these positive statements. We have addressed all comments, and propose a new title. We hope that this new version of the manuscript will be satisfactory.

Associate Editor: 2

Comments to the Authors:

The manuscript has been reviewed by two experts in the field who have both agreed that this is an important manuscript with novel information. Prior to acceptance, the reviewers have raised several issues that should be addressed that will help improve and clarify different parts of the manuscript. Please see the detailed reviews and revise accordingly, or provide explanations if no revision is made.

Response: We appreciate these positive comments. We have treated all comments with due attention. We hope that this new version of the manuscript will be satisfactory.

---

We thank Reviewer 1 for their time and valuable comments. The changes in the manuscript addressing comments from Reviewer 1 are marked in blue.

Reviewer\_1

**Comment:** This manuscript reports on studies of the photobiology of strains of marine *Synechococcus* that are phycocyanin or phycoerythrin rich. The authors have compared responses of these strains to light intensity and photoperiod and the total photon dose. They measured growth rates and a range of photobiological parameters such as effective absorption cross-sectional area of PSII, as well as photosynthetically usable radiation (PUR) and the ratio of PUR to incoming photosynthetically active radiation (PAR). The latter is not often used, but is a highly useful parameter.

The experiments are well designed and are, on the whole, clearly described. The results are presented adequately and discussed thoroughly.

The authors are clear in the conclusions they draw from their data and my only criticisms are about minor points of presentation.

**Response:** We appreciate these positive comments.

**Comment:** I assume from the main data and supplementary information that the authors measured PUR under each specific growth condition to get PUR/PAR ratios. However, since absorbance spectra for only one condition of light treatment for one PE and one PC rich strain are shown in Fig 2, I think that, for clarity, this needs to be explicitly stated in the methods. Adding information about which light conditions were used for the data shown in Fig 2 to the legend would be appropriate.

**Response:** Thank you. We added the relevant text to the Materials & Methods (refer to track changes version: L236-238). The legend description in Fig. 2 also defines the light conditions applicable to the representative spectra presented. All 480 spectra are available on <https://github.com/FundyPhytoPhys/BalticPhotoperiod>, now cited in the Materials & Methods.

**Comment:** Line 119: what is a 'Pre-culture'? Mother cultures used to inoculate experimental tubes are still 'cultures'. Pre-experimental cultures would make more sense, or just say "Picocyanobacterial strains were maintained...."

**Response:** Thank you. We have made appropriate corrections (L147).

**Comment:** Line 149: 8000 x g?

**Response:** We apologize for the error. we corrected it to 8000 x g. This fragment has also been moved to the Supplement, as requested by Reviewer\_2.

**Comment:** Line 628: The first use of phylogeny here is superfluous

**Response:** Thank you. We corrected this mistake.

**Comment:** Line 434 and elsewhere: units for effective absorption cross section of PSII ( $\sigma_{PSII}$ ) are given as  $nm^2 quanta^{-1}$ ) – is this correct? Should it be  $nm^2 \mu mol quanta^{-1}$ ? Or quantum  $^{-1}$ ?

**Response:** Thank you. The unit  $nm^2 quanta^{-1}$  is correct. Some publications and processing softwares use an equivalent non-SI formulation of  $A^2 quanta^{-1}$  ( $5 nm^2 quanta^{-1} = 500 A^2 quanta^{-1}$ ). Other publications have used a short-hand of  $nm^2 PSII^{-1}$  or  $A^2 PSII^{-1}$ , which includes an implicit ratio of 1 quanta  $PSII^{-1}$ . Author DA Campbell apologizes for past sins of inconsistent units.

Minor points of expression:

**Comment:** Line 49: 'pigments of a given cyanobacteria or algae' should be 'pigments of a given cyanobacterium or alga' or 'pigments of given cyanobacteria or algae'

**Response:** Thank you. We corrected this issue.

**Comment:** Line 81: Italicise *Synechococcus*.

**Response:** Thank you for your insightful reading. We corrected this mistake.

**Comment:** Line 231: "...was measured using a Trilogy Laboratory Fluorometer..."

**Response:** Done.

**Comment:** Line 232: "...equipped with a Chlorophyll In-Vivo Module.."

**Response:** Done.

---

We thank Reviewer 2 for their time and valuable comments. The relevant changes in the manuscript are marked in green.

Reviewer\_2

Comments to the Authors LO-24-0249

#### General comments

**Comment:** This paper focuses on physiological differences between strains of PC rich vs. PE rich *Synechococcus* in their response to photic regimes and growth phases. The work is technically sound and well executed. The paper is generally well written. Overall, the results based on these culture experiments point to the potential importance of photoperiod as well as PUR/PAR in explaining the distribution of PC strains. This would seem to be an important aspect of their ecology that has not been fully considered.

**Response:** Thank you for these positive statements, in the revised version we strive to emphasize the importance of photoperiod as a factor with differential influences on growth across strains, and across light levels.

**Comment:** I think this could be more clearly brought forward in the conclusion to the paper. The remarkably high growth rates achieved at 22 C is indeed worth highlighting as a major finding along with behaviour in response to longer photoperiods. However, I would recommend that the authors not generalize based on 2 strains of each type that are all coastal, when there is clearly so much diversity across strains. This generalization needs to be downplayed in the abstract as suggested further below. One generalization that is possible for PC vs PE strains is their light quality niche differentiation (Stomp et al. and references within), but whether this extends to photoperiod length remains to be determined. *Synechococcus* assemblages in coastal areas would tend to be dominated by PC rich strains by virtue of the higher turbidity of these areas relative to the open ocean, perhaps regardless of photoperiod. Based on the present study it would seem that PE rich strains are more susceptible to photoinhibition, and it may indeed be possible to generalize here in reference to other studies based on different strains. I would suggest a concerted literature search of culture studies of PC vs PE to provide further support for this generalization. Using field data as support here is complicated by many other factors that can affect the outcome of competition between species and strains of species.

**Response:** Thank you. We emphasized in the revised Discussion and Conclusions that we recorded the fastest known growth rate for picocyanobacteria at a temperature of 22°C (refer to track changes version: L606, L610-616, L749). We corrected the Abstract to avoid over-generalizing our results to all PC and PE strains (L27-42). We also highlighted the role of photoperiod in revised Discussion and Conclusion (L581-583, L672-675, L752-753) and added literature focused on culture studies of PC vs PE (L602-605) *Synechococcus*.

**Comment:** My other general comment centers around the growth conditions of batch culture (see below) – under the conditions of these experiments, what is the main factor that is triggering the onset of the stationary phase? Is there N limitation, or light limitation (from self-shading) within the cultures once stationary reached? Would picocyanobacteria ever be in stationary under natural conditions? Likely not because their growth rates are very much in sync with loss rates from protozoan grazers - they are essentially kept in exponential growth. Natural conditions are thus more like those of a chemostat.

**Response:** Thank you for this important comment. We removed the passage on cyanobacterial growth phases from the Introduction and moved some parts to Materials & Methods, Results, and Discussion. Due to this comment and the Editor's suggestion, we also decided to change the title (L1-3, L212-214, L367-374, L652-663).

We added text (L 367-374)

"Not all cultures were grown long enough to reach full stationary phase, but onset of stationary phase, when determined, occurred fairly consistently when cultures reached ~ 0.5 OD<sub>720</sub> (PC-rich) or ~ 0.65 OD<sub>720</sub> (PE-rich), no matter the level of culture PAR. It is therefore unlikely that onset of light limitation imposed stationary phase on the cultures, which remained optically fairly thin, with even illumination to each tube from the PSI MultiCultivator array of LED. Based upon parallel studies re-launching growth after stationary phase by dilution with fresh media, with the same strains, under the same growth conditions (unpub.), we hypothesize that nutrient limitation imposes the transition to stationary phase."

Specific comments follow.

Title, Abstract:

**Comment:** Line 25. I think that the forecasting is based on temperature responses as opposed to changes in the depth of the mixing zone which would affect the overall photic regimes. I think here the authors are alluding to the work of Flombaum et al., which is in reference to projected ocean temperatures rather than changes in light regimes.

**Response:** Thank you for this comment. We changed this sentence.

**Comment:** Line 31 here I would specify.. whereas the two PC-rich strains showed...

**Response:** Thank you. We corrected this issue.

**Comment:** Line 33. change to "found that all four coastal strains....showed..."

**Response:** Thank you. We changed this sentence.

## Introduction

**Comment:** Line 51-52. This is not unique to cyanobacteria. Ditto the next sentence (line 54-55) - the challenge of prolonged darkness is not faced just by cyanobacteria at high latitudes. Up until this point the introduction refers to phytoplankton more generally. But the whole first introductory paragraph is pertinent to all phytoplankton taxa even the last two lines (63-64). I would make this clear. The next para introduces *Synechococcus* ... So start here by focusing the background context to this group of phytoplankton, specifically. It is easy to justify the focus on picocyanobacteria, given that they typically dominate the productivity of the open oceans.

**Response:** We thank the Reviewer\_2 for this insightful comment. As suggested by the Reviewer, we changed the Introduction. In the new version of manuscript, the first paragraph focuses on general phytoplankton, the second more clearly on *Synechococcus*.

**Comment:** Line 37 define  $\mu$  or put in brackets when referring to growth rate in line 30 (if this is also  $\mu$  expressed per unit chlorophyll?).

**Response:** Thank you. We added brackets when referring to growth rate.

**Comment:** Line 38. Rephrase coastal picocyanobacteria may easily expand into longer photic regimes...

**Response:** Thank you. We rephrased this sentence.

**Comment:** Line 38-39. This brings us back to the first sentence of the abstract...which makes it seem as if the present work is simply confirmatory when I believe it is not. This study brings in an additional explanation for a potential expansion of marine picocyanobacteria in the face of climate change, that is in addition to temperature.

**Response:** Thank you for this comment. We changed the abstract (L27-42). Additionally, we added a statement to the end of the Introduction (L134-136).

**Comment:** Line 87. This has more to do with the light quality (turbidity) of coastal areas, than the light levels.

**Response:** Thank you. We changed this sentence.

**Comment:** Line 93. This paragraph might be better placed after the one starting line 105? It does not seem to flow well here.

**Response:** Thank you for this comment. We agree. We removed this paragraph from the Introduction and moved the content, with modifications, to the Material and Methods (L212-214) or Discussion (L652-663).

**Comment:** Line 93. Is a batch culture condition the best analogy for growth in nature? Especially when it comes to *Synechococcus*? I think the point about the additional pre-stationary phase is well taken but perhaps move to methods.

**Response:** Thank you for this important comment. We agree. We added information to Materials & Methods (L212-214) and moved this fragment with modifications to the Discussion (L652-663). Due to this and the Editor's suggestion, we also decided to change the title (L1-3).

## Materials & Methods

**Comment:** Line 142 “fiercely”?! replace or just delete this clause. Or change to “pH showed little fluctuation and remained between ~ 8 -9”.

**Response:** Thank you for this comment. We changed this sentence (L169-170).

**Comment:** Line 147. The intro should provide an inkling as to why DNA was extracted...but I see that this was simply to include the phylogenetics of the strains used. Is this line 155 necessary to meet the goals of the paper? Just include this info when strains are described at the start.

**Response:** Thank you for this important comment. We agree. We moved the fragment about phylogenetics to where strains were introduced in Materials & Methods (L143-146). We also added a more detailed description to the legend caption in Fig. S1.

**Comment:** Line 165. Explain the use of the difference between the 2 wavelengths. What information does this provide with respect to growth. It appears further down but explain here and provide a reference for this proxy for chlorophyll a.

**Response:** Thank you for this comment. We explained this fragment and provided a reference for proxy for chlorophyll a (L191-194).

**Comment:** Line 171-172. Fix grammar.

**Response:** Done.

**Comment:** Fig 1. I can't see why the flat part of the curve of the logistic fit is called pre-stationary. Looks like stationary to me...perhaps show Fig. 1 and include the stationary phase so that it is possible to understand the distinction.

**Response:** Thank you for this comment. We added an explanation in the Materials & Methods (L212-214).

**Comment:** Line 203-204. Remove brackets from Morel 1978.

**Response:** Thank you. We fixed this issue.

**Comment:** Fig. 2. Add in the name or number of the strains shown. There were 2 strains of each type, show the patterns for both. It is interesting that for the PE rich strain the relative absorbance of PE peak is much lower under pre-stationary, this would not be expected if light was more limiting (as cell density increased) which suggests that perhaps nitrogen was limiting at this stage?

**Response:** Thank you. We added the strain numbers to the figure caption, and added appropriate statement to the Discussion (L672-675).

## Results

**Comment:** Line 336-227. Fix grammar in this sentence. There were significant effects of all three independent variables on growth rates as well as significant interactions between variables. (these effects are all highly significant based on the p values in Table S2 that really should be provided as the p values are listed as zero ...this of course is not possible. Please fix Table S2 and elsewhere when p values are listed as <0.000 (e.g. Table S1, Table S3...).

**Response:** Thank you. We fixed Tables in the Supplementary materials.

**Comment:** Line 377. I would not refer to 2 of the 4 strains as “exceptions”. There would appear to be a lot of individual strain variation in many of these endpoints and given that only 2 PC rich and 2 PE strains this makes it hard to say what is the “exception” to more “normal”/general results.

**Response:** Thank you. We corrected this issue.

### Discussion

**Comment:** Line 550-553 this is shown well in Fig 5. Cite figures within the paper rather than sup. material when possible.

**Response:** Thank you. We made corrections to the text.

**Comment:** Line 554-556. Yes, this is true and the notion that PE strains are somehow more typical of low light conditions is not a valid generalization. Observations that they may be better adapted for lower light may simply be a consequence of the light quality rather than the light quantity. I have not done a search but there are other studies comparing PE to PC strains with respect to high light requirements, no?

**Response:** Thank you very much for your insightful comment, which helped us improve the manuscript. We added appropriate text to the Discussion (L602-605).

**Comment:** Line 559. Yes, these growth rates are very high, particularly given the temperature of 22 °C. When comparing to the lit. specify the temperature used in those growth experiments because at higher temp higher growth rates are typically seen. The references here to lit. studies should include the temperature at which max. growth rates measured.

**Response:** Thank you. We added the information about temperature to each example cited (L606-616).

**Comment:** 9 figures is a bit much, but I like Fig 9. If a figure has to be moved to sup material, given the audience of typical audience of L&O which may not be so interested in specifics of photo-physiology, perhaps Fig. 7 can be moved to sup. material.

**Response:** Thank you. We understand the Reviewer's concern. However, we believe that both Figure 7 and Figure 9 are both needed in this manuscript, since the combination of high resolution growth measurements, with functional evaluations, is not common. Thus, we prefer to leave the current layout and number of figures, as we believe that they form a logical whole. However, if necessary, we will move Fig. 7 to the Supplement.

### Figures/Tables

Several are mentioned above. But in addition

**Comment:** Fig.1 include in legend light regime used (photoperiod in particular)

**Response:** Thank you. We corrected this issue.

**Comment:** Fix the p values of 0 in the tables S1 etc.,,,

**Response:** Thank you. We corrected Tables in the Supplementary materials.

1   **Long & low; or short & high; photoperiods and light**

2   **differentially influence growth and potential niches of**

3   **PhycoCyanin and PhycoErythrin-rich picocyanobacteria**

4   **Growth yields and light capture in PhycoCyanin and**

5   **PhycoErythrin-rich picocyanobacteria, across photic**

6   **regimes and growth phases**

7

8   **Sylwia Śliwińska-Wilczewska<sup>1,2</sup>, Marta Konik<sup>3,4</sup>, Mireille Savoie<sup>1</sup>, Anabella**

9   **Aguilera<sup>5,6§</sup>, Naaman M. Omar<sup>1</sup>, and Douglas A. Campbell<sup>1,\*</sup>**

10

11   <sup>1</sup> Department of Biology, Mount Allison University, 53 York St., Sackville, NB, E4L 1C9,  
12   Canada

13   <sup>2</sup> Institute of Oceanography, University of Gdańsk, 46 Piłsudskiego St, 81-378, Gdynia, Poland

14   <sup>3</sup> Department of Geography, University of Victoria, Victoria, BC, V8P 5C2, Canada

15   <sup>4</sup> Institute of Oceanology, Polish Academy of Sciences, 81-712 Sopot, Poland

16   <sup>5</sup> Department of Biology and Environmental Science, Centre for Ecology and Evolution in  
17   Microbial Model Systems (EEMiS), Linnaeus University, Kalmar, Sweden

18   <sup>6§</sup> Department of Aquatic Sciences and Assessment, Swedish University of Agricultural  
19   Sciences, Uppsala, Sweden

20   \* Correspondence: Douglas A. Campbell; dubhglascambeuil@gmail.com

21

22 **Running head:** *Picocyanobacteria across photic regimes*

23 **Keywords:** Cumulative diel photon dose; Light-capture, PAR; Photic regime; Phase of growth;  
24 Photoperiod; Picocyanobacteria; PUR

25

26 **Abstract**

27 Strains from the picocyanobacteria genus *Synechococcus* are currently found across a wide  
28 range of photoperiods and photosynthetically active radiation. Future scenarios now forecast  
29 range expansions of marine *Synechococcus* into new photic regimes. We found that temperate  
30 coastal PhycoCyanin(PC)-rich and PhycoErythrin(PE)-rich *Synechococcus* strains grew fastest  
31 under moderate photosynthetically active radiation, and a 24-hour photoperiod, despite a  
32 cumulative diel photon dose equivalent to conditions where growth was slower, under higher  
33 light and shorter photoperiods. Under optimal conditions, a PE-rich *Synechococcus* sp. achieved  
34 a highest recorded cyanobacterial chlorophyll-specific exponential growth rate ( $\mu$ ) of  $4.5\text{ d}^{-1}$ .  
35 Two PE-rich strains demonstrated wider ability to modulate light capture capacity, whereas the  
36 two PC-rich strains showed less change in light capture across increasing cumulative diel photon  
37 dose. We found that all four coastal strains showed consistent patterns of an exponential decay of  
38 effective absorption cross section for PSII photochemistry, versus increasing cumulative diel  
39 PAR doses, although this pattern damped out under stationary phase. Within each strain,  $\mu$   
40 showed saturating responses to increasing cumulative diel PSII electron flux. As photoperiod  
41 opportunists, coastal picocyanobacteria show potential to expand into longer photic regimes as  
42 higher latitudes warm.

43     The genus *Synechococcus* occurs from tropical to arctic zones, with climate scenarios  
44     forecasting range expansions of this picocyanobacteria into new photic regimes. We found that  
45     coastal PhycoCyanin(PC)-rich and PhycoErythrin(PE)-rich *Synechococcus* strains grew fastest  
46     under moderate photosynthetically active radiation, and a 24-hour photoperiod, despite a  
47     cumulative diel photon dose equivalent to conditions where growth was slower, under higher  
48     light and shorter photoperiods. Under optimal conditions, a PE-rich *Synechococcus* sp. achieved  
49     a highest recorded cyanobacterial chlorophyll specific exponential growth rate ( $\mu$ ) of  $4.5\text{ d}^{-1}$ . PE-  
50     rich strains demonstrated wider ability to modulate light capture capacity, whereas the two PC-  
51     rich strains showed less change in light capture across increasing cumulative diel photon dose.  
52     We found that all four coastal strains showed consistent patterns of an exponential decay of  
53     effective absorption cross section for PSII photochemistry, versus increasing cumulative diel  
54     PAR doses. Effective absorption cross section for PSII excited through phycobilisome  
55     absorbance at 590 nm was positively correlated with phycobiliprotein:Chl *a*, particularly during  
56     pre-stationary growth phase. Within each strain,  $\mu$  showed consistent saturating responses to  
57     increasing cumulative diel PSII electron flux. As photoperiod opportunists, coastal  
58     picocyanobacteria may easily expand into longer photic regimes at warming higher latitudes.

59

## 60     **Introduction**

61         The photic regime, comprised of Photosynthetically Active Radiation (PAR), spectral  
62         quality, and photoperiod, is a pivotal influence on the growth and productivity of phytoplankton  
63         within aquatic ecosystems. PAR refers to the spectral range of solar radiation, approximately  
64         400-700 nm, that is capable of driving photosynthesis. The availability and distribution of PAR  
65         in aquatic ecosystems is influenced by cloud cover, water depth, and light attenuation due to

66 water turbidity and suspended particles, including phytoplankton cells (Field et al. 1998;  
67 Torremorell et al. 2009). Photosynthetically Usable Radiation (PUR), in turn is the fraction of  
68 PAR that can be absorbed for photosynthesis by [pigments of given cyanobacteria or algae](#) (Morel  
69 1978). PUR thus depends upon the interaction of PAR, and the phytoplankter expression of  
70 genomic capacities for light capture (Moejes et al. 2017). Cyanobacteria [and algae](#) also respond  
71 to changes in photoperiod, which serves as a key environmental cue for photosynthesis, growth,  
72 reproduction, and nutrient assimilation (LaRoche and Robicheau 2022). Thus, in polar regions,  
73 characterized by prolonged periods of wintertime darkness and continuous daylight during  
74 summer, [phytoplankton](#) encounter unique challenges. Light is the primary limitation on biomass  
75 production in winter, suppressing cyanobacteria [and algae](#) growth and metabolic activity,  
76 whereas extended daylight in summer boosts photosynthetic activity (Arrigo 2014). In temperate  
77 regions, seasonal variation in light-limitation is less pronounced, but [phytoplankton](#) are still  
78 influenced by daily and seasonal fluctuations, with a contrast between more favorable conditions  
79 for [their](#) growth in spring and summer, compared to fall and winter (Huisman et al. 2002;  
80 Holtrop et al. 2021). In the tropics, daylight hours remain nearly constant throughout the year  
81 (Behrenfeld et al. 2006), and [phytoplankton](#) productivity is rather controlled by nutrients  
82 resupplied into the euphotic zone (Li et al. 2015), and mortality through viral lysis (Ortmann et  
83 al. 2002) and zooplankton grazing (Christaki et al. 1999).

84 The picocyanobacterial genus *Synechococcus*, one of the most abundant phytoplankter that  
85 also typically dominates in productivity in the open oceans, comprises a diversity of strains of  
86 differing pigmentations (Śliwińska-Wilczewska et al. 2018 a, b). *Synechococcus*,[a diverse genus](#)  
87 [of picocyanobacteria](#), exhibits a distribution spanning diverse geographical regions (Flombaum  
88 et al. 2013), with strains demonstrating a remarkable range of adaptations to environmental

89 conditions (Śliwińska-Wilczewska et al. 2018a; Aguilera et al. 2023). *Synechococcus* capacities  
90 to thrive across diverse marine and freshwater habitats positions it as a pivotal agent in energy  
91 and nutrient transfer within food webs, connecting the microbial loop with higher trophic levels,  
92 offering direct sustenance to grazers, including zooplankton and small fish (Li 1995). As one of  
93 the two dominant picocyanobacterial genera in oceanic waters, *Synechococcus* contribute  
94 significantly to light attenuation and light availability for other photosynthetic marine organisms,  
95 thereby influencing ocean colour and allowing satellite detection of *Synechococcus*-rich  
96 communities (Xi et al. 2020). General relations among optical absorption spectra and pigment  
97 compositions have been used to determine diagnostic pigment indices of major phytoplankton  
98 functional types (Hirata et al. 2011). Modeling suggests that *Synechococcus* abundance and  
99 ranges will increase due to climate warming (Flombaum et al. 2013). The projected changes may  
100 vary geographically and may include shifts in the spatial distribution of the main  
101 picocyanobacteria, as well as changes in the proportions among *Synechococcus* sp. lineages (Six  
102 et al. 2021), potentially pushing lineages into new photic regimes. *Synechococcus* exhibits  
103 significant phenotypic diversity across lineages, encompassing strains rich in phycobiliprotein  
104 pigments, phycoerythrin (PE-rich) or phycocyanin (PC-rich) (Haverkamp et al. 2009; Aguilera et  
105 al. 2023). Phycobiliprotein pigments are pivotal for light absorption during photosynthesis and  
106 confer distinctive colours to the picocyanobacteria (Stomp et al. 2007). The disparate light  
107 preferences between PC-rich and PE-rich *Synechococcus* sp. strains influence their ecological  
108 niches. PC-rich strains thrive in environments with elevated light levels, such as surface waters  
109 and coastal regions. PE-rich strains exhibit adaptation to lower-light conditions, primarily  
110 inhabiting the deeper layers of the water column. PC-rich and PE-rich *Synechococcus* sp. strains  
111 thus predominantly occupy complementary habitats (Six et al. 2007; Haverkamp et al. 2009; Six

112 et al. 2021), although differential responses of *Synechococcus* lineages to photoperiod, have not  
113 been studied in detail, except for thermophilic PC-rich *Synechococcus* PCC 6715 (Klepacz-  
114 Smółka et al. 2020).

115 ~~Cyanobacteria growth includes lag, exponential growth, stationary, and death phases~~  
116 ~~(Reynolds 2006). During the lag phase, cyanobacteria acclimate to the environment and prepare~~  
117 ~~for active growth by synthesizing essential cellular components. Exponential growth phase is~~  
118 ~~marked by cell division and biomass accumulation, fueled by nutrient and light availability. If~~  
119 ~~growth is limited by declining nutrients, by light, or by accumulation of inhibitory factors, algae~~  
120 ~~enter stationary phase, characterized by a balance between cell division and death, leading to a~~  
121 ~~plateau in population. The death phase occurs when cyanobacteria cell death outruns division,~~  
122 ~~leading to net decomposition, contributing to nutrient recycling in aquatic ecosystems (Reynolds~~  
123 ~~2006). Moreover, Schuurmans et al. (2017) proposed an additional phase between the~~  
124 ~~exponential and stationary phases of picocyanobacteria growth, which is often neglected in~~  
125 ~~physiological studies. Herein, we examined the physiological responses of PC-rich and PE-rich~~  
126 ~~*Synechococcus* sp. in this phase, which we termed the pre-stationary phase of growth.~~

127 Picocyanobacteria are the most abundant phytoplankters in aquatic ecosystems and are  
128 crucial to the optical properties of ocean water, by influencing its colour and transparency. PC-  
129 rich and PE-rich *Synechococcus* sp. may have different costs and physiological strategies for  
130 growth under different photic regimes, which could drive spatial and temporal variability of  
131 picocyanobacteria biomass and community composition, in current and potential future aquatic  
132 habitats. Therefore, our aim was to determine whether ~~photoperiod and light photic regimes and~~  
133 ~~growth phases~~ differentially affect growth and light-capture, between representative PC-rich and  
134 PE-rich *Synechococcus* sp. This study emphasizes the potential importance of photoperiod as a

135 factor influencing poleward expansions of marine picocyanobacteria in the face of climate  
136 change.

137

138 **Materials and Methods**

139 **Experimental setup**

140 Two xenic PhycoCyanin(PC)-rich (CCBA\_056 or CCBA\_077) strains and two  
141 PhycoErythrin(PE)-rich (CCBA\_048 or CCBA\_127) strains of *Synechococcus* were obtained  
142 from the Culture Collection of Baltic Algae (CCBA; <https://ccba.ug.edu.pl/pages/en/home.php>).  
143 The phylogenetic placement of CCBA strains (Fig. S1 in Supporting Information) within cluster  
144 5 picocyanobacteria was explored by amplifying and sequencing a fragment of the 16S rRNA  
145 gene using universal primers 27F and 1492R (Lane 1991). 16S rRNA gene sequences were  
146 aligned with MAFFT v. 7.5 using the G-INS-I algorithm (Katoh et al. 2019).

147 Picocyanobacteria strains were maintained in Tissue Culture Flasks (VWR International,  
148 Cat. No. 10062-872, PA, USA) and were transferred to fresh f/2 media (Guillard 1975) at  
149 salinity of 8 PSU (which corresponds to their natural habitat) every two weeks, under a  
150 photoperiod of 12 h and Photosynthetically Active Radiation (PAR) of 10  $\mu\text{mol photons m}^{-2}\text{s}^{-1}$   
151 supplied from cool white fluorescent tubes, at 22°C.

152 Experimental cultures of each strain were grown in 8 x 80 mL round bottom cylindrical  
153 glass tubes in a Multi-Cultivator MC 1000-OD (Photon Systems Instruments, Drásov, Czech  
154 Republic). Each culture tube contained 75 mL of f/2 medium inoculated with 5 mL of growing  
155 pre-culture, to achieve exponential growth from the beginning of the experiment, with little to no  
156 lag phase upon inoculation. Culture tubes were inoculated in the afternoon while the

157 photoregime of a sinuisoidal photoperiod commenced the following morning such that peak PAR  
158 occurred at noon each day.

159 Cultures grew at 22°C, with photoperiods of 8, 12, 16, or 24 h, with peak PAR of 30, 90,  
160 180, 300, 600, or 900  $\mu\text{mol photons m}^{-2}\text{s}^{-1}$  independently supplied to each culture tube from  
161 white LED lamps. To approximate diel cycles, the photoperiods of 8 – 16 h were applied in a  
162 sinuisoidal shape, while the 24-hour photoperiod was applied continuously in a square shape.  
163 The area under the sinuisoidal curve is 1/2 the area under a square of equal width, therefore at  
164 equivalent peak PAR the 24 h square photoperiod cultures received 4 times the diel photon doses  
165 of the 12 h sinuisoidal photoperiod cultures.

166 Culture tubes were closed with a silicone inert silicone stopper perforated by an aeration  
167 input tube extending to the bottom of the culture tube, and a pressure outlet tube. Aeration with a  
168 total air flow rate of around  $\sim 140 \text{ mL min}^{-1} \text{ tube}^{-1}$  through a  $0.2\mu\text{m}$  filter ensured mixing and  
169 provided sufficient air/ $\text{CO}_2$  supply to cultures through the entire culture volume. The pH showed  
170 little fluctuation and remained between  $\sim 8 – 9$ . Light, temperature, optical density, and aeration  
171 gas of the Multi-Cultivator system were monitored and controlled via the Photobioreactor  
172 Control Software (Photon Systems Instruments, Drásov, Czech Republic).

173

#### 174 **DNA extractions**

175 Samples for total genomic DNA were collected by harvesting 10 mL of each culture and  
176 centrifuging for 8 minutes at  $8,000 \times g$ . DNA was extracted using the FastDNA™ SPIN Kit for  
177 Soil (MP Biomedicals) with Matrix E columns following manufacturer instructions with the  
178 addition of an incubation with proteinase K (1% final concentration) at 55°C for one hour. DNA  
179 concentration was measured using an Invitrogen Qubit 2.0 fluorometer (Thermo Fisher Scientific

180 Ine.) and purity was assessed using a Thermo Scientific™ NanoDrop 2000 spectrophotometer  
181 (Thermo Fisher Scientific Inc.).

182 The phylogenetic placement of CCBA strains (Fig. S1 in Supporting Information) within  
183 cluster 5 picocyanobacteria was explored by amplifying and sequencing a fragment of the 16S  
184 rRNA gene using universal primers 27F and 1492R (Lane 1991). 16S rRNA gene sequences  
185 were aligned with MAFFT v. 7.5 using the G-INS-I algorithm (Katoh et al. 2019). Phylogenetic  
186 trees were created using IQ-TREE v. 1.6.12 (Hoang et al. 2018), using GTR+F+I+R3 model  
187 determined by ModelFinder (Kalyaanamoorthy et al. 2017). Bootstrap values were calculated  
188 with 1000 replicates (Hoang et al. 2018).

189

## 190 Growth curves and chlorophyll-specific exponential growth rates

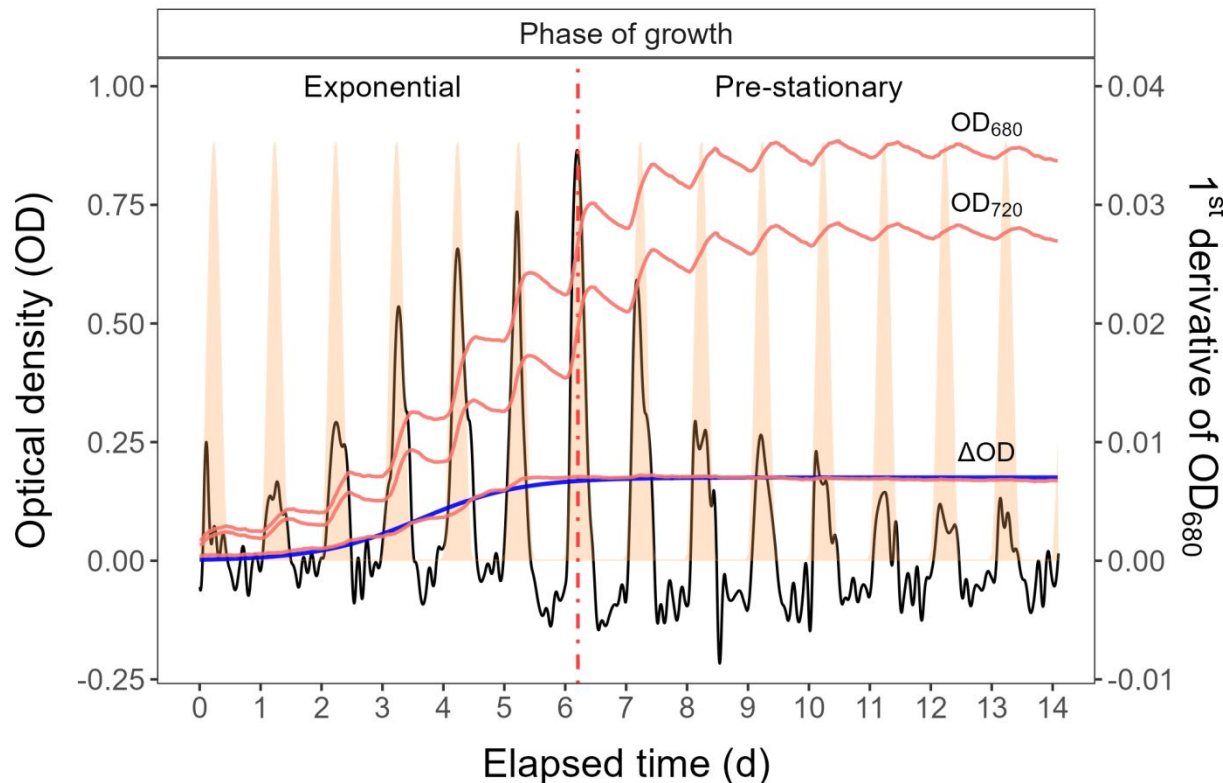
191 Picocyanobacterial growth was monitored every 5 minutes for 14 days, independently for  
192 each culture tube, by automatically recording OD<sub>680</sub>; a proxy for chlorophyll *a* content, cell  
193 scatter, OD<sub>720</sub>; a proxy for cell scatter, and ΔOD ( $\Delta\text{OD} = \text{OD}_{680} - \text{OD}_{720}$ ); a proxy for  
194 chlorophyll *a* content (Nedbal et al. 2008). The exceptions were experiments conducted with a  
195 photoperiod of 24 h and light of 600 or 900  $\mu\text{mol photons m}^{-2}\text{s}^{-1}$ , which lasted 7 days (Fig. S2).  
196 The chlorophyll-specific exponential growth rates ( $\mu$ ) were determined by fitting logistic growth  
197 curves using a modified Levenberg-Marquardt fitting algorithm (Elzhov et al. 2023) to plots of  
198 the chlorophyll *a* proxy of ΔOD vs. elapsed time for each combination of strain, photoperiod,  
199 and peak PAR (Fig. S3).

200 To summarize the growth responses of the four picocyanobacterial strains we used a  
201 Generalized Additive Model (GAM) (Wood 2017). GAM was applied to the relation of  
202 chlorophyll-specific  $\mu$ ,  $\text{d}^{-1}$  to photoperiod and PAR level. The R package *mgcv* (Wood 2017)

203 was used to model the growth rate with smoothing terms and indicate the 90, 50 and 10%  
204 quantiles for growth rate across the levels of factors. Only growth rate estimates for which the  
205 amplitude of standard error was smaller than 50% of the fitted growth rate were included in the  
206 GAM. We visually compared the GAM contours to isolines of equal cumulative diel PAR  
207 ( $\mu\text{mol photons m}^{-2}\text{d}^{-1}$ ).

208 The 1<sup>st</sup> derivative of OD<sub>680</sub> taken over 1 h increments was computed using *xts*: eXtensible  
209 Time Series (Ryan et al. 2024) and *signal*: Signal Processing (Ligges et al. 2024) R packages.  
210 The time when the cultures reached their maximum absolute hourly growth (tMaxAHG) of the  
211 1<sup>st</sup> derivative of OD<sub>680</sub> was taken as the time of transition from exponential to pre-stationary  
212 growth phases (Fig. 1). This phase progresses to the stationary growth phase. In this work, all  
213 measurements obtained after transition time were termed the pre-stationary phase of growth,  
214 according to Schuurmans et al. (2017).

215



216

217 **Fig. 1.** Example of a growth curve (tracked as  $\text{OD}_{720}$ ,  $\text{OD}_{680}$ , or  $\Delta\text{OD}$ ; red solid lines, left y-axis) of PE-rich culture  
 218 of *Synechococcus* sp. (0448; grown at 180 peak PAR  $\mu\text{mol photons m}^{-2}\text{s}^{-1}$ ; and photoperiods of 12 h) vs. elapsed  
 219 time (d, x-axis). 1<sup>st</sup> derivative of  $\text{OD}_{680}$  taken over 1 h increments (black solid line, right y-axis); solid blue line  
 220 shows logistic fits of chlorophyll proxy  $\text{OD}_{680} - \text{OD}_{720}$  ( $\Delta\text{OD}$ ) vs. elapsed time. The vertical red dot dash line  
 221 represents the time when the culture reached the maximum of the 1<sup>st</sup> derivative of  $\text{OD}_{680}$ , or maximum absolute  
 222 hourly growth (tMaxAHG), taken as the time of transition from exponential to pre-stationary growth phases.  
 223

## 224 Whole-cell absorbance spectra

225 Absorbance measurements on intact cells in suspension were conducted in an integrating  
 226 cavity upgrade spectrophotometer (CLARiT<sup>Y</sup> 17 UV/Vis/NIR, On-Line Instrument Systems,  
 227 Inc., Bogart, GA, USA). 8 mL of f/2 medium were added to both the sample and reference  
 228 observation cavities of the spectrophotometer. After recording a baseline from 375 to 710 nm, 1  
 229 mL was withdrawn from the sample cavity and replaced with 1 mL of picocyanobacteria cell

230 suspension. The pathlength corrected absorbance per cm was performed by determining the  
231 Javorfi coefficients (Javorfi et al. 2006) as described in the equipment manual.

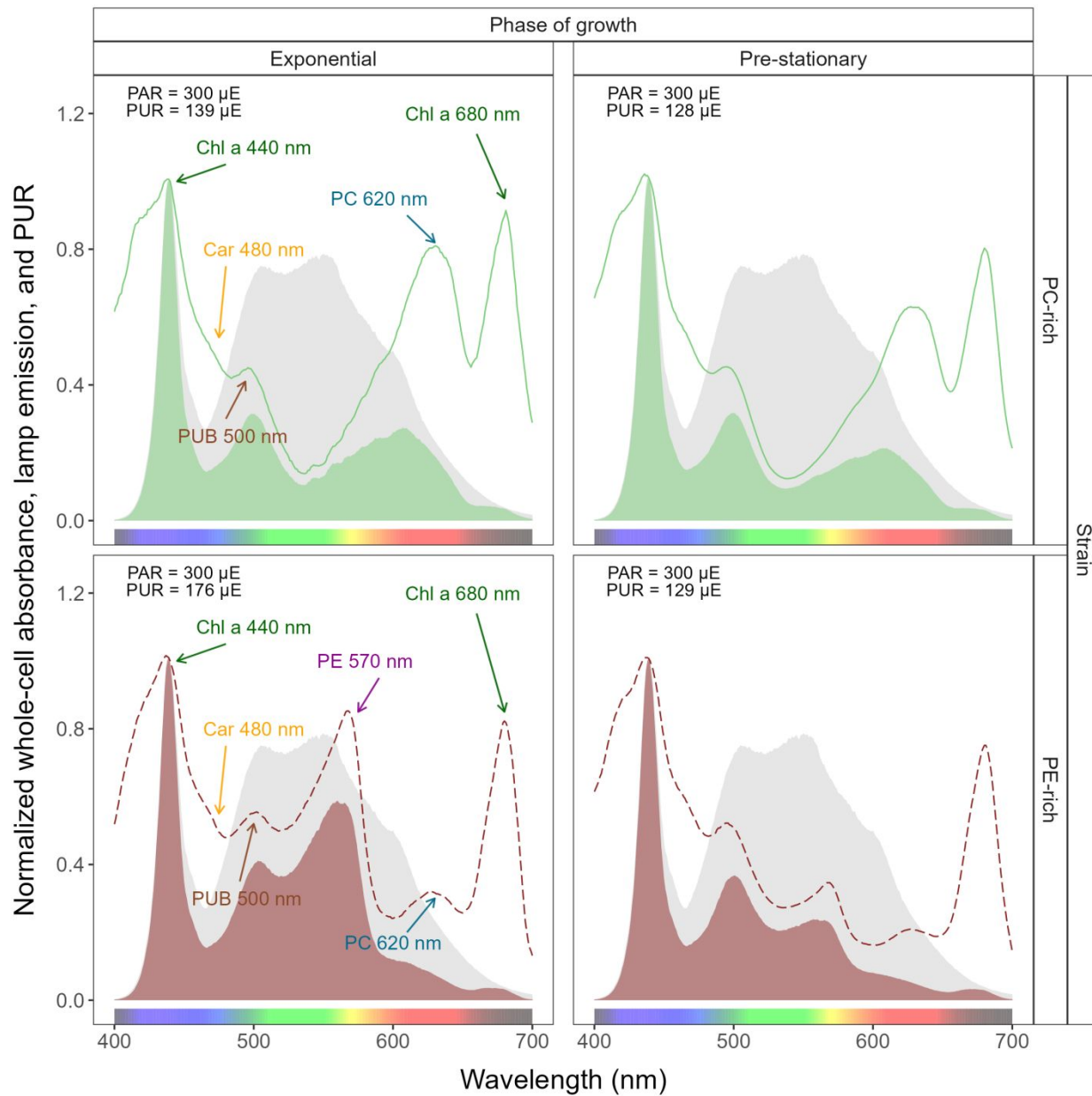
232

### 233 Photosynthetically Usable Radiation (PUR)

234 Using whole-cell absorbance spectra of *Synechococcus* sp. cultures (Fig. 2), we estimated  
235 Photosynthetically Usable Radiation (PUR;  $\mu E = \mu\text{mol photons m}^{-2}\text{s}^{-1}$ ) according to Morel  
236 (1978). Representative absorbance spectra for one growth light treatment (300  $\mu\text{mol photons}$   
237  $\text{m}^{-2}\text{s}^{-1}$ ), for one PE and one PC rich strain, are shown in Fig. 2. The other 476 spectra used to  
238 estimate PUR are available at <https://github.com/FundyPhytoPhys/BalticPhotoperiod>. We  
239 normalized the obtained whole-cell Absorbances (A) and the Emission spectra of the white LED  
240 lamps (Em) from 400 nm to 700 nm to a reference wavelength of 440 nm. PUR is then the ratio  
241 of the sum of Absorbance Normalized to 440 nm (NormA<sub>440</sub>) multiplied by the sum of Emission  
242 spectra Normalized to 440 nm (NormEm<sub>440</sub>) to the sum of the Emission spectra Normalized to  
243 440 nm (NormEm<sub>440</sub>), multiplied by the PAR (Eq. (1)).

$$244 PUR (\mu E) = \frac{\sum(NormA_{440} \times NormEm_{440})}{\sum(NormEm_{440})} \times PAR (\mu E) \quad (1)$$

245



246

247 **Fig. 2.** Whole-cell absorbance spectra of PC-rich (077; solid light green lines) or PE-rich (127; dashed dark red  
 248 lines) cultures of *Synechococcus* sp. Representative absorbance spectra, normalized to 440 nm (NormA<sub>440</sub>), were  
 249 measured from the exponential or pre-stationary phases of growth, together with emission spectra of the white LED  
 250 lamp used for PAR, normalized to emission at 440 nm (NormEm<sub>440</sub>, light gray area), in this example PAR was 300  
 251  $\mu\text{mol photons m}^{-2}\text{s}^{-1}$ . Estimated Photosynthetically Usable Radiation (PUR) is shown as a darker green area for the  
 252 PC-rich strain and a darker red area for the PE-rich strain, with PUR given for each culture ( $\mu\text{E} = \mu\text{mol photons}$

253  $\text{m}^{-2}\text{s}^{-1}$ ). Peaks characteristic of known pigments are labeled; Chl *a*, chlorophyll *a*; PC, phycocyanin; PE,  
254 phycoerythrin; PUB, phycourobilin; Car, carotenoids.

255

## 256 Cumulative diel PAR and PUR

257 Based on the length and shape of the photoperiod (sinuisoidal wave for photoperiods of 8,  
258 12, 16 h; square for photoperiod of 24 h) and the peak PAR ( $\mu\text{E} = \mu\text{mol photons m}^{-2}\text{s}^{-1}$ ), we  
259 estimated the value of the cumulative diel PAR ( $\mu\text{mol photons m}^{-2}\text{d}^{-1}$ ). For sinuisoidal  
260 photoperiods we used Eq. (2); for the continuous 24 h photoperiod we used Eq. (3). Cumulative  
261 diel PUR was estimated similarly after estimation of peak PUR from peak PAR.

$$262 \frac{\text{Cumulative diel PAR } (\mu\text{mol photons m}^{-2} \text{ d}^{-1})}{\text{PAR } (\mu\text{E}) \times 60 \text{ (s min}^{-1}\text{)} \times 60 \text{ (min h}^{-1}\text{)} \times \text{photoperiod (h d}^{-1}\text{)}} = \quad (2)$$

$$263 \frac{\text{Cumulative diel PAR } (\mu\text{mol photons m}^{-2} \text{ d}^{-1})}{\text{PAR } (\mu\text{E}) \times 60 \text{ (s min}^{-1}\text{)} \times 60 \text{ (min h}^{-1}\text{)} \times \text{photoperiod (h d}^{-1}\text{)}} = \quad (3)$$

264

## 265 Pigment content

266 Chlorophyll *a* (Chl *a*) ( $\mu\text{g mL}^{-1}$ ) was measured using a Trilogy Laboratory Fluorometer  
267 (Turner Designs, Inc., CA, USA) equipped with a Chlorophyll In-Vivo Module, previously  
268 calibrated using 20 mL ampoules with known Chl *a* concentrations in 3:2 90% acetone:DMSO  
269 solution. Quantitative analysis of Chl *a* was obtained after adding 50  $\mu\text{L}$  of culture and 2 mL of a  
270 90% acetone:DMSO solution in a 3:2 ratio.

271 We also estimated the pigment content ( $\mu\text{g mL}^{-1}$ ): chlorophyll *a* (Chl *a*), carotenoids (Car),  
272 phycoerythrin (PE), phycocyanin (PC), and allophycocyanin (APC) in *Synechococcus* sp.  
273 cultures over time using previously determined linear correlations between pigment content  
274 obtained by extraction (Strickland and Parsons 1972; Bennett and Bogorad 1973) and absorbance

275 values of individual pigment peaks (Car; 480, PE; 565, PC; 620, APC; 650, and Chl *a*; 665 nm)  
276 obtained from the whole-cell absorbance spectra using integrating cavity upgrade  
277 spectrophotometer (CLARiTY 17 UV/Vis/NIR, On-Line Instrument Systems, Inc., Bogart, GA,  
278 USA) (Tab. S1 in Supporting Information). The sum of phycobiliproteins (PE, PC, APC protein)  
279 to Chl *a* ratio ( $\mu\text{g}:\mu\text{g}$ ) for individual strains was also calculated.

280

## 281 **PSII The effective absorption cross section of PSII and electron flux**

282 We harvested 2 mL of cultures for photophysiological characterizations repeatedly across  
283 the growth trajectories. We used Fast Repetition Rate fluorometry (Kolber et al. 1998) (FRRf,  
284 Solisense, USA), with a lab built temperature control jacket (22°C), to apply series of flashlets to  
285 drive saturation induction/relaxation trajectories, fit using the onboard Solisense LIFT software  
286 (Falkowski and Kolber 1993; Kolber et al. 1998). From the model fits we took the initial  
287 fluorescence before induction ( $F_0$ ,  $F_0'$ , or  $F_S$ , depending upon the level of actinic light and step  
288 in the light response curve); the maximum fluorescence ( $F_M$  or  $F_M'$ ) once Photosystem II (PSII)  
289 was driven to closure; and the effective absorption cross section for PSII photochemistry ( $\sigma_{\text{PSII}}$  or  
290  $\sigma_{\text{PSII}}'$ ;  $\text{nm}^2 \text{ quanta}^{-1}$ ) (Tortell and Suggett 2021). We used a double tap protocol (Xu et al. 2017),  
291 where FRRf induction/relaxation trajectories were collected during a rapid light curve sequence  
292 increasing in steps of 10 s at 0, 20, 40, 80, 160, and 320  $\mu\text{mol photons m}^{-2}\text{s}^{-1}$  PAR, delivered  
293 from LED emitters centred at 445, preferentially exciting chlorophyll, or 590 nm, preferentially  
294 exciting phycobiliproteins. Flash Power for 445 nm excitation was 60000  $\mu\text{mol photons m}^{-2}\text{s}^{-1}$   
295 PAR, while for 590 nm excitation power was 14000  $\mu\text{mol photons m}^{-2}\text{s}^{-1}$ , calibrated using a  
296 quantum sensor (LI-250, LI-COR, Inc.). We applied 1 s darkness between sequential light steps,

297 to allow re-opening of PSII. FRRf excitation flashlets were applied at the same wavebands, 445  
 298 or 590 nm, as the actinic light steps.

299 We calculated (Eq. (4)) an uncalibrated fluorescence based estimator for volumetric  
 300 electron transport,  $JV_{PSII}$ , ( $\text{km} \times \text{e}^- \text{ L}^{-1} \text{ s}^{-1}$ ) under both 445 and 590 nm excitation bands  
 301 (Oxborough et al. 2012; Boatman et al. 2019; Tortell and Suggett 2021).

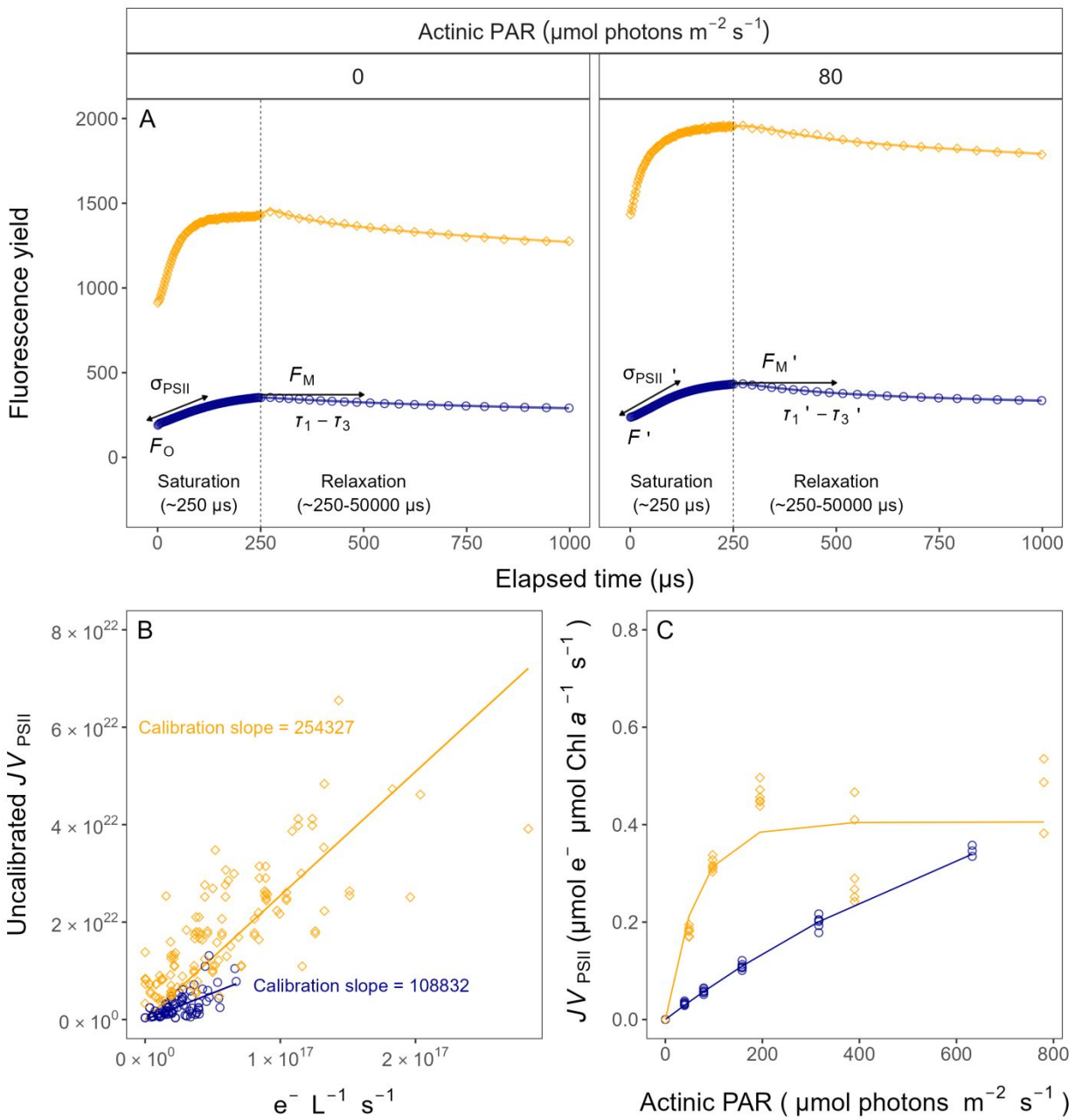
$$302 \quad JV_{PSII} = \frac{\sigma_{PSII}' \times qP \times I \times F_O}{\sigma_{PSII}} \quad (4)$$

303 where  $\sigma_{PSII}'$  is effective absorption cross section for PSII photochemistry under the relevant  
 304 actinic PAR step ( $\text{nm}^2 \text{ quanta}^{-1}$ ); qP is an estimate of the fraction of PSII open for  
 305 photochemistry estimated according to Oxborough and Baker (1997); I is the applied PAR ( $\mu\text{mol}$   
 306 photons  $\text{m}^{-2}\text{s}^{-1}$ );  $F_O$  is the minimum fluorescence from a given sample and excitation bandwidth  
 307 (relative fluorescence) and  $\sigma_{PSII}$  is the maximum effective absorption cross section for PSII  
 308 photochemistry from a given sample and excitation bandwidth ( $\text{nm}^2 \text{ quanta}^{-1}$ ). We compared  
 309 several other algorithms for  $JV_{PSII}$  (Tortell and Suggett 2021) and found similar results.

310 We calibrated the  $JV_{PSII}$  estimator to absolute rates of electron transport (Eq. (5)) using  
 311 parallel measures of oxygen evolution ( $\mu\text{mol O}_2 \text{ L}^{-1} \text{ s}^{-1}$ ), captured simultaneously with the FRRf  
 312 measures, below light saturation of electron transport, using a FireSting robust oxygen probe  
 313 (PyroScience, Germany) inserted in the cuvette for select Rapid Light Curve (RLC) runs (Fig. 3).  
 314 For the blue LED ( $\text{Ex}_{445\text{nm}}$ ) excitation we used a calibration slope of 108832, while for orange  
 315 LED ( $\text{Ex}_{590\text{nm}}$ ) excitation we used a calibration slope of 254327

$$316 \quad JV_{PSII}(\text{e}^- \text{ L}^{-1} \text{ s}^{-1}) = \frac{\text{Uncalibrated } JV_{PSII}(\text{e}^- \text{ L}^{-1} \text{ s}^{-1})}{\text{Calibration slope}} \quad (5)$$

317



318

319 **Fig. 3.** Single turnover (ST) fluorescence induction by Fast Repetition Rate fluorometry (FRRf). (A) Examples of  
 320 fluorescence yield vs. elapsed time ( $\mu\text{s}$ ) for PE-rich culture of *Synechococcus* sp. (048) in the dark (dark-relaxed; 0  
 321  $\mu\text{mol photons m}^{-2}\text{s}^{-1}$ ) and under actinic PAR (in this example  $80 \mu\text{mol photons m}^{-2}\text{s}^{-1}$ ) using blue LED ( $Ex_{445\text{nm}}$ ;  
 322 open blue circles) or orange ( $Ex_{590\text{nm}}$ ; open orange diamonds) excitation. The ST technique delivers a series of  
 323 flashlets for non-intrusive, repeated monitoring of chlorophyll fluorescence parameters (including  $F_O$ ,  $F'$ ,  $F_M$ ,  $F'_M$ ,  
 324  $\tau_1 - \tau_3$ ,  $\tau'_1 - \tau'_3$ ,  $\sigma_{PSII}$ , and  $\sigma_{PSII}'$ ). (B) Linear regressions of uncalibrated PSII electron flux ( $JV_{PSII}$ ) vs.  $e^- L^{-1} s^{-1}$  derived

325 from simultaneously measured oxygen evolution Light Response Curves (LRC) under blue LED ( $\text{Ex}_{445\text{nm}}$ ; open blue  
326 circles) or orange ( $\text{Ex}_{590\text{nm}}$ ; open orange diamonds) excitation. (C) Rapid Light Curve (RLC), fit with a three  
327 parameter model (Harrison and Platt 1986), for PSII electron flux ( $JV_{\text{PSII}}$ ;  $\mu\text{mol e}^{-} \mu\text{mol Chl } a^{-1} s^{-1}$ ) vs. actinic PAR  
328 measured under blue LED ( $\text{Ex}_{445\text{nm}}$ ; open blue circles) or orange ( $\text{Ex}_{590\text{nm}}$ ; open orange diamonds) excitation.

329

330 **Statistical analysis**

331 We used R version 4.3.0 (R Core Team 2023) running under RStudio (Posit team 2022).  
332 We performed three-way factorial ANOVA (*aov()* function; R Base package) to determine  
333 whether peak PAR, photoperiod, strain, and their interactions, significantly influence the  
334 chlorophyll-specific exponential growth rate ( $\mu$ ;  $d^{-1}$ ), estimated from logistic fits (*nlsLM()*  
335 function; Elzhov et al. (2023)) of chlorophyll proxy  $OD_{680} - OD_{720}$  vs. cumulative diel PUR  
336 (Table S2). We also used the *nlsLM()* function to fit a three parameter light response model  
337 (Harrison and Platt 1986) of growth rates ( $\alpha$ , initial slope of curve;  $\beta$ , reflecting the  
338 photoinhibition process;  $P_{\text{max}}$ , the maximum rate of growth curve).

339 To examine statistical differences between fits of light responses, we performed one-way  
340 ANOVA (*aov()* function) of the three parameter model (Harrison and Platt 1986) fit to pooled  
341 data for each taxa, compared to separate fits for each different photoperiod (8, 12, 16, or 24); or  
342 to separate fits for each different peak PAR (30, 90, 180, 300, 600 together with 900). These  
343 comparisons were run for chlorophyll-specific exponential growth rate vs. cumulative diel PUR  
344 (Table S3, S4); vs. cumulative diel PAR (Table S5, S6) or vs. PSII electron flux ( $JV_{\text{PSII}}$ ;  $\mu\text{mol e}^{-}$   
345  $\mu\text{mol Chl } a^{-1} d^{-1}$ ; Table S7, S8). One-way ANOVA was also used to examine statistical  
346 differences between single phase exponential decay fits (*SSasymp()* function; Serway et al.  
347 (2004)) of pooled data across different strains for a given phase of growth and across different  
348 phase of growth for a given strain for PUR/PAR ratio (Table S9); Phycobiliprotein to Chl  $a$  ratio

349 (Table S10); or effective absorption cross section of PSII ( $\sigma_{PSII}'$ ; nm<sup>2</sup> quanta<sup>-1</sup>) measured under  
350 diel peak PAR growth light under Ex<sub>590nm</sub> (orange) excitation in relation to the cumulative diel  
351 PAR ( $\mu\text{mol photons m}^{-2}\text{d}^{-1}$ ) (Table S11).

352 We used *t*-tests (*t.test()* function; R Base package) of linear fits (*lm()* function) to compare  
353 pooled data across different strains for a given phase of growth, and across different phases of  
354 growth, for a given strain, for effective absorption cross section of PSII ( $\sigma_{PSII}'$ ; nm<sup>2</sup> quanta<sup>-1</sup>)  
355 measured under diel peak PAR growth light under Ex<sub>445nm</sub> (blue) excitation vs. the cumulative  
356 diel PAR ( $\mu\text{mol photons m}^{-2}\text{d}^{-1}$ ; Table S12); or vs. the Phycobiliprotein to Chl *a* ratio (Table  
357 S13). The same *t*-test analyses were performed for effective absorption cross section of PSII  
358 ( $\sigma_{PSII}'$  or  $\sigma_{PSII}$ ; nm<sup>2</sup> quanta<sup>-1</sup>) measured under Ex<sub>590nm</sub> (orange) excitation vs. the Phycobiliprotein  
359 to Chl *a* ratio (Table S14, S15).

360 Statistical differences for all analyses were determined at significance level  $\alpha = 0.05$ . The  
361 manuscript was prepared as a Rmarkdown document (Handel 2020) with figures plotted using  
362 ggplot2 (Wickham 2016) and patchwork (Pedersen 2024) packages. All metadata, data and code  
363 is available on GitHub (<https://github.com/FundyPhytoPhys/BalticPhotoperiod>).

364

## 365 **Results**

### 366 **Chlorophyll-specific exponential growth rate**

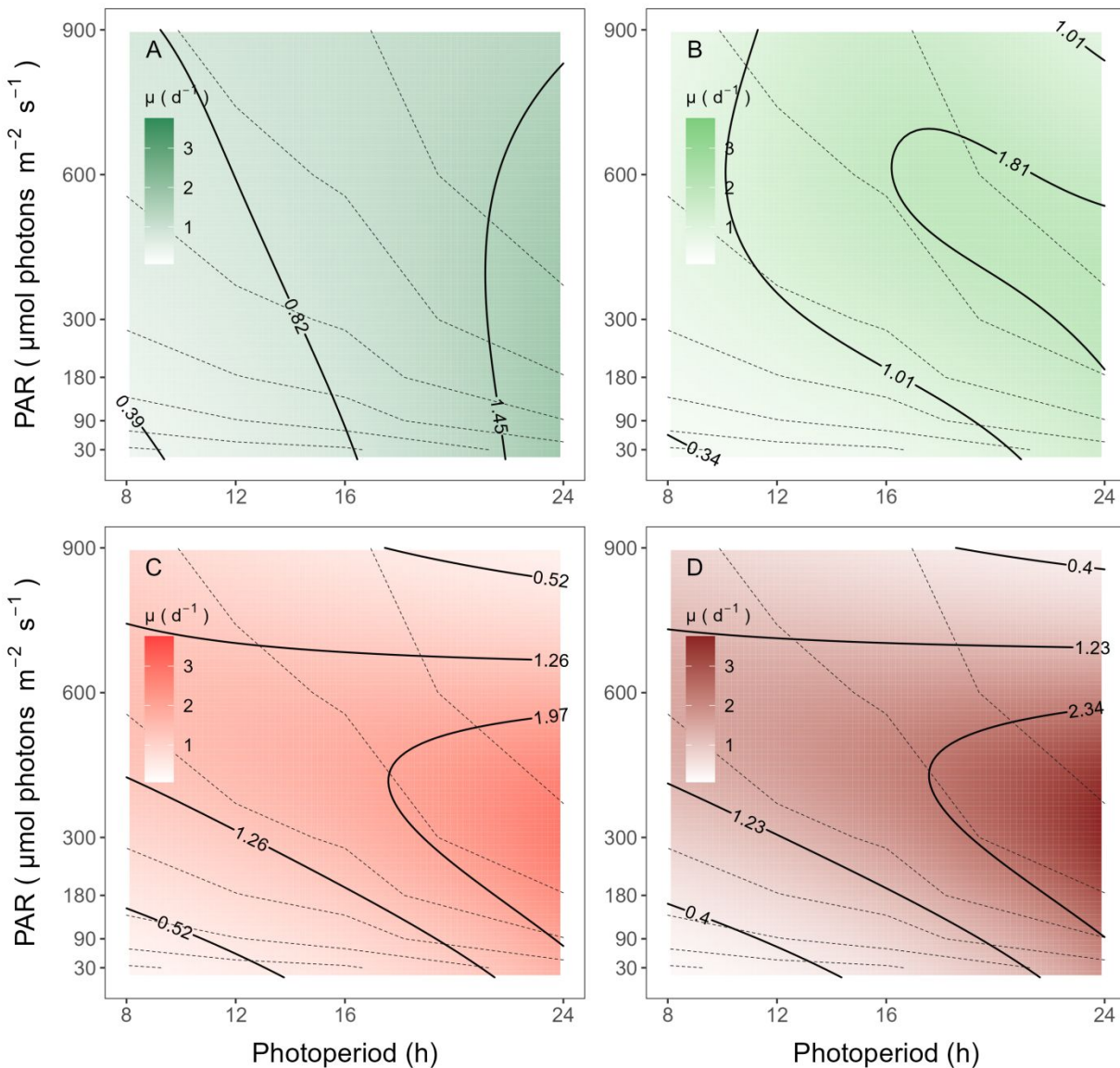
367 Not all cultures were grown long enough to reach full stationary phase, but onset of  
368 stationary phase, when determined, occurred fairly consistently when cultures reached  $\sim 0.5$   
369 OD<sub>720</sub> (PC-rich) or  $\sim 0.65$  OD<sub>720</sub> (PE-rich), no matter the level of culture PAR. It is therefore  
370 unlikely that onset of light limitation imposed stationary phase on the cultures, which remained  
371 optically fairly thin, with even illumination to each tube from the PSI MultiCultivator array of

372 LED. Based upon parallel studies re-launching growth after stationary phase by dilution with  
373 fresh media, with the same strains, under the same growth conditions (unpub.), we hypothesize  
374 that nutrient limitation imposes the transition to stationary phase.

375 We used logistic curve fits (Fig. S3B) to determine chlorophyll-specific exponential  
376 growth rates ( $\mu$ ;  $d^{-1}$ ), for two PhycoCyanin(PC)-rich cultures (056, 077) and two  
377 PhycoErythrin(PE)-rich cultures (048, 127) of *Synechococcus* sp. grown at 30, 90, 180, 300, 600,  
378 or 900 peak PAR  $\mu\text{mol photons m}^{-2}\text{s}^{-1}$  ( $\mu\text{E}$ ); and photoperiods of 8, 12, 16, or 24 h. ~~Three-way~~  
379 ~~factorial ANOVA showed that peak PAR, photoperiod, strain, and their interactions,~~  
380 ~~significantly affected  $\mu$  (ANOVA,  $p < 0.05$  for all; Table S2).~~ There were significant effects of  
381 all three independent variables on  $\mu$  as well as significant interactions between variables  
382 (ANOVA,  $p < 0.05$ ; Table S2). All tested strains, except PE-rich\_048, grew even under peak  
383 PAR 900  $\mu\text{mol photons m}^{-2}\text{s}^{-1}$  and 24 h photoperiod. The highest growth rate was recorded for  
384 *Synechococcus* sp. PE-rich\_127 ( $\mu = 4.5 \text{ d}^{-1}$ ; 3.7 h doubling time) and PC-rich\_056 ( $\mu = 3.4 \text{ d}^{-1}$ ;  
385 4.9 h doubling time) at 180  $\mu\text{mol photons m}^{-2}\text{s}^{-1}$  peak PAR and photoperiod of 24 h.

386 The GAM model in Fig. 4 summarizes the growth responses of the PC-rich and PE-rich  
387 picocyanobacteria to peak PAR and photoperiod. PC-rich\_056 *Synechococcus* sp. showed  
388 highest growth rates under a photoperiod of 24 h, across a wide range of peak PAR indicated by  
389 the contour line labeled  $1.45 \text{ d}^{-1}$ , representing the 90<sup>th</sup> percentile of achieved growth rates for the  
390 strain. On the other hand, the other tested PC-rich strain (077) showed highest growth rates in the  
391 range of photoperiod 16–24 h and peak PAR between 300 – 700  $\mu\text{mol photons m}^{-2}\text{s}^{-1}$ , indicated  
392 by the  $1.81 \text{ d}^{-1}$  contour line again representing the 90<sup>th</sup> percentile of maximum achieved growth  
393 rates for the strain. For both PC-rich strains, growth was slowest under 30  $\mu\text{mol photons m}^{-2}\text{s}^{-1}$   
394 and a photoperiod of 8 h.

395 Both PE-rich strains achieved fastest growth rates above peak PAR of ~300  $\mu\text{mol}$  photons  
396  $\text{m}^{-2}\text{s}^{-1}$ , under the longest photoperiod of 24 h, indicated by the  $1.97 \text{ d}^{-1}$  for PE-rich\_048, and  
397  $2.34 \text{ d}^{-1}$  for PE-rich\_127, contour lines. For the PE-rich strains growth decreased with decreasing  
398 photoperiod and decreasing peak PAR. Moreover, PE-rich strains showed photoinhibition of  
399 growth at peak PAR of 900  $\mu\text{mol}$  photons  $\text{m}^{-2}\text{s}^{-1}$  and photoperiods of 16- 24 h. The growth rate  
400 contours for PC-rich and PE-rich *Synechococcus* sp. did not generally follow isoclines of  
401 cumulative diel photon dose ( $\mu\text{mol}$  photons  $\text{m}^{-2}\text{d}^{-1}$ , dashed lines), showing that photoperiod, and  
402 peak PAR influenced growth rates beyond cumulative diel photon dose.



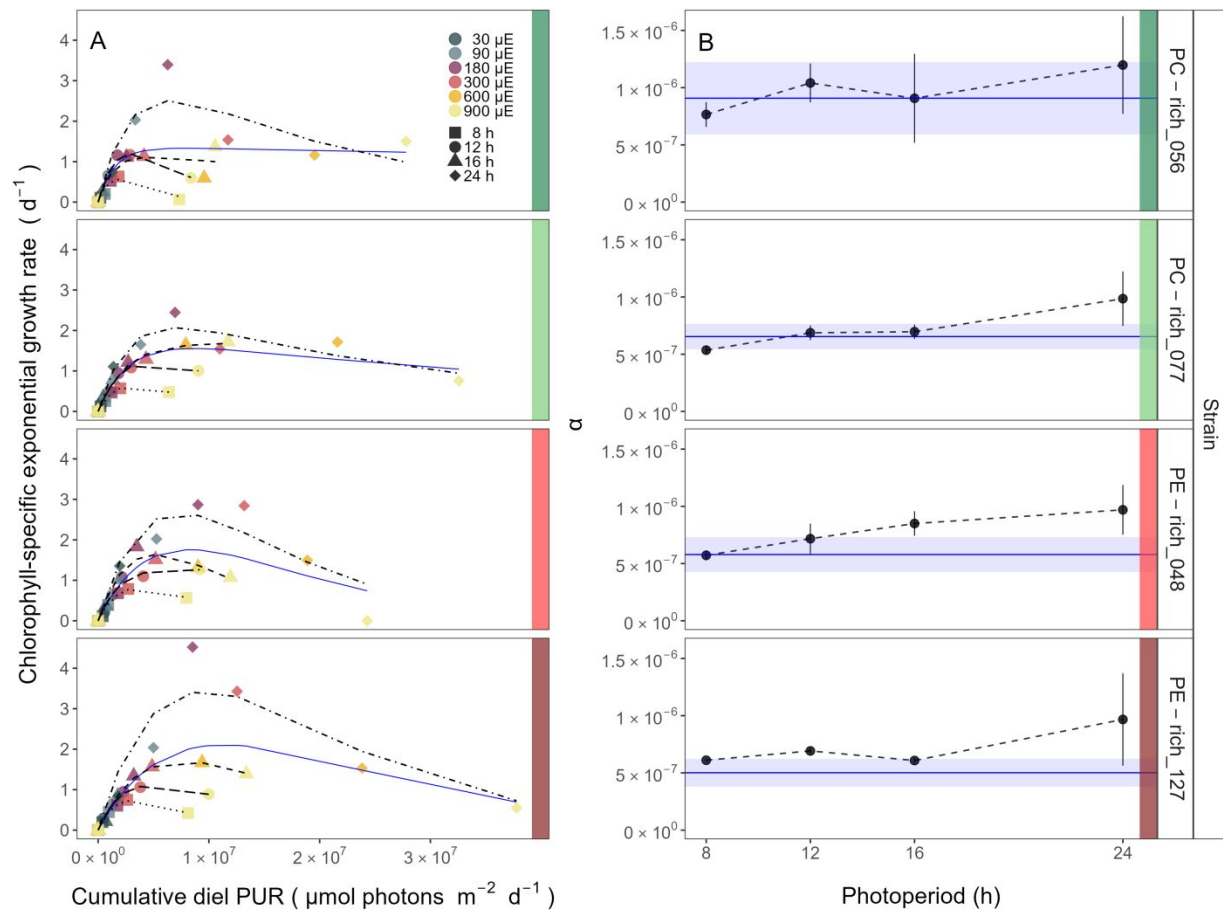
403

404 **Fig. 4.** A contour plot of a Generalized Additive Model (GAM) of chlorophyll-specific growth rates ( $d^{-1}$ ) for two  
 405 PC-rich cultures: **(A)** 056, **(B)** 077 and two PE-rich cultures: **(C)** 048, **(D)** 127 of *Synechococcus* sp. grown at 30, 90,  
 406 180, 300, 600, or 900 peak PAR  $\mu\text{mol photons m}^{-2}\text{s}^{-1}$ ; and photoperiods of 8, 12, 16, or 24 h. Legends show colour  
 407 gradients of growth rate ( $\mu$ ;  $d^{-1}$ ) from no growth (white) to 3.0  $d^{-1}$  (dark green for PC-rich\_056, light green for PC-  
 408 rich\_077, light red for PE-rich\_048 or dark red for PE-rich\_127 strains). Labeled contour lines indicate the 90%,  
 409 50%, and 10% quantiles for achieved growth rate. Dotted lines show isoclines of cumulative diel photon dose ( $\mu\text{mol}$   
 410  $\text{photons m}^{-2} d^{-1}$ ).

411

412 A three parameter light response model fit (Harrison and Platt 1986) of chlorophyll-  
413 specific exponential growth rates vs. cumulative diel PUR dose for two PC-rich and two PE-rich  
414 cultures of *Synechococcus* sp. showed significant differences between model fits of the pooled  
415 data vs. fits for all tested photoperiods (8, 12, 16, or 24 h; ANOVA,  $p < 0.05$ ; Fig. 5A, Table S3).  
416 The alpha parameters of the initial rise of growth rate ( $\alpha$ ) vs. cumulative diel PUR, estimated  
417 from data pooled for each photoperiod increased with increasing photoperiod for all strains. The  
418 highest increase (>2-fold) of  $\alpha$  with increasing photoperiod was recorded for PC-rich\_056 (Fig.  
419 5B). Strains also showed distinct growth rate responses to cumulative diel PUR, depending upon  
420 peak PAR (Fig. S4A, Table S4), that differ from a single light response model fit to the pooled  
421 data across all peak PAR from a strain. Differences were observed in the strains PC-rich\_077 and  
422 PE-rich\_048 with the peak PAR of 600 or 900  $\mu\text{mol photons m}^{-2}\text{s}^{-1}$ , which were not  
423 significantly different from the pooled data model. A caveat to these findings is that cumulative  
424 diel photon dose is a product of photoperiod and PAR, so the highest levels of cumulative PUR  
425 dose are only achieved under the 600 or 900  $\mu\text{mol photons m}^{-2}\text{s}^{-1}$ . The alpha parameters of the  
426 initial rise of growth rate ( $\alpha$ ) vs. cumulative diel PUR, estimated from data pooled for each peak  
427 PAR decreased across peak PAR for all tested strains (Fig. S4B).

428 Growth rate saturated under increasing cumulative diel PUR for all strains, however, the  
429 achieved estimates of  $\mu_{\max}$  varied depending upon photoperiod and peak diel PAR. Growth rates  
430 vs. cumulative diel PAR relationships, estimated for exponential phase cultures, followed similar  
431 patterns (Fig. S5, Fig. S6 and Table S5, S6 in Supporting Information).



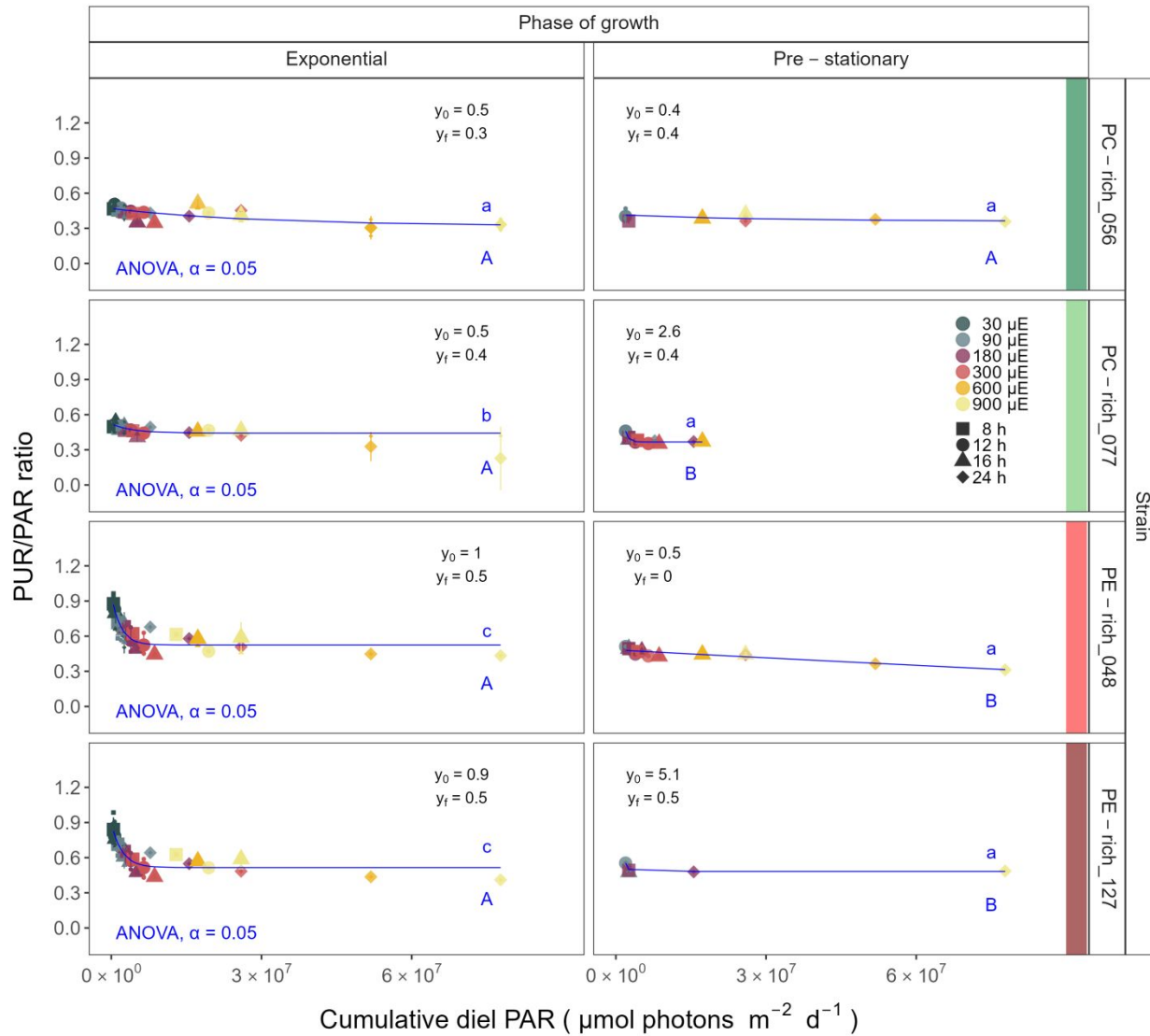
432

433 **Fig. 5.** (A) Chlorophyll-specific exponential growth rates ( $d^{-1}$ ) vs. cumulative diel Photosynthetically Usable  
 434 Radiation (PUR,  $\mu\text{mol photons m}^{-2}\text{d}^{-1}$ ). Growth rates ( $\pm$  SE falling within symbols) were estimated from logistic fits  
 435 of chlorophyll proxy  $\text{OD}_{680} - \text{OD}_{720}$  ( $\Delta\text{OD}$ ) vs. elapsed time (Fig. 1, Fig. S3B), for two PC-rich cultures (056; dark  
 436 green, 077; light green) and two PE-rich cultures (048; light red, 127; dark red) of *Synechococcus* sp. grown at 30  
 437 ( $\mu\text{E}$ ), 90 (light gray), 180 (purple), 300 (red), 600 (orange), or 900 (yellow) peak PAR  $\mu\text{mol photons m}^{-2}\text{s}^{-1}$   
 438 ( $\mu\text{E}$ ); and photoperiods of 8 (square), 12 (circle), 16 (triangle), or 24 (diamond) h. Solid blue line shows a fit of the  
 439 pooled growth rates through photoperiods for each strain, with a three parameter model (Harrison and Platt 1986).  
 440 We also fit the same model separately for 8 (dotted line), 12 (long dash line), 16 (dashed line), or 24 (two dash line)  
 441 h photoperiods, since for all strains they were each significantly different (ANOVA,  $p < 0.05$ ) from the fit of pooled  
 442 data. (B) Alpha parameters of the initial rise of growth rate ( $\alpha$ ) vs. cumulative diel Photosynthetically Usable  
 443 Radiation (PUR), estimated from data pooled for each photoperiod (points ( $\pm$  SE) connected by dashed lines), and  
 444 estimated for all data across photoperiods (solid blue horizontal line  $\pm$  SE), for each strain.

445

446 **PUR/PAR ratio vs. cumulative diel PAR**

447 The PUR/PAR ratio is an index of the efficacy of light capture for a culture under a given  
448 growth condition; showing the fraction of PAR that can be captured by the absorbance of the  
449 cells (Fig. 6). For the two PC-rich and, particularly, for the two PE-rich cultures of  
450 *Synechococcus* sp. PUR/PAR decayed exponentially to a plateau, with increasing cumulative  
451 diel PAR, when pooling PUR/PAR data across different combinations of photoperiod and peak  
452 PAR. Although all strains followed a similar trend, the single phase exponential decay model fit  
453 parameters varied significantly among strains, during their exponential phase of growth  
454 (ANOVA,  $p < 0.05$ ), except the model fits from PE-rich\_048 and PE-rich\_127 (ANOVA,  $p >$   
455 0.05; Table S9). Moreover, the PUR/PAR ratio was higher in the PE-rich strains under low  
456 cumulative diel photon dose during their exponential phase of growth ( $y_0$  greater or equal to 0.9),  
457 but decayed towards a plateau close to the PC-rich strains as cumulative diel photon dose  
458 increases ( $y_f = 0.5$ ). On the other hand, the single phase exponential decay model fits did not  
459 differ significantly among strains, during their pre-stationary phase of growth (ANOVA,  $p >$   
460 0.05; Table S9). During this phase, response of PUR/PAR ratio to increasing cumulative diel  
461 PAR exhibits damping, maintaining a consistent trend across all strains within the  $y_f$  range of 0.4  
462 to 0.5, with the exception of the PE-rich\_048 strain. We also find that model fits from different  
463 phases of growth differed within a given strain, with the exception of PC-rich\_056 (ANOVA;  $p$   
464  $< 0.05$ , Table S9). A similar decay trend was observed for Phycobiliprotein to Chl *a* ratio  
465 ( $\mu\text{g}:\mu\text{g}$ ) across cumulative diel PAR (Fig. S7).



466

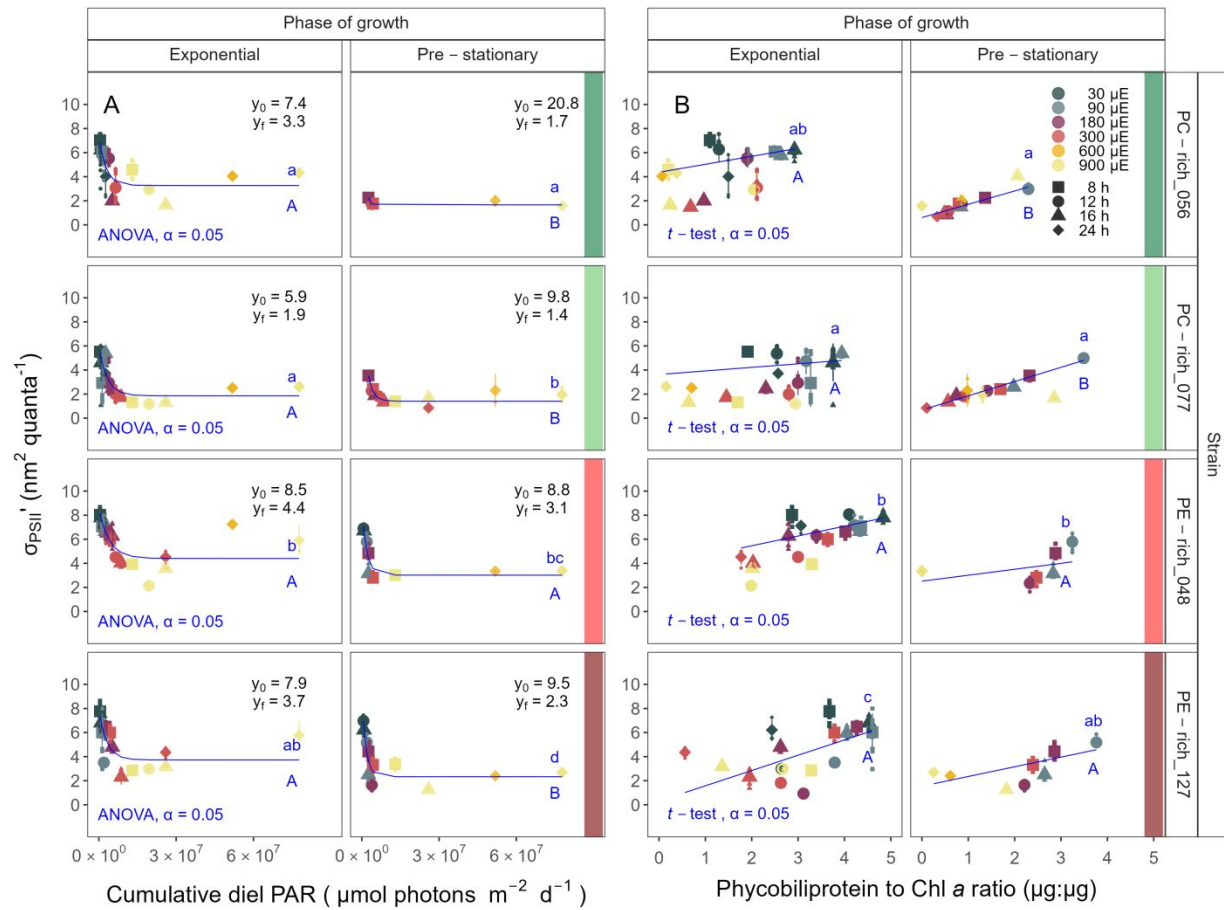
467 **Fig. 6.** Changes in PUR/PAR ratio vs. cumulative diel PAR ( $\mu\text{mol photons m}^{-2} \text{d}^{-1}$ ). PUR/PAR ratio was estimated  
468 for two PC-rich cultures (056; dark green, 077; light green) and two PE-rich cultures (048; light red, 127; dark red)  
469 of *Synechococcus* sp. grown at 30 (dark gray), 90 (light gray), 180 (purple), 300 (red), 600 (orange), or 900 (yellow)  
470 peak PAR  $\mu\text{mol photons m}^{-2} \text{s}^{-1}$  ( $\mu\text{E}$ ); and photoperiods of 8 (square), 12 (circle), 16 (triangle), or 24 (diamond) h.  
471 Figure presents data (smaller symbols) and means (bigger symbols) from exponential or pre-stationary phase of  
472 growth. Blue solid line shows single phase exponential decay fit for data from each strain and growth phase, with fit  
473 parameters presented. Different lowercase letters indicate statistically significant differences between the fit models  
474 for different strains within a given phase of growth. Different uppercase letters indicate statistically significant  
475 differences between the fit models for different phases of growth within a given strain (ANOVA;  $p < 0.05$ ).

476

477 **Effective absorption cross section of PSII of picocyanobacteria**

478 The effective absorption cross section of PSII ( $\sigma_{PSII}'$ ,  $\text{nm}^2 \text{ quanta}^{-1}$ ), was estimated using  
479 FRRf induction curves using  $\text{Ex}_{590\text{nm}}$  (orange) excitation, for two PC-rich (056, 077) and two PE-  
480 rich (048, 127) cultures of *Synechococcus* sp. grown at 30, 90, 180, 300, 600, or 900 peak PAR  
481  $\mu\text{mol photons m}^{-2}\text{s}^{-1}$  ( $\mu\text{E}$ ); and photoperiods of 8, 12, 16, or 24 h (Fig. 7). The  $\sigma_{PSII}'$  measured  
482 under diel peak PAR growth light under  $\text{Ex}_{445\text{nm}}$  (blue) excitation vs. cumulative diel photon  
483 dose is shown in Supporting Information (Fig. S8, Table S12).

484 All strains showed consistent patterns of sharp, exponential decay of effective absorption  
485 cross section for PSII photochemistry vs. cumulative diel photon doses, across different  
486 combinations of photoperiod and peak PAR (Fig. 7A). Although all strains showed this response  
487 pattern, the exponential decay fits differed significantly among two PC-rich strains and PE-  
488 rich\_048 strains during their exponential phase of growth (ANOVA,  $p < 0.05$ ; Table S11). PE-  
489 rich strains showed higher  $\sigma_{PSII}'$  under low cumulative diel photon dose ( $y_0$  about 0.8 and  $y_f$   
490 about 4) than did PC-rich strains. During pre-stationary phase this response dampens in the PC-  
491 rich strains but persists in the PE-rich strains (Table S11).  $\sigma_{PSII}'$  for the PE-rich strains during  
492 pre-stationary phase of growth still remain higher ( $y_f$  between 2.3 – 3.0) than in the PC-rich  
493 strains ( $y_f$  between 1.4 – 1.7) even as cumulative diel photon dose increases. Model fits from  
494 different phases of growth differed within a given strain, with the exception of PE-rich\_048  
495 (ANOVA;  $p < 0.05$ , Table S11).



496

497 **Fig. 7. (A)** Effective absorption cross section of PSII ( $\sigma_{\text{PSII}'}$ ;  $\text{nm}^2 \text{ quanta}^{-1}$ ) measured under diel peak PAR growth  
 498 light vs. cumulative diel PAR ( $\mu\text{mol photons m}^{-2} \text{ d}^{-1}$ ); blue solid line shows single phase exponential decay fit for  
 499 data from each strain and growth phase. **(B)** Changes of  $\sigma_{\text{PSII}'}$  measured under diel peak PAR growth light vs. the  
 500 ratio of sum of  $\mu\text{g}$  phycobilins (PE, PC, APC protein, Phycobiliprotein) to  $\mu\text{g}$  Chl *a*; blue solid line shows linear  
 501 model fit for data from each strain and growth phase.  $\sigma_{\text{PSII}'}$  was estimated using FRRf induction curves with  
 502 excitation of phycobilisomes (Ex<sub>590nm</sub>, orange), for two PC-rich cultures (056; dark green, 077; light green) and two  
 503 PE-rich cultures (048; light red, 127; dark red) of *Synechococcus* sp. grown at 30 (dark gray), 90 (light gray), 180  
 504 (purple), 300 (red), 600 (orange), or 900 (yellow) peak PAR  $\mu\text{mol photons m}^{-2} \text{ s}^{-1}$  ( $\mu\text{E}$ ); and photoperiods of 8  
 505 (square), 12 (circle), 16 (triangle), or 24 (diamond) h. Figure presents data (smaller symbols) and means (bigger  
 506 symbols) from exponential or pre-stationary phase of growth. Different lowercase letters indicate statistically  
 507 significant differences between the fit models for different strains within a given phase of growth. Different

508 uppercase letters indicate statistically significant differences between the fit models for different phases of growth  
509 within a given strain ( $p < 0.05$ ).

510

511 Effective absorption cross section of PSII ( $\sigma_{PSII}'$ ;  $\text{nm}^2 \text{ quanta}^{-1}$ ), measured under diel peak  
512 PAR growth light with  $\text{Ex}_{590\text{nm}}$  (orange) excitation, varies with Phycobiliprotein to Chl *a* ratio  
513 (Fig. 7B).  $\sigma_{PSII}'$  excited through phycobilisome absorbance at  $\text{Ex}_{590\text{nm}}$  shows positive linear  
514 correlations with the Phycobiliprotein to Chl *a* ratio, although strains in exponential growth show  
515 significant scatter around this positive relation, likely related to regulatory control of  $\sigma_{PSII}'$  under  
516 different measurement PAR, beyond pigment composition. Under pre-stationary phase the  
517 relationship between  $\sigma_{PSII}'$  and Phycobiliprotein to Chl *a* ratio was more consistent, suggesting  
518 increased reliance upon compositional regulation to control light delivery to PSII, as opposed to  
519 shorter-term physiological regulation under changing light. The linear fits of  $\sigma_{PSII}'$   
520 vs. Phycobiliprotein to Chl *a* ratio also vary significantly between PC-rich\_077 and two PE-rich  
521 strains during their exponential phase of growth. During pre-stationary phase we noted  
522 significant differences between two PC-rich strains and PE-rich\_048. Moreover, significant  
523 differences between the fit models for varying phases of growth were noted for PC-rich strains  
524 056 and 077 (*t*-test;  $p < 0.05$ , Table S14).

525 Changes in effective absorption cross section of PSII ( $\sigma_{PSII}$ ;  $\text{nm}^2 \text{ quanta}^{-1}$ ) measured in the  
526 dark with  $\text{Ex}_{590\text{nm}}$  (orange) excitation vs. Phycobiliprotein to Chl *a* ratio (Fig. S9A, Table S15)  
527 and  $\sigma_{PSII}'$  measured under diel peak PAR growth light under  $\text{Ex}_{445\text{nm}}$  (blue) excitation  
528 vs. Phycobiliprotein to Chl *a* ratio (Fig. S9B and Table S13) are shown in Supporting  
529 Information.

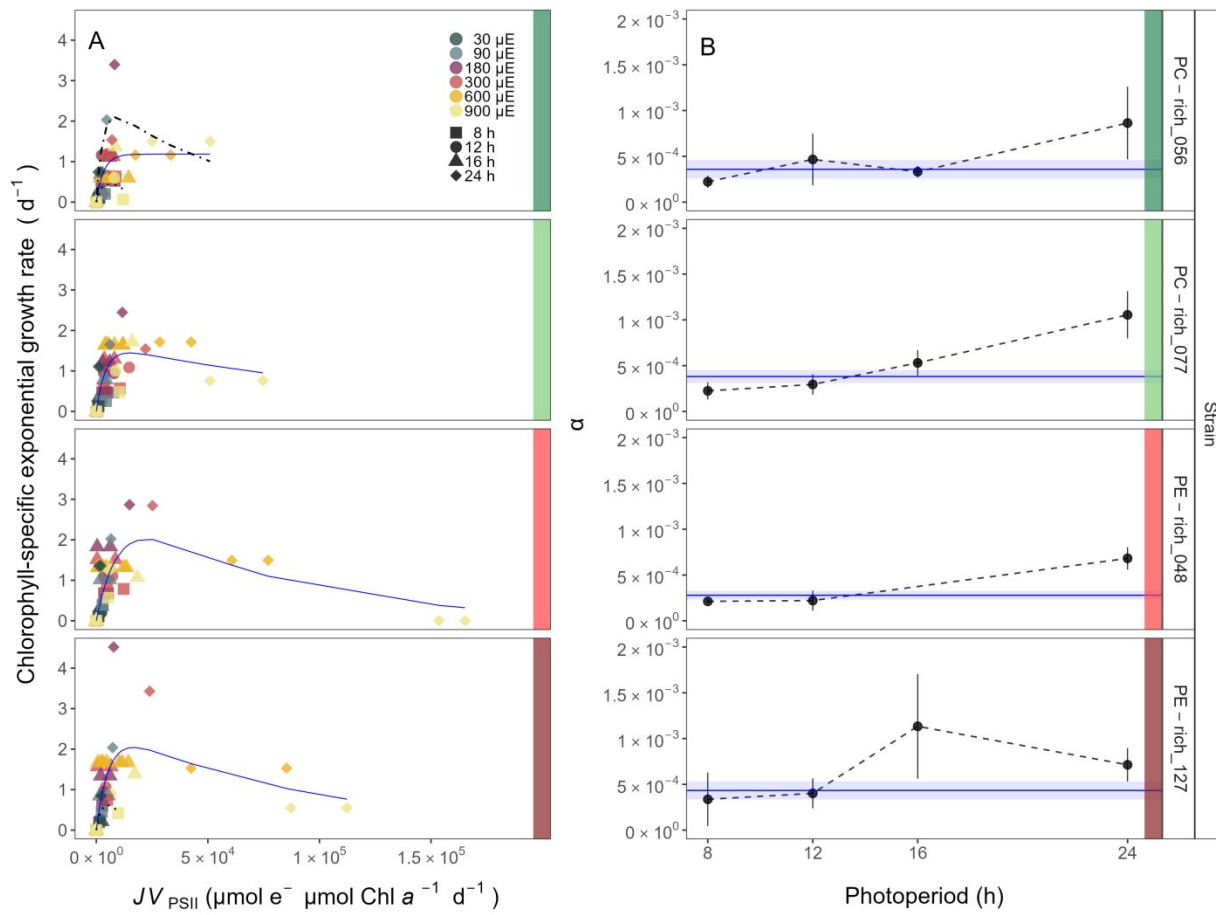
530

### 531    **Growth rates vs. cumulative diel PSII electron flux**

532       Chlorophyll-specific exponential growth rates ( $d^{-1}$ ), within each strain, show fairly  
533       consistent saturating responses to increasing cumulative diel PSII electron flux ( $JV_{PSII}$ ;  $\mu\text{mol e}^-$   
534        $\mu\text{mol Chl } a^{-1} d^{-1}$ ) estimated under diel peak PAR growth light, and estimated using FRRf  
535       induction curves with excitation of chlorophyll (Ex<sub>445nm</sub>, blue), although photoperiod (Fig. 8A,  
536       Table S7) and peak PAR (Fig. S10, Table S8) retained a secondary influence on achieved growth  
537       responses for some growth conditions.

538       A three parameter model fit of (Harrison and Platt 1986) vs. cumulative diel PSII electron  
539       flux ( $JV_{PSII}$ ;  $\mu\text{mol e}^- \mu\text{mol Chl } a^{-1} d^{-1}$ ) for two PC-rich and two PE-rich cultures of  
540       *Synechococcus* sp. showed no significant differences between fits of the pooled data vs. fits for  
541       different photoperiods (8, 12, 16, or 24 h; ANOVA,  $p < 0.05$ ), with exception of 8 and 24 h  
542       photoperiod for PC-rich\_056 and 8 h photoperiod for PE-rich\_127 strains (ANOVA,  $p > 0.05$ ;  
543       Table S7).

544       Alpha parameters of the initial rise of growth rate ( $\alpha$ ) vs. cumulative diel  $JV_{PSII}$ , estimated  
545       from data pooled for each photoperiod showed an increase across increasing photoperiods for  
546       each strain except for PE-rich\_0127. The highest increase (>2-fold) of  $\alpha$  from the lowest to the  
547       highest photoperiod was recorded for PC-rich\_077 (Fig. 8B).



548

549 **Fig. 8.** (A) Chlorophyll-specific exponential growth rates ( $d^{-1}$ ) vs. cumulative diel PSII electron flux ( $JV_{PSII}$ ;  $\mu\text{mol e}^-$   
 550  $\mu\text{mol Chl } a^{-1} d^{-1}$ ) measured under diel peak PAR growth light. Growth rates ( $\pm$  SE falling within symbols) were  
 551 estimated from logistic fits of chlorophyll proxy  $OD_{680} - OD_{720}$  ( $\Delta OD$ ) vs. elapsed time (Fig. S3B).  $JV_{PSII}$  was  
 552 estimated using FRRf induction curves with excitation of chlorophyll ( $Ex_{445\text{nm}}$ , blue), for two PC-rich cultures (056;  
 553 dark green, 077; light green) and two PE-rich cultures (048; light red, 127; dark red) of *Synechococcus* sp. grown at  
 554 30 (dark gray), 90 (light gray), 180 (purple), 300 (red), 600 (orange), or 900 (yellow) peak PAR  $\mu\text{mol photons}$   
 555  $\text{m}^{-2}\text{s}^{-1}$  ( $\mu\text{E}$ ); and photoperiods of 8 (square), 12 (circle), 16 (triangle), or 24 (diamond) h. Solid blue line shows a fit  
 556 of the pooled growth rates for each strain, with a three parameter model (Harrison and Platt 1986). We also fit the  
 557 same model separately for 8 (dotted line) and 24 (two dash line) h photoperiods, when they were significantly  
 558 different (ANOVA,  $p < 0.05$ ) from the fit of pooled data. (B) Alpha parameters of the initial rise of growth rate ( $\alpha$ )  
 559 vs. cumulative diel  $JV_{PSII}$ , estimated from data pooled for each photoperiod (points ( $\pm$  SE) connected by dashed  
 560 lines), and estimated for all data across photoperiods (horizontal line  $\pm$  SE), for each strain.

561

562 **Discussion**563 **Photic regimes - implications for picocyanobacteria growth and distribution**

564 Light regimes, including photoperiod, and peak PAR, are major factors affecting the  
565 distribution and seasonality of phytoplankters (Erga and Heimdal 1984). Changes in photoperiod  
566 trigger acclimation responses, shaping the temporal dynamics and community structure of  
567 phytoplankton (Theus et al. 2022; Longobardi et al. 2022). Each tested picocyanobacterial strain  
568 showed influences of photoperiod upon the responses of growth rate to cumulative diel PUR  
569 (Fig. 5) and PAR (Fig. S5). To our surprise, increasing photoperiod increased the ranges of  
570 response to PAR and PUR. Both the PC-rich and the PE-rich strains of *Synechococcus* sp.  
571 exhibited their highest initial responses of growth to increasing PUR and PAR (alpha, (Fig. 5B),  
572 Fig. S5B), and their fastest growth rates under continuous light (24 h photoperiod), consistent  
573 with some other strains (Jacob-Lopes et al. 2009; Klepacz-Smólka et al. 2020). Yet, 24 h  
574 photoperiod also exacerbated eventual photoinhibition under excess cumulative diel PUR and  
575 PAR. Our four temperate strains do not experience direct selective pressures to exploit a  
576 continuous 24 photoperiod (Brand and Guillard 1981), so achieving maximum growth under a 24  
577 h photoperiod rather suggests lack of a requirement for a dark period, and lack of requirement for  
578 a regular photoperiod. Coastal phytoplankton strains are selected to exploit instantaneous light  
579 (Brand and Guillard 1981), of whatever duration, to cope with fluctuating light and nutrients in  
580 coastal environments (MacIntyre et al. 2000; Litchman et al. 2009), leading to a pleiotropic  
581 capacity for exploiting continuous light. *Synechococcus* assemblages in coastal areas would tend  
582 to be dominated by PC-rich strains by virtue of the higher turbidity of these areas relative to the  
583 open ocean, perhaps regardless of photoperiod. However, the ability of both PC-rich and PE-rich

584 coastal picocyanobacteria to exploit continuous light means they could, potentially, grow rapidly  
585 at higher latitudes, in a future warmer polar summer water.

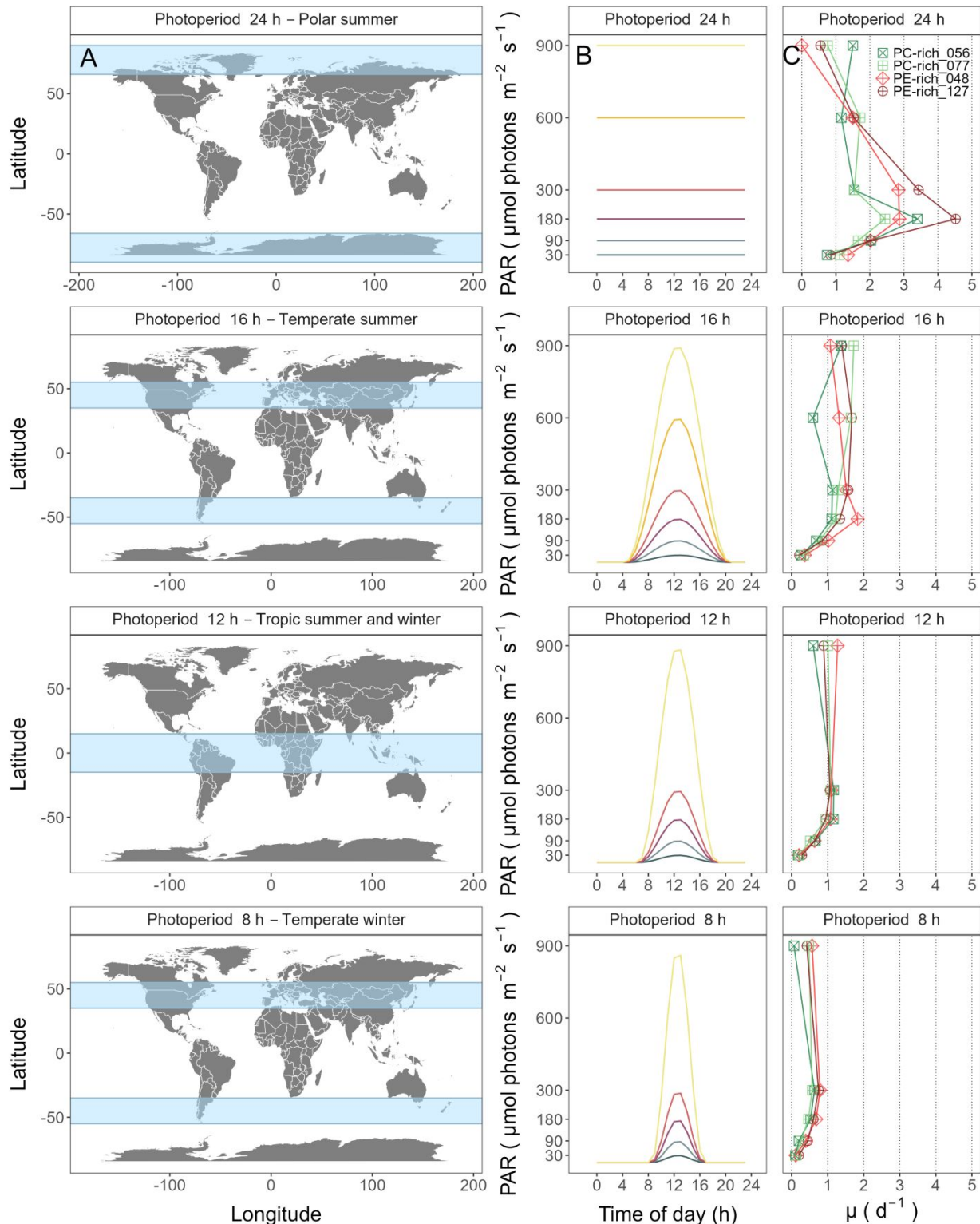
586 Light level is another key driver of picocyanobacteria productivity (Pick 1991; Six et al.  
587 2007; Aguilera et al. 2023). The spatial and temporal distribution of PAR within aquatic  
588 ecosystems is influenced by solar angle, water depth, water clarity, and the presence of light-  
589 absorbing substances such as dissolved organic matter (Morel 1978, 1988) and phytoplankton  
590 cells. PUR then represents the light potentially available for phytoplankton to photosynthesize.  
591 PUR is always smaller than PAR ( $\text{PUR} < \text{PAR}$ ), and depends on the spectral composition of the  
592 PAR, versus the phytoplankton pigment composition, determining cellular spectral absorption  
593 (Morel 1978), which changes depending upon growth conditions and the phase of growth.

594 PE-rich and PC-rich *Synechococcus* sp. strains show distinct growth responses to  
595 cumulative diel photon dose, depending upon the peak PAR or PUR of the applied photoregime  
596 (Fig. 5S4, Fig. S6). Chlorophyll-specific exponential growth rates of the PE-rich and PC-rich  
597 *Synechococcus* sp. strains increased with increasing light levels, to a plateau in the range of 180  
598 – 300  $\mu\text{mol photons m}^{-2}\text{s}^{-1}$ . Growth above 600  $\mu\text{mol photons m}^{-2}\text{s}^{-1}$  occurred with a growth  
599 yield per cumulative diel photon lower than under moderate light, particularly when combined  
600 with short 8 h or long 24 h photoperiods. Even though PE-rich *Synechococcus* sp. are more  
601 adapted to lower-light conditions deeper in the water column (Stomp et al. 2007), our findings  
602 show that PE-rich strains will grow under higher irradiance, which is generally contradictory to  
603 previous literature reports (Vörös et al. 1998; Moser et al. 2009). Observations that PE-rich  
604 picocyanobacteria may be better adapted for lower light may simply be a consequence of the  
605 light quality rather than the light quantity (Hauschild et al. 1991; Pick, 1991).

606        The maximum growth rate of *Synechococcus* sp. PE-rich\_127 strain under 22°C, 24 h  
607        photoperiod and peak PAR of 180  $\mu\text{mol photons m}^{-2}\text{s}^{-1}$  was 4.5  $\text{d}^{-1}$  ( $\mu = 0.187 \text{ h}^{-1}$ ),  
608        corresponding to a doubling time of 3.7 h (Fig. 5, Fig. S4); faster than previously reported for  
609        marine picocyanobacteria, and indeed faster than for the model freshwater cyanobacteria  
610        *Synechococcus* sp. PCC6301 (doubling time of 4.5-5 h under 38°C, constant illumination, and  
611        250  $\mu\text{mol photons m}^{-2}\text{s}^{-1}$ ) (Sakamoto and Bryant 1999), or *Synechocystis* sp. PCC 6803  
612        (doubling time of 4.3 h under 30°C and 120  $\mu\text{mol photons m}^{-2}\text{s}^{-1}$ ) (van Alphen et al. 2018). The  
613        fastest growth rate as yet achieved for any phytoplankton occurs in a genetically modified green  
614        algae *Picochlorum celeri*, with a maximum of about 6.78  $\text{d}^{-1}$  and ~2.5 h doubling time (under  
615        30°C, constant illumination, and 900  $\mu\text{mol photons m}^{-2}\text{s}^{-1}$ ), ~~in bioreactors~~ (Weissman et al.  
616        2018 Krishnan et al. 2021). The Baltic *Synechococcus* sp. strains, not genetically modified,  
617        preferred 24 h photoperiod and moderate peak PAR of 180  $\mu\text{mol photons m}^{-2}\text{s}^{-1}$ , suggesting they  
618        could, potentially, thrive in warming polar latitude waters. *Synechococcus* sp. strains indeed  
619        already occur across geographical regions (Śliwińska-Wilczewska et al. 2018b) with different  
620        photic regimes, including polar regions (reviewed by Velichko et al. (2021)), exceeding latitude  
621        80°S and 80°N. The prolonged daylight hours of polar summers, coupled with nutrient-rich  
622        waters, promote growth of genetically diverse *Synechococcus* populations (Vincent et al. 2000),  
623        contributing significantly to primary productivity. Gradinger and Lenz (1989) suggested that  
624        *Synechococcus*-type picocyanobacteria may serve as indicator organisms for the advection of  
625        warm water masses into polar regions, important in the context of monitoring upcoming climate  
626        changes.

627        The coastal PC-rich and PE-rich strains of *Synechococcus* showed saturation, and then  
628        photoinhibition of growth rates under increasing cumulative diel PUR, although the achieved

estimates of  $\mu_{\max}$ , and the onset of photoinhibition of growth, varied depending upon strain, photoperiod and peak PAR (Fig. 4). The tested strains were generally opportunistic in exploiting longer photoperiods to achieve faster  $\mu$ , although PE-rich strains suffered strong photoinhibition of growth under peak PAR above 600  $\mu\text{mol photons m}^{-2}\text{s}^{-1}$  and 24 h photoperiod (Fig. 5, Fig. S4), suggesting the PE-rich strains are better adapted to lower light and deeper parts of the water column. The least favorable growth conditions for both PE-rich and PC-rich strains of *Synechococcus* sp. were under high light ( $> 600 \mu\text{mol photons m}^{-2}\text{s}^{-1}$ ) and the shortest photoperiod (8 h), even though the cumulative diel PUR dose was equivalent to conditions where the light intensity was lower, and the photoperiod was longer. Thus, these Baltic picocyanobacteria are prone to photoinhibition under both the longest, and the shortest, photoperiod regimes, with flatter light responses of growth under intermediate photoperiods. In regions and periods with a longer photoperiod, both PC-rich and PE-rich *Synechococcus* sp. could become dominant species in surface waters but could suffer under shorter photoperiods (Fig. 9).



643

644 **Fig. 9.** Latitudinal bands, equivalent summer or winter photoperiods, and picocyanobacterial growth responses. **(A)**  
 645 Latitudinal bands corresponding to tested growth photoperiods. **(B)** Tested photoperiod and peak PAR regimes used

646 for growth experiments. (C) Chlorophyll specific exponential growth rates ( $\pm$  SE falling within symbols) for two  
647 PhycoCyanin(PC)-rich cultures (056; dark green, 077; light green) and two PhycoErythrin(PE)-rich cultures (048;  
648 light red, 127; dark red) of *Synechococcus* sp. under tested photoperiod and peak PAR regimes.

649

650 **Photic regimes and growth phase both influence cellular absorbance and light**  
651 **use**

652 Cyanobacteria growth includes lag, exponential growth, stationary, and death phases  
653 (Reynolds 2006). During the lag phase, cyanobacteria acclimate to the environment and prepare  
654 for active growth by synthesizing essential cellular components. Exponential growth phase is  
655 marked by cell division and biomass accumulation, fueled by nutrient and light availability. If  
656 growth is limited by declining nutrients, by light, or by accumulation of inhibitory factors, algae  
657 enter stationary phase, characterized by a balance between cell division and death, leading to a  
658 plateau in population. The death phase occurs when cyanobacteria cell death outruns division,  
659 leading to net decomposition, contributing to nutrient recycling in aquatic ecosystems (Reynolds  
660 2006). Moreover, Schuurmans et al. (2017) proposed an additional phase between the  
661 exponential and stationary phases of picocyanobacteria growth, which is often neglected in  
662 physiological studies. Herein, we summarize the results obtained both in the exponential phase  
663 of growth and after the transition to the pre-stationary and stationary growth phases.

664 Under nutrient replete exponential growth, the picocyanobacterial strains show ~~eonsistent~~  
665 ~~patterns of~~ an exponential decline in PUR/PAR ratio versus cumulative diel photon doses, ~~across~~  
666 ~~different combinations of photoperiod and peak PAR~~. Thus, under nutrient repletion the  
667 picocyanobacteria balance pigment composition to match light conditions (Fig. 6). In addition to  
668 chlorophyll *a*, picocyanobacteria use phycobilins, including phycocyanin (harvesting red light at  
669 620 nm) and phycoerythrin (harvesting yellow light at 570 nm), as accessory pigments to

enhance light harvesting efficiency. Picocyanobacteria enhance phycobilin production to compensate for limited irradiance, thereby optimizing their photosynthetic capabilities (Śliwińska-Wilczewska et al. 2018a) and increasing their PUR/PAR. However, during the pre-stationary phase, the PE-rich strains lose these capabilities and the fact that the relative absorbance of PE peak was much lower, which would not be expected if light was more limiting (as cell density increased), suggests that nitrogen could be limiting factor at this stage.

The effective absorption cross section for photochemistry of PSII in the light ( $\sigma_{PSII}'$ ) comprises the probability of light capture by PSII and the quantum yield for subsequent photochemistry. PC-rich and PE-rich strains of *Synechococcus* again show consistent patterns of an exponential decay to a plateau with increasing cumulative diel PAR doses, for  $\sigma_{PSII}'$  ( $\text{nm}^2 \text{ quanta}^{-1}$ ), measured under diel peak PAR growth light under  $\text{Ex}_{590\text{nm}}$  (orange) excitation), without detectable influences of photoperiod, nor of peak PAR (Fig. 7A).  $\sigma_{PSII}'$  excited through chlorophyll absorbance at 445 nm was, in contrast, consistently small across strains and growth conditions (Fig. S8, Fig. S9), since in cyanobacteria the number of chlorophyll serving each PSII is nearly fixed (Xu et al. 2018).  $\sigma_{PSII}'$  excited through phycobilisome absorbance at 590 nm shows, as expected, a positive correlation with Phycobiliprotein:Chl *a*. Growth under low cumulative diel PAR results in an increased Phycobiliprotein:Chl *a*, as the picocyanobacteria allocate protein resources towards phycobiliprotein-mediated light capture (Beale 1994; Stadnichuk et al. 2015; Chakdar and Pabbi 2016). PC-rich and PE-rich strains of *Synechococcus* sp. in exponential growth nonetheless show significant scatter around this pattern, likely related to regulatory control of  $\sigma_{PSII}'$ , beyond pigment composition. In pre-stationary phase  $\sigma_{PSII}'$  vs. Phycobiliprotein:Chl *a* was better aligned, suggesting reliance upon fixed compositional

692 regulation of phycobiliprotein content to control light delivery to PSII, as opposed to shorter-  
693 term regulation.

694 **A 16S rRNA gene phylogeny** (amplicon average 1385 bp) placed the tested strains in order  
695 Synechococcales and family Synechoccaceae, within the cluster 5 picocyanobacterial lineage, in  
696 sub-cluster 5.2 together with freshwater, brackish and halotolerant strains, separated from marine  
697 sub-clusters 5.1 and 5.3 (Fig. 1S). The 16S rRNA of the strains showed ~100% identity with  
698 strains assigned to *Synechococcus* spp. or to *Cyanobium* spp. It is worth emphasizing that light  
699 capture and light absorption abilities differed significantly among tested strains (Six et al. 2021).  
700 The PE-rich strains show a much higher PUR/PAR ratio under low cumulative diel photon doses  
701 during exponential phase, but decay towards a plateau and reach a similar value to the PC-rich  
702 strains as cumulative diel photon dose increases. Thus, the PE-rich strains in exponential phase  
703 demonstrated higher ability to modulate light absorbance capacity, whereas PC-rich strains  
704 retained a more stable PUR/PAR across cumulative diel photon doses. What is more, during  
705 exponential phase, the PE-rich strains show a much higher  $\sigma_{PSII}'$  under low cumulative diel  
706 photon dose, and their  $\sigma_{PSII}'$  remains higher than the PC-rich strains, even as cumulative diel  
707 photon dose increases. Hence, PE-rich strains exhibit higher light harvesting efficiency, at the  
708 expense of susceptibility to higher light levels, particularly under the shortest (8h) and longest  
709 (24h) photoperiods.

710 *Synechococcus* exhibits remarkable acclimation within a strain to different environmental  
711 conditions (Śliwińska-Wilczewska et al. 2018a, 2020; Aguilera et al. 2023). Under high  
712 cumulative diel photon dose, *Synechococcus* employs photoprotective mechanisms to prevent the  
713 harmful effects of excess light energy. These include the dissipation of excess energy as heat via  
714 non-photochemical quenching (NPQ) and the regulation of phycobilisome antenna pigments, to

715 balance light absorption and energy transfer. In contrast, under conditions of low cumulative diel  
716 PAR dose, *Synechococcus* sp. increases the expression of light-harvesting complexes to enhance  
717 light absorption (Fig. 6) and capture (Fig. 7).

718 Available photic regimes, combining photoperiod and peak PAR, may determine the  
719 occurrences of PC-rich and PE-rich picocyanobacterial phenotypes. Nitrogen (N) is an essential  
720 element for cyanobacteria, while the N costs to produce photosynthetic pigments varies. The  
721 molecular weight of the two phycoerythrin (PE; phycoerythrobilin) subunits is about 20,000 and  
722 18,300 g mol<sup>-1</sup>, while the two phycocyanin (PC; phycocyanobilin) subunits are about 17,600 and  
723 16,300 g mol<sup>-1</sup>, and allophycocyanin (APC) is lower still, about 16,000 g mol<sup>-1</sup> (Bennett and  
724 Bogorad 1971)~~and cell-specific content of this pigment is usually low in both phenotypes~~  
725 ~~(Śliwińska-Wilezewska et al. 2020)~~. It follows that N-cost of producing PE is higher than that of  
726 PC, even though PE-rich picocyanobacteria capture light better than PC-rich phenotypes (Fig. 6;  
727 Fig. 7). Our results confirm that PE-rich strains are stronger light-harvesting competitors, while  
728 the PC-rich strains have lower N-quotients for their phycobilin light capture system.

729

### 730 **Photic regimes - implications for cumulative diel PSII electron flux**

731 Algal dynamics respond rapidly to changes in environmental conditions (Connor 2018).  
732 We used Fast Repetition Rate fluorometry (FRRf; Fig. 3) (Kolber et al. 1998) to generate an  
733 index of PSII electron transport rate per unit volume ( $JV_{PSII}$ ) (Oxborough et al. 2012; Tortell and  
734 Suggett 2021; Berman-Frank et al. 2023), calibrated to absolute rates of electron transport  
735 measured through oxygen evolution. Across different photic regimes the growth rates,  $\mu$ , of PC-  
736 rich and PE-rich picocyanobacteria show fairly consistent saturating responses to increasing  
737 cumulative diel PSII electron flux ( $JV_{PSII}$ ;  $\mu\text{mol e}^- \mu\text{mol Chl } a^{-1} d^{-1}$ ; Fig. 8). As previously found

738 for diatoms (Li et al. 2017) cumulative diel reductant generation was indeed a better predictor of  
739  $\mu$  than was cumulative diel PUR, although photoperiod and peak PAR retain secondary  
740 influences on achieved growth responses of the picocyanobacteria under some conditions.

741

742 **Conclusions**

743 Coastal picocyanobacteria show different growth responses to photoperiod and light level,  
744 even under combinations giving equivalent cumulative diel PUR. Both PE-rich and PC-rich  
745 strains of *Synechococcus* sp., grew fastest under moderate light and a 24 h photoperiod.  
746 Consequently, these coastal strains from *Synechococcus* cluster 5.2 show potential to emerge as  
747 components of the phytoplankton during the Arctic or Antarctic summer under future, warmed,  
748 polar regions. In optimal conditions (24 h of photoperiod, a peak PAR of 180  $\mu\text{mol}$  photons  
749  $\text{m}^{-2}\text{s}^{-1}$ , and only 22°C), one of the PE-rich *Synechococcus* sp., reached a chlorophyll-specific  
750 exponential growth rate of 4.5  $\text{d}^{-1}$  (3.7 h doubling time), a record for a cyanobacteria. PE-rich  
751 strains in the exponential phase of growth also demonstrated high ability to modulate their  
752 PUR/PAR ratio by adjusting pigment composition, giving an advantage in the competition for  
753 light. However, based on the present study it would seem that PE-rich strains are more  
754 susceptible to photoinhibition. We determined that growth yields of PC-rich and PE-rich  
755 picocyanobacteria are well predicted by cumulative diel PSII electron fluxes, across different  
756 photic regimes. PE-rich phenotypes of picocyanobacteria currently predominate in abundance  
757 and genetic diversity in the Baltic Sea (Aguilera et al. 2023). This dominance may be the result  
758 of eutrophication in the Baltic Sea, providing higher nitrogen for phycobiliprotein synthesis, and  
759 leading to lower light even in near-surface waters. Our results suggest possible expansion of the  
760 range of picocyanobacteria to new photic regimes in a warmed future and indicate that PE-rich

761 *Synechococcus* sp. may be a dominant component of picophytoplankton in nutrient-rich  
762 environments.

763

764 **Additional Supporting Information may be found in the online version of this article.**

765

766 **Authors Contribution Statement:** S.S-W. designed the study with input from D.A.C. M.K.  
767 estimated the transition point between exponential and pre-stationary phase of growth. M.S.  
768 ensured the proper operation of the photobioreactors. A.A. conducted genetic analysis. N.M.O.  
769 solved technical problems related to computer operation and software. S.S-W., M.S., N.M.O.,  
770 D.A.C. contributed to R coding and data analysis. S.S-W. conducted the experiments, created  
771 plots and wrote the manuscript, with support from D.A.C. All authors contributed to the  
772 discussion of the results, supported manuscript preparation, and approved the final submitted  
773 manuscript.

774

775 ***Data availability statement***

776 Data supporting this study is available on:

777 <https://github.com/FundyPhytoPhys/BalticPhotoperiod> (public GitHub Repository) and

778 <https://docs.google.com/spreadsheets/d/1ZXpwR7Gfto->

779 [uRzVdXzMpQF4frbrvMLH\\_IyLqonFZRSw/edit#gid=0](#) (URL for MetaDataCatalog).

780 Code to perform data processing and analyses is available at

781 <https://github.com/FundyPhytoPhys/BalticPhotoperiod>.

782 16S rRNA sequences used in this study are available in GenBank under the accession  
783 numbers PP034393, PP034394, PP034396 and PP034403.

784

785 **Acknowledgements**

786 We would like to express our sincere gratitude to the two Editors, Ilana Berman-Frank and Elisa  
787 Schaum, and two Reviewers for their efforts reviewing and improving this manuscript. We thank  
788 Maximilian Berthold for the code for the GAM model; Miranda Corkum who maintained  
789 cultures and trained personnel in culture handling; Laurel Genge, and Carlie Barnhill (Mount  
790 Allison students) who assisted with R code. This work was supported by Canada Research Chair  
791 in Phytoplankton Ecophysiology (D.A.C) and Latitude & Light; NSERC of Canada Discovery  
792 Grant (D.A.C).

793

794 **Conflict of Interest**

795 None declared.

796

797 **References**

- 798 Aguilera, A., J. Alegria Zufia, L. Bas Conn, and others. 2023. Ecophysiological analysis reveals  
799 distinct environmental preferences in closely related Baltic Sea picocyanobacteria.  
800 Environmental Microbiology **25**: 1674–1695. doi:10.1111/1462-2920.16384
- 801 Arrigo, K. R. 2014. Sea ice ecosystems. Annual Review of Marine Science **6**: 439–467.  
802 doi:10.1146/annurev-marine-010213-135103
- 803 Beale, S. I. 1994. Biosynthesis of cyanobacterial tetrapyrrole pigments: Hemes, chlorophylls,  
804 and phycobilins, p. 519–558. In D.A. Bryant [ed.], The Molecular Biology of Cyanobacteria.  
805 Springer Netherlands.

- 806 Behrenfeld, M. J., R. T. O'Malley, D. A. Siegel, and others. 2006. Climate-driven trends in  
807 contemporary ocean productivity. *Nature* **444**: 752–755. doi:10.1038/nature05317
- 808 Bennett, A., and L. Bogorad. 1971. Properties of subunits and aggregates of blue-green algal  
809 biliproteins. *Biochemistry* **10**: 3625–3634. doi:10.1021/bi00795a022
- 810 Bennett, A., and L. Bogorad. 1973. Complementary Chromatic Adaptation in a filamentous blue-  
811 green alga. *Journal of Cell Biology* **58**: 419–435. doi:10.1083/jcb.58.2.419
- 812 Berman-Frank, I., D. Campbell, A. Ciotti, and others. 2023. Application of Single Turnover  
813 Active Chlorophyll Fluorescence for Phytoplankton Productivity Measurements. Version 2.0,  
814 June, 26, 2023. Report Scientific Committee on Oceanic Research (SCOR) Working Group 156.
- 815 Boatman, T. G., R. J. Geider, and K. Oxborough. 2019. Improving the accuracy of Single  
816 Turnover Active Fluorometry (STAF) for the estimation of Phytoplankton Primary Productivity  
817 (PhytoPP). *Frontiers in Marine Science* **6**. doi:10.3389/fmars.2019.00319
- 818 Brand, L. E., and R. R. L. Guillard. 1981. The effects of continuous light and light intensity on  
819 the reproduction rates of twenty-two species of marine phytoplankton. *Journal of Experimental  
820 Marine Biology and Ecology* **50**: 119–132. doi:10.1016/0022-0981(81)90045-9
- 821 Chakdar, H., and S. Pabbi. 2016. Cyanobacterial phycobilins: Production, purification, and  
822 regulation, p. 45–69. In P. Shukla [ed.], *Frontier Discoveries and Innovations in Interdisciplinary  
823 Microbiology*. Springer India.
- 824 Christaki, U., S. Jacquet, J. R. Dolan, D. Vaulot, and F. Rassoulzadegan. 1999. Growth and  
825 grazing on *Prochlorococcus* and *Synechococcus* by two marine ciliates. *Limnology and  
826 Oceanography* **44**: 52–61. doi:10.4319/lo.1999.44.1.0052

- 827 Connor, D. 2018. Investigating the use of fast repetition rate fluorometry in understanding algal  
828 physiology in optically complex oceans.
- 829 Elzhov, T. V., K. M. Mullen, A.-N. Spiess, and B. Bolker. 2023. Minpack.lm: R Interface to the  
830 Levenberg-Marquardt Nonlinear Least-Squares Algorithm Found in MINPACK, Plus Support  
831 for Bounds.
- 832 Erga, S. R., and B. R. Heimdal. 1984. Ecological studies on the phytoplankton of Korsfjorden,  
833 western Norway. The dynamics of a spring bloom seen in relation to hydrographical conditions  
834 and light regime. *Journal of Plankton Research* **6**: 67–90. doi:10.1093/plankt/6.1.67
- 835 Falkowski, P., and Z. Kolber. 1993. Estimation of phytoplankton photosynthesis by active  
836 fluorescence. *ICES Marine Science Symposium* **197**: 92–103.
- 837 Field, C. B., M. J. Behrenfeld, J. T. Randerson, and P. Falkowski. 1998. Primary production of  
838 the biosphere: Integrating terrestrial and oceanic components. *Science* **281**: 237–240.  
839 doi:10.1126/science.281.5374.237
- 840 Flombaum, P., J. L. Gallegos, R. A. Gordillo, and others. 2013. Present and future global  
841 distributions of the marine Cyanobacteria *Prochlorococcus* and *Synechococcus*. *Proceedings of*  
842 *the National Academy of Sciences* **110**: 9824–9829. doi:10.1073/pnas.1307701110
- 843 Gradinger, R., and J. Lenz. 1989. Picocyanobacteria in the high Arctic. *Marine Ecology Progress Series*  
844 **52**: 99–101. doi:10.3354/meps052099
- 845 Guillard, R. R. L. 1975. Culture of phytoplankton for feeding marine invertebrates, p. 29–60. *In*  
846 W.L. Smith and M.H. Chanley [eds.], *Culture of Marine Invertebrate Animals: Proceedings —*  
847 *1st Conference on Culture of Marine Invertebrate Animals* Greenport. Springer US.

- 848 Handel, A. 2020. Andreas Handel - Custom Word formatting using R Markdown.
- 849 Harrison, W. G., and T. Platt. 1986. Photosynthesis-irradiance relationships in polar and  
850 temperate phytoplankton populations. *Polar biology* **5**: 153–164.
- 851 Haverkamp, T. H. A., D. Schouten, M. Doeleman, U. Wollenzien, J. Huisman, and L. J. Stal.  
852 2009. Colorful microdiversity of *Synechococcus* strains (picocyanobacteria) isolated from the  
853 Baltic Sea. *The ISME Journal* **3**: 397–408. doi:10.1038/ismej.2008.118
- 854 Hirata, T., N. J. Hardman-Mountford, R. J. W. Brewin, and others. 2011. Synoptic relationships  
855 between surface Chlorophyll-*a* and diagnostic pigments specific to phytoplankton functional  
856 types. *Biogeosciences* **8**: 311–327. doi:10.5194/bg-8-311-2011
- 857 Hoang, D. T., O. Chernomor, A. von Haeseler, B. Q. Minh, and L. S. Vinh. 2018. UFBoot2:  
858 Improving the Ultrafast Bootstrap Approximation. *Molecular Biology and Evolution* **35**: 518–  
859 522. doi:10.1093/molbev/msx281
- 860 Holtrop, T., J. Huisman, M. Stomp, and others. 2021. Vibrational modes of water predict spectral  
861 niches for photosynthesis in lakes and oceans. *Nature Ecology & Evolution* **5**: 55–66.  
862 doi:10.1038/s41559-020-01330-x
- 863 Huisman, J., M. Arrayás, U. Ebert, and B. Sommeijer. 2002. How do sinking phytoplankton  
864 species manage to persist? *The American Naturalist* **159**: 245–254. doi:10.1086/338511
- 865 Jacob-Lopes, E., C. H. G. Scoparo, L. M. C. F. Lacerda, and T. T. Franco. 2009. Effect of light  
866 cycles (night/day) on CO<sub>2</sub> fixation and biomass production by microalgae in photobioreactors.  
867 *Chemical Engineering and Processing: Process Intensification* **48**: 306–310.  
868 doi:10.1016/j.cep.2008.04.007

- 869 Jávorfi, T., J. Erostyák, J. Gál, A. Buzády, L. Menczel, G. Garab, and K. Razi Naqvi. 2006.
- 870 Quantitative spectrophotometry using integrating cavities. *Journal of Photochemistry and*
- 871 *Photobiology B: Biology* **82**: 127–131. doi:10.1016/j.jphotobiol.2005.10.002
- 872 Kalyaanamoorthy, S., B. Q. Minh, T. K. F. Wong, A. von Haeseler, and L. S. Jermiin. 2017.
- 873 ModelFinder: Fast model selection for accurate phylogenetic estimates. *Nature Methods* **14**:
- 874 587–589. doi:10.1038/nmeth.4285
- 875 Katoh, K., J. Rozewicki, and K. D. Yamada. 2019. MAFFT online service: Multiple sequence
- 876 alignment, interactive sequence choice and visualization. *Briefings in Bioinformatics* **20**: 1160–
- 877 1166. doi:10.1093/bib/bbx108
- 878 Klepacz-Smólka, A., D. Pietrzyk, R. Szeląg, P. Głuszcza, M. Daroch, J. Tang, and S. Ledakowicz.
- 879 2020. Effect of light colour and photoperiod on biomass growth and phycocyanin production by
- 880 *Synechococcus* PCC 6715. *Bioresource Technology* **313**: 123700.
- 881 doi:10.1016/j.biortech.2020.123700
- 882 Kolber, Z. S., O. Prášil, and P. G. Falkowski. 1998. Measurements of variable chlorophyll
- 883 fluorescence using fast repetition rate techniques: Defining methodology and experimental
- 884 protocols. *Biochimica et Biophysica Acta (BBA) - Bioenergetics* **1367**: 88–106.
- 885 doi:10.1016/S0005-2728(98)00135-2
- 886 Krishnan, A., M. Likhogrud, M. Cano, and others. 2021. *Picochlorum Celeri* as a model system
- 887 for robust outdoor algal growth in seawater. *Scientific Reports* **11**: 11649. doi:10.1038/s41598-
- 888 021-91106-5

- 889 Lane, D. J. 1991. 16S/23S rRNA sequencing. Nucleic acid techniques in bacterial systematics  
890 115–175.
- 891 LaRoche, J., and B. M. Robicheau. 2022. The Pelagic Light-Dependent Microbiome, p. 395–  
892 423. In L.J. Stal and M.S. Cretoiu [eds.], *The Marine Microbiome*. Springer International  
893 Publishing.
- 894 Li, G., D. Talmy, and D. A. Campbell. 2017. Diatom growth responses to photoperiod and light  
895 are predictable from diel reductant generation. *Journal of Phycology* **53**: 95–107.  
896 doi:10.1111/jpy.12483
- 897 Li, Q., L. Legendre, and N. Jiao. 2015. Phytoplankton responses to nitrogen and iron limitation  
898 in the tropical and subtropical Pacific Ocean. *Journal of Plankton Research* **37**: 306–319.  
899 doi:10.1093/plankt/fbv008
- 900 Li, W. K. W. 1995. Composition of ultraphytoplankton in the central North Atlantic. *Marine  
901 Ecology Progress Series* **122**: 1–8.
- 902 Ligges, U., T. Short, P. Kienzle, and others. 2024. Signal: Signal Processing.
- 903 Litchman, E., C. A. Klausmeier, and K. Yoshiyama. 2009. Contrasting size evolution in marine  
904 and freshwater diatoms. *Proceedings of the National Academy of Sciences* **106**: 2665–2670.  
905 doi:10.1073/pnas.0810891106
- 906 Longobardi, L., L. Dubroca, F. Margiotta, D. Sarno, and A. Zingone. 2022. Photoperiod-driven  
907 rhythms reveal multi-decadal stability of phytoplankton communities in a highly fluctuating  
908 coastal environment. *Scientific Reports* **12**: 3908. doi:10.1038/s41598-022-07009-6

- 909 MacIntyre, H. L., T. M. Kana, R. J. Geider, H. L. MacIntyre, T. M. Kana, and R. J. Geider. 2000.  
910 The effect of water motion on short-term rates of photosynthesis by marine phytoplankton.  
911 Trends in Plant Science **5**: 12–17. doi:10.1016/S1360-1385(99)01504-6
- 912 Moejes, F. W., A. Matuszyńska, K. Adhikari, and others. 2017. A systems-wide understanding  
913 of photosynthetic acclimation in algae and higher plants. Journal of Experimental Botany **68**:  
914 2667–2681. doi:10.1093/jxb/erx137
- 915 Morel, A. 1978. Available, usable, and stored radiant energy in relation to marine  
916 photosynthesis. Deep Sea Research **25**: 673–688. doi:10.1016/0146-6291(78)90623-9
- 917 Morel, A. 1988. Optical modeling of the upper ocean in relation to its biogenous matter content  
918 (case I waters). Journal of Geophysical Research: Oceans **93**: 10749–10768.  
919 doi:10.1029/JC093iC09p10749
- 920 Oxborough, K., and N. R. Baker. 1997. Resolving chlorophyll *a* fluorescence images of  
921 photosynthetic efficiency into photochemical and non-photochemical components – calculation  
922 of qP and Fv-/Fm-; without measuring Fo-; Photosynthesis Research **54**: 135–142.  
923 doi:10.1023/A:1005936823310
- 924 Oxborough, K., C. M. Moore, D. J. Suggett, T. Lawson, H. G. Chan, and R. J. Geider. 2012.  
925 Direct estimation of functional PSII reaction center concentration and PSII electron flux on a  
926 volume basis: A new approach to the analysis of Fast Repetition Rate fluorometry (FRRf) data.  
927 Limnology and Oceanography: Methods **10**: 142–154. doi:10.4319/lom.2012.10.142
- 928 Pedersen, T. L. 2024. Patchwork: The Composer of Plots.

- 929 Pick, F. R. 1991. The abundance and composition of freshwater picocyanobacteria in relation to  
930 light penetration. Limnology and Oceanography **36**: 1457–1462. doi:10.4319/lo.1991.36.7.1457
- 931 Posit team. 2022. RStudio: Integrated development environment for r, Posit Software, PBC.
- 932 R Core Team. 2023. R: A language and environment for statistical computing, R Foundation for  
933 Statistical Computing.
- 934 Reynolds, C. S. 2006. The Ecology of Phytoplankton, Cambridge University Press.
- 935 Ryan, J. A., J. M. Ulrich, R. Bennett, and C. Joy. 2024. Xts: eXtensible Time Series.
- 936 Sakamoto, T., and D. A. Bryant. 1999. Nitrate transport and not photoinhibition limits growth of  
937 the freshwater cyanobacterium *Synechococcus* species PCC 6301 at low temperature. Plant  
938 Physiology **119**: 785–794. doi:10.1104/pp.119.2.785
- 939 Schuurmans, R. M., J. C. P. Matthijs, and K. J. Hellingwerf. 2017. Transition from exponential  
940 to linear photoautotrophic growth changes the physiology of *Synechocystis* sp. PCC 6803.  
Photosynthesis Research **132**: 69–82. doi:10.1007/s11120-016-0329-8
- 942 Serway, R. A., C. J. Moses, and C. A. Moyer. 2004. Modern Physics, Cengage Learning.
- 943 Six, C., Z. V. Finkel, A. J. Irwin, and D. A. Campbell. 2007. Light variability illuminates niche-  
944 partitioning among marine picocyanobacteria. PLOS ONE **2**: e1341.  
doi:10.1371/journal.pone.0001341
- 946 Six, C., M. Ratin, D. Marie, and E. Corre. 2021. Marine *Synechococcus* picocyanobacteria: Light  
947 utilization across latitudes. Proceedings of the National Academy of Sciences **118**: e2111300118.  
doi:10.1073/pnas.2111300118

- 949 Śliwińska-Wilczewska, S., A. Cieszyńska, J. Maculewicz, and A. Latała. 2018a.  
950 Ecophysiological characteristics of red, green, and brown strains of the Baltic  
951 picocyanobacterium *Synechococcus* sp. – a laboratory study. Biogeosciences **15**: 6257–6276.  
952 doi:10.5194/bg-15-6257-2018
- 953 Śliwińska-Wilczewska, S., Z. Konarzewska, K. Wiśniewska, and M. Konik. 2020.  
954 Photosynthetic pigments changes of three phenotypes of picocyanobacteria *Synechococcus* sp.  
955 Under different light and temperature conditions. Cells **9**: 2030. doi:10.3390/cells9092030
- 956 Śliwińska-Wilczewska, S., J. Maculewicz, A. Barreiro Felpeto, and A. Latała. 2018b.  
957 Allelopathic and bloom-forming picocyanobacteria in a changing world. Toxins **10**: 48.  
958 doi:10.3390/toxins10010048
- 959 Stadnichuk, I. N., P. M. Krasilnikov, and D. V. Zlenko. 2015. Cyanobacterial phycobilisomes  
960 and phycobiliproteins. Microbiology **84**: 101–111. doi:10.1134/S0026261715020150
- 961 Stomp, M., J. Huisman, L. Vörös, F. R. Pick, M. Laamanen, T. Haverkamp, and L. J. Stal. 2007.  
962 Colourful coexistence of red and green picocyanobacteria in lakes and seas. Ecology Letters **10**:  
963 290–298. doi:10.1111/j.1461-0248.2007.01026.x
- 964 Strickland, J. D., and T. R. Parsons. 1972. Practical Hand Book of Seawater Analysis. Fisheries  
965 Research Board of Canada **167 (2nd edition)**: 1–311. doi:DOI: <http://dx.doi.org/10.25607/OPB-1791>
- 966
- 967 Theus, M. E., T. J. Layden, N. McWilliams, S. Crafton-Tempel, C. T. Kremer, and S. B. Fey.  
968 2022. Photoperiod influences the shape and scaling of freshwater phytoplankton responses to  
969 light and temperature. Oikos **2022**: e08839. doi:10.1111/oik.08839

- 970 Torremorell, A., M. E. Llames, G. L. Pérez, R. Escaray, J. Bustingorry, and H. Zagarese. 2009.
- 971 Annual patterns of phytoplankton density and primary production in a large, shallow lake: The  
972 central role of light. *Freshwater Biology* **54**: 437–449. doi:10.1111/j.1365-2427.2008.02119.x
- 973 Tortell, P., and D. J. Suggett. 2021. A user guide for the application of Single Turnover active  
974 chlorophyll fluorescence for phytoplankton productivity measurements. Version 1. Report  
975 Scientific Committee on Oceanic Research (SCOR) Working Group 156.
- 976 van Alphen, P., H. Abedini Najafabadi, F. Branco dos Santos, and K. J. Hellingwerf. 2018.  
977 Increasing the photoautotrophic growth rate of *Synechocystis* sp. PCC 6803 by identifying the  
978 limitations of its cultivation. *Biotechnology Journal* **13**: 1700764. doi:10.1002/biot.201700764
- 979 Velichko, N., S. Smirnova, S. Averina, and A. Pinevich. 2021. A survey of Antarctic  
980 cyanobacteria. *Hydrobiologia* **848**: 2627–2653.
- 981 Vincent, W. F., J. P. Bowman, L. M. Rankin, and T. A. McMeekin. 2000. Phylogenetic diversity  
982 of picocyanobacteria in Arctic and Antarctic ecosystems. *Microbial biosystems: new frontiers.*  
983 Proceedings of the 8th International Symposium on Microbial Ecology 317–322.
- 984 Wickham, H. 2016. Data Analysis, p. 189–201. In H. Wickham [ed.], *Ggplot2: Elegant Graphics*  
985 for Data Analysis. Springer International Publishing.
- 986 Wood, S. N. 2017. Generalized Additive Models: An Introduction with R, Second Edition, 2nd  
987 ed. Chapman and Hall/CRC.
- 988 Xi, H., S. N. Losa, A. Mangin, and others. 2020. Global retrieval of phytoplankton functional  
989 types based on empirical orthogonal functions using CMEMS GlobColour merged products and

990 further extension to OLCI data. *Remote Sensing of Environment* **240**: 111704.  
991 doi:10.1016/j.rse.2020.111704

992 Xu, K., J. L. Grant-Burt, N. Donaher, and D. A. Campbell. 2017. Connectivity among  
993 Photosystem II centers in phytoplankters: Patterns and responses. *Biochimica et Biophysica Acta*  
994 (*BBA*) - *Bioenergetics* **1858**: 459–474. doi:10.1016/j.bbabi.2017.03.003

995 Xu, K., J. Lavaud, R. Perkins, E. Austen, M. Bonnanfant, and D. A. Campbell. 2018.  
996 Phytoplankton  $\sigma$ PSII and excitation dissipation; implications for estimates of primary  
997 productivity. *Frontiers in Marine Science* **5**. doi:10.3389/fmars.2018.00281

1   **Long & low; or short & high; photoperiods and light**  
2   **differentially influence growth and potential niches of**  
3   **PhycoCyanin and PhycoErythrin-rich picocyanobacteria**

4

5   **Sylwia Śliwińska-Wilczewska<sup>1,2</sup>, Marta Konik<sup>3,4</sup>, Mireille Savoie<sup>1</sup>, Anabella**  
6   **Aguilera<sup>5,6</sup>, Naaman M. Omar<sup>1</sup>, and Douglas A. Campbell<sup>1,✉</sup>**

7

8   <sup>1</sup> Department of Biology, Mount Allison University, 53 York St., Sackville, NB, E4L 1C9,  
9   Canada

10   <sup>2</sup> Institute of Oceanography, University of Gdańsk, 46 Piłsudskiego St, 81-378, Gdynia, Poland

11   <sup>3</sup> Department of Geography, University of Victoria, Victoria, BC, V8P 5C2, Canada

12   <sup>4</sup> Institute of Oceanology, Polish Academy of Sciences, 81-712 Sopot, Poland

13   <sup>5</sup> Department of Biology and Environmental Science, Centre for Ecology and Evolution in  
14   Microbial Model Systems (EEMiS), Linnaeus University, Kalmar, Sweden

15   <sup>6</sup> Department of Aquatic Sciences and Assessment, Swedish University of Agricultural Sciences,  
16   Uppsala, Sweden (present address)

17   ✉ Correspondence: Douglas A. Campbell; dubhglas.cambeuil@gmail.com

18

19   **Running head:** *Picocyanobacteria across photic regimes*

20   **Keywords:** Cumulative diel photon dose; Light-capture, PAR; Photic regime; Phase of growth;  
21   Photoperiod; Picocyanobacteria; PUR

## 22     **Abstract**

23       Strains from the picocyanobacteria genus *Synechococcus* are currently found across a wide  
24       range of photoperiods and photosynthetically active radiation. Future scenarios now forecast  
25       range expansions of marine *Synechococcus* into new photic regimes. We found that temperate  
26       coastal PhycoCyanin(PC)-rich and PhycoErythrin(PE)-rich *Synechococcus* strains grew fastest  
27       under moderate photosynthetically active radiation, and a 24-hour photoperiod, despite a  
28       cumulative diel photon dose equivalent to conditions where growth was slower, under higher  
29       light and shorter photoperiods. Under optimal conditions, a PE-rich *Synechococcus* sp. achieved  
30       a highest recorded cyanobacterial chlorophyll-specific exponential growth rate ( $\mu$ ) of  $4.5\text{ d}^{-1}$ .  
31       Two PE-rich strains demonstrated wider ability to modulate light capture capacity, whereas the  
32       two PC-rich strains showed less change in light capture across increasing cumulative diel photon  
33       dose. We found that all four coastal strains showed consistent patterns of an exponential decay of  
34       effective absorption cross section for PSII photochemistry, versus increasing cumulative diel  
35       PAR doses, although this pattern damped out under stationary phase. Within each strain,  $\mu$   
36       showed saturating responses to increasing cumulative diel PSII electron flux. As photoperiod  
37       opportunists, coastal picocyanobacteria show potential to expand into longer photic regimes as  
38       higher latitudes warm.

39

## 40     **Introduction**

41       The photic regime, comprised of Photosynthetically Active Radiation (PAR), spectral  
42       quality, and photoperiod, is a pivotal influence on the growth and productivity of phytoplankton  
43       within aquatic ecosystems. PAR refers to the spectral range of solar radiation, approximately  
44       400-700 nm, that is capable of driving photosynthesis. The availability and distribution of PAR

45 in aquatic ecosystems is influenced by cloud cover, water depth, and light attenuation due to  
46 water turbidity and suspended particles, including a feedback loop whereby phytoplankton cells  
47 themselves contribute to light attenuation (Field et al. 1998; Torremorell et al. 2009).

48 Photosynthetically Usable Radiation (PUR), is, in turn, the fraction of PAR that can be absorbed  
49 for photosynthesis by pigments of given cyanobacteria or algae (Morel 1978). PUR thus depends  
50 upon the interaction of PAR, and the phytoplankton expression of genomic capacities for light  
51 capture under a given condition (Moejes et al. 2017). Cyanobacteria and algae also respond to  
52 changes in photoperiod, which serves as a key environmental cue for photosynthesis, growth,  
53 reproduction, and nutrient assimilation (LaRoche and Robicheau 2022). Thus, in polar regions,  
54 prolonged periods of wintertime darkness place a primary limitation on phytoplankton biomass  
55 production, while extended daylight during summer boosts photosynthetic activity (Arrigo  
56 2014). In temperate regions, seasonal variation in light-limitation is less pronounced, but  
57 phytoplankton are still influenced by daily and seasonal fluctuations, with a contrast between  
58 more favorable conditions for their growth in spring and summer, compared to fall and winter  
59 (Huisman et al. 2002; Holtrop et al. 2021). In the tropics, daylight hours remain nearly constant  
60 throughout the year (Behrenfeld et al. 2006), and phytoplankton productivity is primarily  
61 controlled by nutrients resupplied into the euphotic zone (Li et al. 2015), and mortality through  
62 viral lysis (Ortmann et al. 2002) or zooplankton grazing (Christaki et al. 1999).

63 The picocyanobacterial genus *Synechococcus*, one of the most abundant phytoplankton  
64 primary producer in oceans, comprises a diversity of strains of differing pigmentations  
65 (Śliwińska-Wilczewska et al. 2018a; b). *Synechococcus* collectively exhibits a distribution  
66 spanning diverse geographical regions (Flombaum et al. 2013), with strains demonstrating a  
67 remarkable range of adaptations to environmental conditions (Śliwińska-Wilczewska et al.

68 2018a; Aguilera et al. 2023). *Synechococcus* capacities to thrive across diverse marine and  
69 freshwater habitats positions it as a pivotal agent in energy and nutrient transfer within food  
70 webs, connecting the microbial loop with higher trophic levels, offering direct sustenance to  
71 grazers, including zooplankton and small fish (Li 1995). As one of the two dominant  
72 picocyanobacterial genera in oceanic waters, *Synechococcus* contribute significantly to light  
73 attenuation and light availability for other photosynthetic marine organisms, thereby influencing  
74 ocean colour and allowing satellite detection of *Synechococcus*-rich communities (Xi et al.  
75 2020). General relations among optical absorption spectra and pigment compositions have been  
76 used to determine diagnostic pigment indices of major phytoplankton functional types (Hirata et  
77 al. 2011). Modeling suggests that *Synechococcus* abundance and ranges will increase due to  
78 climate warming (Flombaum et al. 2013). The projected changes may vary geographically and  
79 may include shifts in the spatial distribution of the main picocyanobacteria, as well as changes in  
80 the proportions among *Synechococcus* sp. lineages (Six et al. 2021), potentially pushing lineages  
81 into new photic regimes. *Synechococcus* exhibits significant phenotypic diversity across  
82 lineages, encompassing strains rich in phycobiliprotein pigments, phycoerythrin (PE-rich) or  
83 phycocyanin (PC-rich) (Haverkamp et al. 2009; Aguilera et al. 2023). Phycobiliprotein pigments  
84 are pivotal for light absorption during photosynthesis and confer distinctive colours to the  
85 picocyanobacteria (Stomp et al. 2007). The disparate light preferences between PC-rich and PE-  
86 rich *Synechococcus* sp. strains influence their ecological niches. PC-rich strains thrive in surface  
87 waters and coastal regions. PE-rich strains exhibit adaptation to lower-light conditions, primarily  
88 inhabiting the deeper layers of the water column. PC-rich and PE-rich *Synechococcus* sp. strains  
89 thus predominantly occupy complementary habitats (Six et al. 2007; Haverkamp et al. 2009; Six  
90 et al. 2021), although differential responses of *Synechococcus* lineages to photoperiod, have not

91 been studied in detail, except for thermophilic PC-rich *Synechococcus* PCC 6715 (Klepacz-  
92 Smółka et al. 2020).

93 Picocyanobacteria are the most abundant phytoplankters in aquatic ecosystems and are  
94 crucial to the optical properties of ocean water, by influencing its colour and transparency. PC-  
95 rich and PE-rich *Synechococcus* sp. may have different costs and physiological strategies for  
96 growth under different photic regimes, which could drive spatial and temporal variability of  
97 picocyanobacteria biomass and community composition, in current and potential future aquatic  
98 habitats. Therefore, our aim was to determine whether photoperiod and light differentially affect  
99 growth and light-capture, between representative PC-rich and PE-rich *Synechococcus* sp. This  
100 study emphasizes the potential importance of photoperiod as a factor influencing poleward  
101 expansions of marine picocyanobacteria in the face of climate change.

102

## 103 **Materials and Methods**

### 104 **Experimental setup**

105 Two xenic PhycoCyanin(PC)-rich (CCBA\_056 or CCBA\_077) strains and two  
106 PhycoErythrin(PE)-rich (CCBA\_048 or CCBA\_127) strains of *Synechococcus* were obtained  
107 from the Culture Collection of Baltic Algae (CCBA; <https://ccba.ug.edu.pl/pages/en/home.php>).  
108 The phylogenetic placement of CCBA strains (Fig. S1 in Supporting Information) within cluster  
109 5 picocyanobacteria was explored by amplifying and sequencing a fragment of the 16S rRNA  
110 gene using universal primers 27F and 1492R (Lane 1991). 16S rRNA gene sequences were  
111 aligned with MAFFT v. 7.5 using the G-INS-I algorithm (Katoh et al. 2019).

112 Picocyanobacteria strains were maintained in Tissue Culture Flasks (VWR International,  
113 Cat. No. 10062-872, PA, USA) and were transferred to fresh f/2 media (Guillard 1975) at

114 salinity of 8 PSU (which corresponds to their natural habitat) every two weeks, under a  
115 photoperiod of 12 h and Photosynthetically Active Radiation (PAR) of  $10 \mu\text{mol photons m}^{-2}\text{s}^{-1}$   
116 supplied from cool white fluorescent tubes, at  $22^\circ\text{C}$ .

117 Experimental cultures of each strain were grown in  $8 \times 80 \text{ mL}$  round bottom cylindrical  
118 glass tubes in a Multi-Cultivator MC 1000-OD (Photon Systems Instruments, Drásov, Czech  
119 Republic). Each culture tube contained  $75 \text{ mL}$  of f/2 medium inoculated with  $5 \text{ mL}$  of growing  
120 pre-culture, to achieve exponential growth from the beginning of the experiment, with little to no  
121 lag phase upon inoculation. Culture tubes were inoculated in the afternoon while the  
122 photoregime of a sinuisoidal photoperiod commenced the following morning such that peak PAR  
123 occurred at noon each day.

124 Cultures grew at  $22^\circ\text{C}$ , with photoperiods of 8, 12, 16, or 24 h, with peak PAR of 30, 90,  
125  $180$ ,  $300$ ,  $600$ , or  $900 \mu\text{mol photons m}^{-2}\text{s}^{-1}$  independently supplied to each culture tube from  
126 white LED lamps. To approximate diel cycles, the photoperiods of 8 – 16 h were applied in a  
127 sinuisoidal shape, while the 24-hour photoperiod was applied continuously. The area under the  
128 sinuisoidal curve is  $1/2$  the area under a rectangle of equal 24-hour width, therefore at equivalent  
129 peak PAR the 24 h square photoperiod cultures received 4 times the diel photon doses of the 12 h  
130 sinuisoidal photoperiod cultures.

131 Culture tubes were closed with a silicone inert silicone stopper perforated by an aeration  
132 input tube extending to the bottom of the culture tube, and a pressure outlet tube. Aeration with a  
133 total air flow rate of around  $\sim 140 \text{ mL min}^{-1} \text{ tube}^{-1}$  through a  $0.2 \mu\text{m}$  filter ensured mixing and  
134 provided air and  $\text{CO}_2$  to cultures through the entire culture volume. The pH showed little  
135 fluctuation and remained between  $\sim 8 – 9$ . Light, temperature, optical density, and aeration gas of

136 the Multi-Cultivator system were monitored and controlled via the Photobioreactor Control  
137 Software (Photon Systems Instruments, Drásov, Czech Republic).

138

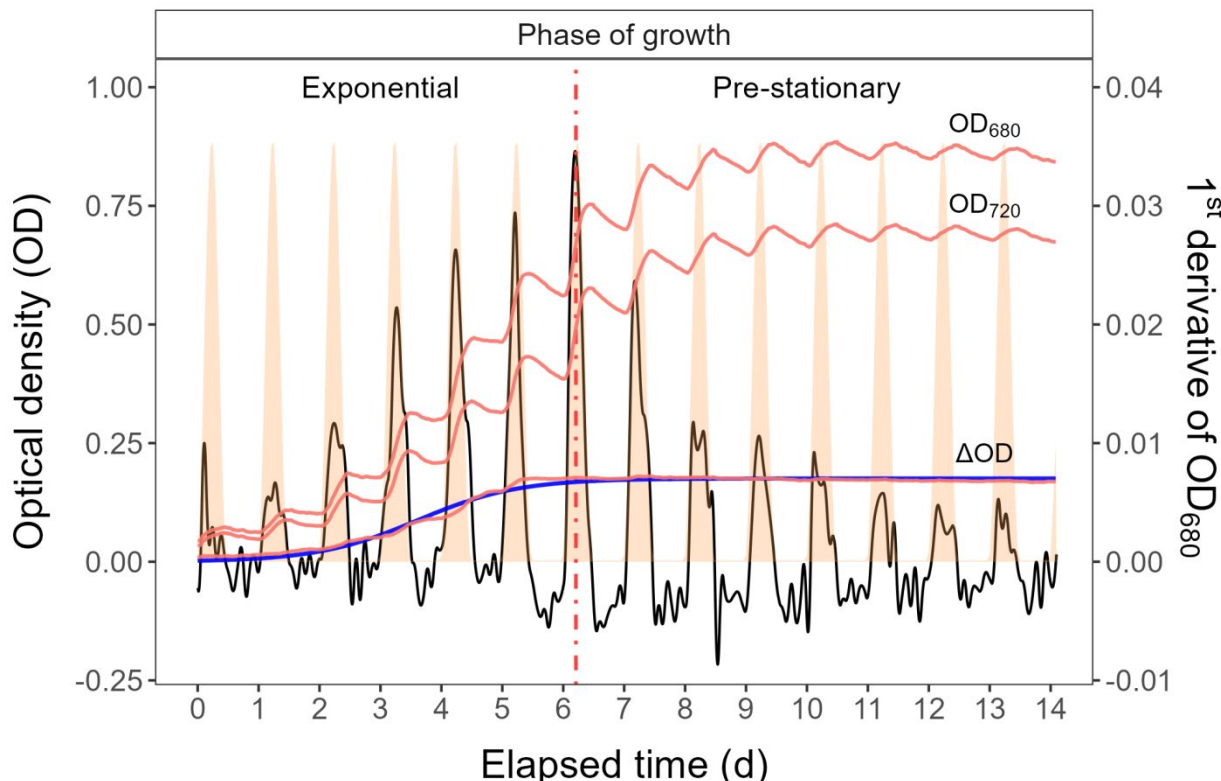
### 139 **Growth curves and chlorophyll-specific exponential growth rates**

140 Picocyanobacterial growth was monitored every 5 minutes for 14 days, independently for  
141 each culture tube, by automatically recording OD<sub>680</sub>, a proxy for chlorophyll *a* content; OD<sub>720</sub>; a  
142 proxy for cell scatter; and ΔOD (ΔOD = OD<sub>680</sub> – OD<sub>720</sub>), a proxy for chlorophyll *a* content  
143 (Nedbal et al. 2008). The exceptions were experiments conducted with a photoperiod of 24 h and  
144 light of 600 or 900 μmol photons m<sup>-2</sup>s<sup>-1</sup>, which lasted 7 days (Fig. S2). The chlorophyll-specific  
145 exponential growth rates ( $\mu$ ) were determined by fitting logistic growth curves using a modified  
146 Levenberg-Marquardt fitting algorithm (Elzhov et al. 2023) to plots of the chlorophyll *a* proxy of  
147 ΔOD vs. elapsed time for each combination of strain, photoperiod, and peak PAR (Fig. S3).

148 To summarize the growth responses of the four picocyanobacterial strains we used a  
149 Generalized Additive Model (GAM) (Wood 2017) applied to the relation of chlorophyll-specific  
150  $\mu$ , d<sup>-1</sup> to photoperiod and PAR level. The R package *mgcv* (Wood 2017) was used to model the  
151 growth rate with smoothing terms and indicate the 90, 50 and 10% quantiles for growth rate  
152 across the levels of factors. Only growth rate estimates for which the amplitude of standard error  
153 was smaller than 50% of the fitted growth rate were included in the GAM. We visually  
154 compared the GAM contours to isolines of equal cumulative diel PAR (μmol photons m<sup>-2</sup>d<sup>-1</sup>).

155 The 1<sup>st</sup> derivative of OD<sub>680</sub> taken over 1 h increments was computed using *xts*: eXtensible  
156 Time Series (Ryan et al. 2024) and *signal*: Signal Processing (Ligges et al. 2024) R packages.  
157 The time when the cultures reached their maximum absolute hourly growth (tMaxAHG) of the  
158 1<sup>st</sup> derivative of OD<sub>680</sub> was taken as the time of transition from exponential to pre-stationary

159 growth phases (Fig. 1). This phase progresses to the stationary growth phase. In this work, all  
 160 measurements obtained after transition time were termed the pre-stationary phase of growth,  
 161 according to Schuurmans et al. (2017).



162

163 **Fig. 1.** Example of a growth curve (tracked as  $OD_{720}$ ,  $OD_{680}$ , or  $\Delta OD$ ; red solid lines, left y-axis) of PE-rich culture  
 164 of *Synechococcus* sp. (048; grown at 180 peak PAR  $\mu\text{mol photons m}^{-2}\text{s}^{-1}$ ; and photoperiods of 12 h) vs. elapsed  
 165 time (d, x-axis). 1<sup>st</sup> derivative of  $OD_{680}$  taken over 1 h increments (black solid line, right y-axis); solid blue line  
 166 shows logistic fits of chlorophyll proxy  $OD_{680} - OD_{720}$  ( $\Delta OD$ ) vs. elapsed time. The vertical red dot dash line  
 167 represents the time when the culture reached the maximum of the 1<sup>st</sup> derivative of  $OD_{680}$ , or maximum absolute  
 168 hourly growth (tMaxAHG), taken as the time of transition from exponential to pre-stationary growth phases.

169

## 170 Whole-cell absorbance spectra

171 Absorbance measurements on intact cells in suspension were conducted in an integrating  
 172 cavity upgrade spectrophotometer (CLARiT<sup>Y</sup> 17 UV/Vis/NIR, On-Line Instrument Systems,

173 Inc., Bogart, GA, USA). 8 mL of f/2 medium were added to both the sample and reference  
174 observation cavities of the spectrophotometer. After recording a baseline from 375 to 710 nm, 1  
175 mL was withdrawn from the sample cavity and replaced with 1 mL of picocyanobacteria cell  
176 suspension. The pathlength corrected absorbance per cm was performed by determining the  
177 Javorfi coefficients (Jávorfi et al. 2006) as described in the equipment manual.

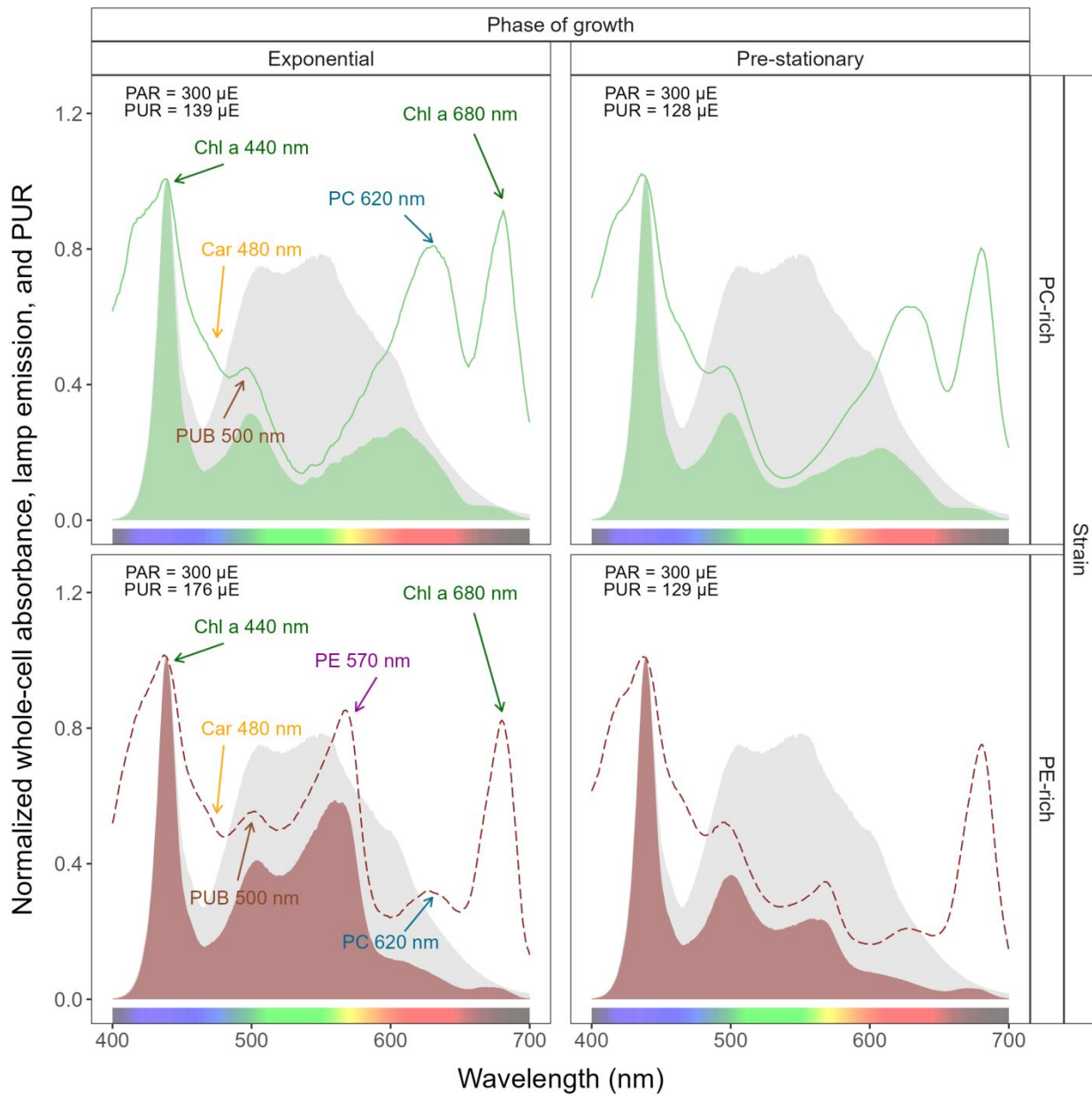
178

## 179 Photosynthetically Usable Radiation (PUR)

180 Using whole-cell absorbance spectra of *Synechococcus* sp. cultures, we estimated  
181 Photosynthetically Usable Radiation (PUR;  $\mu E = \mu\text{mol photons m}^{-2}\text{s}^{-1}$ ) according to Morel  
182 (1978). Representative absorbance spectra for one growth light treatment (300  $\mu\text{mol photons}$   
183  $\text{m}^{-2}\text{s}^{-1}$ ), for one PE and one PC rich strain, are shown in Fig. 2. The other 476 spectra used to  
184 estimate PUR are available at <https://github.com/FundyPhytoPhys/BalticPhotoperiod>. We  
185 normalized the obtained whole-cell Absorbances (A) and the Emission spectra of the white LED  
186 lamps (Em) from 400 nm to 700 nm to a reference wavelength of 440 nm. PUR is then the ratio  
187 of the sum of Absorbance Normalized to 440 nm (NormA<sub>440</sub>) multiplied by the sum of Emission  
188 spectra Normalized to 440 nm (NormEm<sub>440</sub>) to the sum of the Emission spectra Normalized to  
189 440 nm (NormEm<sub>440</sub>), multiplied by the PAR (Eq. (1)).

$$190 PUR (\mu E) = \frac{\sum(NormA_{440} \times NormEm_{440})}{\sum(NormEm_{440})} \times PAR (\mu E) \quad (1)$$

191



193 **Fig. 2.** Whole-cell absorbance spectra of PC-rich (077; solid light green lines) or PE-rich (127; dashed dark red  
 194 lines) cultures of *Synechococcus* sp. Representative absorbance spectra, normalized to 440 nm (NormA<sub>440</sub>), were  
 195 measured from the exponential or pre-stationary phases of growth, together with emission spectra of the white LED  
 196 lamp used for PAR, normalized to emission at 440 nm (NormEm<sub>440</sub>, light gray area), in this example PAR was 300  
 197  $\mu\text{mol photons m}^{-2}\text{s}^{-1}$ . Estimated Photosynthetically Usable Radiation (PUR) is shown as a darker green area for the  
 198 PC-rich strain and a darker red area for the PE-rich strain, with PUR given for each culture ( $\mu\text{E} = \mu\text{mol photons}$

199  $\text{m}^{-2}\text{s}^{-1}$ ). Peaks characteristic of known pigments are labeled; Chl *a*, chlorophyll *a*; PC, phycocyanin; PE,  
200 phycoerythrin; PUB, phycourobilin; Car, carotenoids.

201

## 202 Cumulative diel PAR and PUR

203 Based on the length and shape of the photoperiod (sinuisoidal wave for photoperiods of 8,  
204 12, 16 h; square for photoperiod of 24 h) and the peak PAR ( $\mu\text{E} = \mu\text{mol photons m}^{-2}\text{s}^{-1}$ ), we  
205 estimated the value of the cumulative diel PAR ( $\mu\text{mol photons m}^{-2}\text{d}^{-1}$ ). For sinuisoidal  
206 photoperiods we used Eq. (2); for the continuous 24 h photoperiod we used Eq. (3). Cumulative  
207 diel PUR was estimated similarly after estimation of peak PUR from peak PAR.

$$208 \frac{\text{Cumulative diel PAR } (\mu\text{mol photons m}^{-2} \text{ d}^{-1})}{\text{PAR } (\mu\text{E}) \times 60 \text{ (s min}^{-1}\text{)} \times 60 \text{ (min h}^{-1}\text{)} \times \text{photoperiod (h d}^{-1}\text{)}} = \quad (2)$$

$$209 \frac{\text{Cumulative diel PAR } (\mu\text{mol photons m}^{-2} \text{ d}^{-1})}{\text{PAR } (\mu\text{E}) \times 60 \text{ (s min}^{-1}\text{)} \times 60 \text{ (min h}^{-1}\text{)} \times \text{photoperiod (h d}^{-1}\text{)}} = \quad (3)$$

210

## 211 Pigment content

212 Chlorophyll *a* (Chl *a*) ( $\mu\text{g mL}^{-1}$ ) was measured using Trilogy Laboratory Fluorometer  
213 (Turner Designs, Inc., CA, USA) equipped with Chlorophyll In-Vivo Module, previously  
214 calibrated using 20 mL ampoules with known Chl *a* concentrations in 3:2 90% acetone:DMSO  
215 solution. Quantitative analysis of Chl *a* was obtained after adding 50  $\mu\text{L}$  of culture and 2 mL of a  
216 90% acetone:DMSO solution in a 3:2 ratio.

217 We also estimated the pigment content ( $\mu\text{g mL}^{-1}$ ): chlorophyll *a* (Chl *a*), carotenoids (Car),  
218 phycoerythrin (PE), phycocyanin (PC), and allophycocyanin (APC) in *Synechococcus* sp.  
219 cultures over time using previously determined linear correlations between pigment content  
220 obtained by extraction (Strickland and Parsons 1972; Bennett and Bogorad 1973) and absorbance

221 values of individual pigment peaks (Car; 480, PE; 565, PC; 620, APC; 650, and Chl *a*; 665 nm)  
222 obtained from the whole-cell absorbance spectra using integrating cavity upgrade  
223 spectrophotometer (CLARiTY 17 UV/Vis/NIR, On-Line Instrument Systems, Inc., Bogart, GA,  
224 USA) (Tab. S1 in Supporting Information). The sum of phycobiliproteins (PE, PC, APC protein)  
225 to Chl *a* ratio ( $\mu\text{g}:\mu\text{g}$ ) for individual strains was also calculated.

226

## 227 **The effective absorption cross section of PSII and electron flux**

228 We harvested 2 mL of cultures for photophysiological characterizations repeatedly across  
229 the growth trajectories. We used Fast Repetition Rate fluorometry (Kolber et al. 1998) (FRRf,  
230 Solisense, USA), with a lab built temperature control jacket (22°C), to apply series of flashlets to  
231 drive saturation induction/relaxation trajectories, fit using the onboard Solisense LIFT software  
232 (Falkowski and Kolber 1993; Kolber et al. 1998). From the model fits we took the initial  
233 fluorescence before induction ( $F_0$ ,  $F_0'$ , or  $F_s$ , depending upon the level of actinic light and step  
234 in the light response curve); the maximum fluorescence ( $F_M$  or  $F_M'$ ) once Photosystem II (PSII)  
235 was driven to closure by the saturation induction flashlet train; and the effective absorption cross  
236 section for PSII photochemistry ( $\sigma_{\text{PSII}}$  or  $\sigma_{\text{PSII}}'$ ;  $\text{nm}^2 \text{ quanta}^{-1}$ ) (Tortell and Suggett 2021). We  
237 used a double tap protocol (Xu et al. 2017), where FRRf induction/relaxation trajectories were  
238 collected during a rapid light curve sequence increasing in steps of 10 s at 0, 20, 40, 80, 160, and  
239 320  $\mu\text{mol photons m}^{-2}\text{s}^{-1}$  PAR, delivered from LED emitters centred at 445, preferentially  
240 exciting chlorophyll, or 590 nm, preferentially exciting phycobiliproteins. Flash Power for 445  
241 nm excitation was 60000  $\mu\text{mol photons m}^{-2}\text{s}^{-1}$  PAR, while for 590 nm excitation power was  
242 14000  $\mu\text{mol photons m}^{-2}\text{s}^{-1}$ , calibrated using a quantum sensor (LI-250, LI-COR, Inc.). We

243 applied 1 s darkness between sequential light steps, to allow re-opening of PSII. FRRf excitation  
 244 flashlets were applied at the same wavebands, 445 or 590 nm, as the actinic light steps.

245 We calculated (Eq. (4)) an uncalibrated fluorescence based estimator for volumetric  
 246 electron transport,  $JV_{PSII}$ , ( $\text{kmol e}^- \text{ L}^{-1} \text{ s}^{-1}$ ) under both 445 and 590 nm excitation bands  
 247 (Oxborough et al. 2012; Boatman et al. 2019; Tortell and Suggett 2021).

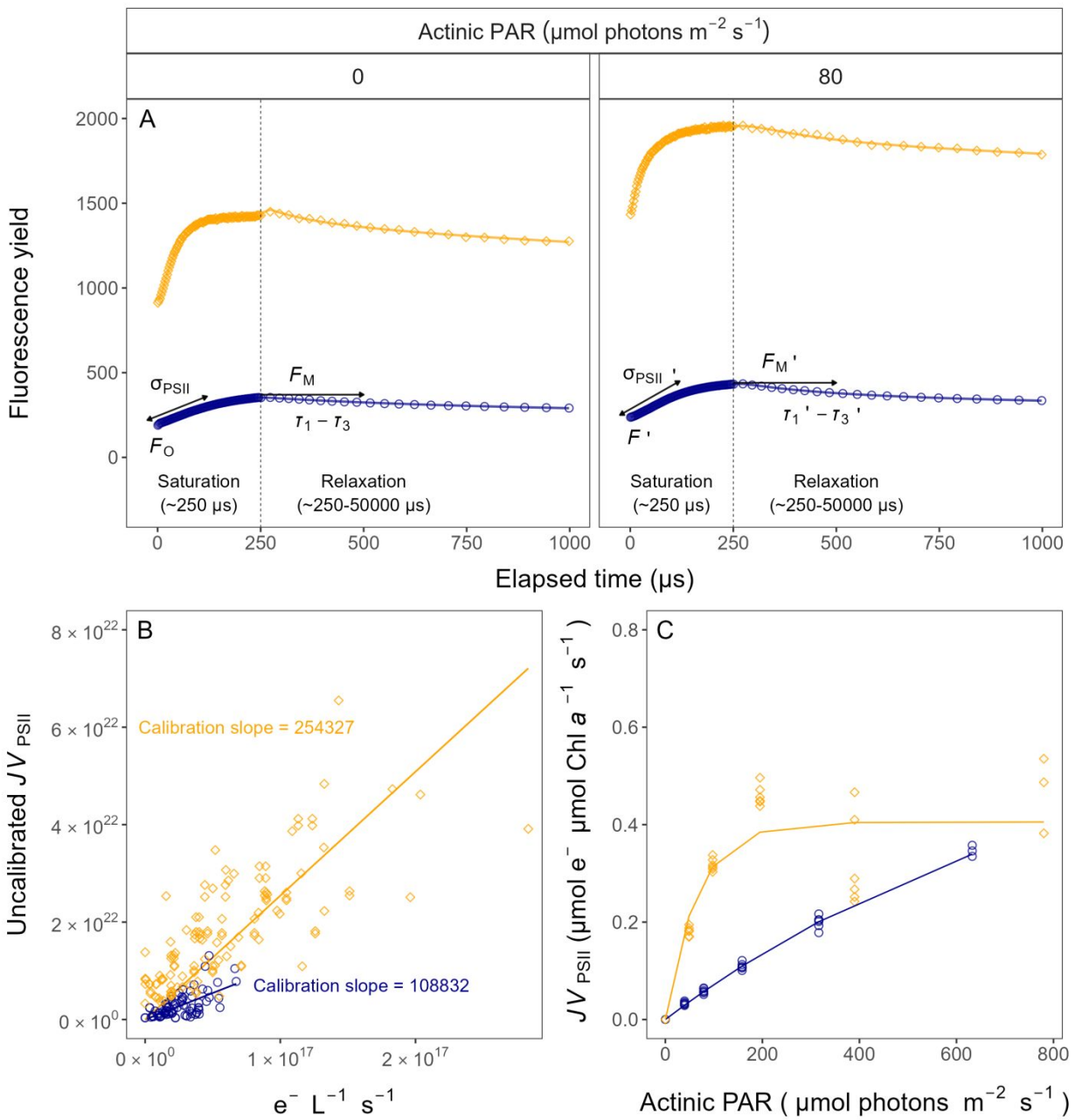
$$248 JV_{PSII} = \frac{\sigma_{PSII}' \times qP \times I \times F_O}{\sigma_{PSII}} \quad (4)$$

249 where  $\sigma_{PSII}'$  is effective absorption cross section for PSII photochemistry under the relevant  
 250 actinic PAR step ( $\text{nm}^2 \text{ quanta}^{-1}$ ); qP is the fraction of PSII open for photochemistry estimated  
 251 according to Oxborough and Baker (1997); I is the applied PAR ( $\mu\text{mol photons m}^{-2}\text{s}^{-1}$ );  $F_O$  is the  
 252 minimum fluorescence from a given sample and excitation bandwidth (relative fluorescence) and  
 253  $\sigma_{PSII}$  is the maximum effective absorption cross section for PSII photochemistry from a given  
 254 sample and excitation bandwidth ( $\text{nm}^2 \text{ quanta}^{-1}$ ). We compared several other algorithms for  
 255  $JV_{PSII}$  (Tortell and Suggett 2021) and found similar results.

256 We calibrated the  $JV_{PSII}$  estimator to absolute rates of electron transport (Eq. (5)) using  
 257 parallel measures of oxygen evolution ( $\mu\text{mol O}_2 \text{ L}^{-1} \text{ s}^{-1}$ ), captured simultaneously with the FRRf  
 258 measures, below light saturation of electron transport, using a FireSting robust oxygen probe  
 259 (PyroScience, Germany) inserted in the cuvette for select Rapid Light Curve (RLC) runs (Fig. 3).  
 260 For the blue LED ( $\text{Ex}_{445\text{nm}}$ ) excitation we used a calibration slope of 108832, while for orange  
 261 LED ( $\text{Ex}_{590\text{nm}}$ ) excitation we used a calibration slope of 254327

$$262 JV_{PSII}(e^- \text{ L}^{-1} \text{ s}^{-1}) = \frac{\text{Uncalibrated } JV_{PSII}(e^- \text{ L}^{-1} \text{ s}^{-1})}{\text{Calibration slope}} \quad (5)$$

263



264

265 **Fig. 3.** Single turnover (ST) fluorescence induction by Fast Repetition Rate fluorometry (FRRf). (A) Examples of  
 266 fluorescence yield vs. elapsed time ( $\mu\text{s}$ ) for PE-rich culture of *Synechococcus* sp. (048) in the dark (dark-relaxed; 0  
 267  $\mu\text{mol photons m}^{-2}\text{s}^{-1}$ ) and under actinic PAR (in this example  $80 \mu\text{mol photons m}^{-2}\text{s}^{-1}$ ) using blue LED (Ex<sub>445nm</sub>;  
 268 open blue circles) or orange (Ex<sub>590nm</sub>; open orange diamonds) excitation. The ST technique delivers a series of  
 269 flashlets for non-intrusive, repeated monitoring of chlorophyll fluorescence parameters (including  $F_O$ ,  $F'$ ,  $F_M$ ,  $F'_M$ ,  
 270  $\tau_1 - \tau_3$ ,  $\tau'_1 - \tau'_3$ ,  $\sigma_{PSII}$ , and  $\sigma_{PSII}'$ ). (B) Linear regressions of uncalibrated PSII electron flux ( $JV_{PSII}$ ) vs.  $e^- \text{ L}^{-1} \text{ s}^{-1}$  derived

271 from simultaneously measured oxygen evolution Light Response Curves (LRC) under blue LED ( $\text{Ex}_{445\text{nm}}$ ; open blue  
272 circles) or orange ( $\text{Ex}_{590\text{nm}}$ ; open orange diamonds) excitation. (C) Rapid Light Curve (RLC), fit with a three  
273 parameter model (Harrison and Platt 1986), for PSII electron flux ( $JV_{\text{PSII}}$ ;  $\mu\text{mol e}^{-} \mu\text{mol Chl } a^{-1} s^{-1}$ ) vs. actinic PAR  
274 measured under blue LED ( $\text{Ex}_{445\text{nm}}$ ; open blue circles) or orange ( $\text{Ex}_{590\text{nm}}$ ; open orange diamonds) excitation.

275

## 276 Statistical analysis

277 We used R version 4.3.0 (R Core Team 2023) running under RStudio (Posit team 2022).  
278 We performed three-way factorial ANOVA (*aov()* function; R Base package) to determine  
279 whether peak PAR, photoperiod, strain, and their interactions, significantly influence the  
280 chlorophyll-specific exponential growth rate ( $\mu$ ;  $d^{-1}$ ), estimated from logistic fits (*nlsLM()*  
281 function; Elzhov et al. (2023)) of chlorophyll proxy  $\text{OD}_{680} - \text{OD}_{720}$  vs. cumulative diel PUR  
282 (Table S2). We also used the *nlsLM()* function to fit a three parameter light response model  
283 (Harrison and Platt 1986) of growth rates ( $\alpha$ , initial slope of curve;  $\beta$ , reflecting the  
284 photoinhibition process;  $P_{\text{max}}$ , the maximum rate of growth curve).

285 To examine statistical differences between fits of light responses, we performed one-way  
286 ANOVA (*aov()* function) of the three parameter model (Harrison and Platt 1986) fit to pooled  
287 data for each taxa, compared to separate fits for each different photoperiod (8, 12, 16, or 24); or  
288 to separate fits for each different peak PAR (30, 90, 180, 300, 600 together with 900). These  
289 comparisons were run for chlorophyll-specific exponential growth rate vs. cumulative diel PUR  
290 (Table S3, S4); vs. cumulative diel PAR (Table S5, S6) or vs. PSII electron flux ( $JV_{\text{PSII}}$ ;  $\mu\text{mol e}^{-}$   
291  $\mu\text{mol Chl } a^{-1} d^{-1}$ ; Table S7, S8). One-way ANOVA was also used to examine statistical  
292 differences between single phase exponential decay fits (*SSasymp()* function; Serway et al.  
293 (2004)) of pooled data across different strains for a given phase of growth and across different  
294 phase of growth for a given strain for PUR/PAR ratio (Table S9); Phycobiliprotein to Chl  $a$  ratio

295 (Table S10); or effective absorption cross section of PSII ( $\sigma_{PSII}'$ ; nm<sup>2</sup> quanta<sup>-1</sup>) measured under  
296 diel peak PAR growth light under Ex<sub>590nm</sub> (orange) excitation in relation to the cumulative diel  
297 PAR ( $\mu\text{mol photons m}^{-2}\text{d}^{-1}$ ) (Table S11).

298 We used *t*-tests (*t.test()* function; R Base package) of linear fits (*lm()* function) to compare  
299 pooled data across different strains for a given phase of growth, and across different phases of  
300 growth, for a given strain, for effective absorption cross section of PSII ( $\sigma_{PSII}'$ ; nm<sup>2</sup> quanta<sup>-1</sup>)  
301 measured under diel peak PAR growth light under Ex<sub>445nm</sub> (blue) excitation vs. the cumulative  
302 diel PAR ( $\mu\text{mol photons m}^{-2}\text{d}^{-1}$ ; Table S12); or vs. the Phycobiliprotein to Chl *a* ratio (Table  
303 S13). The same *t*-test analyses were performed for effective absorption cross section of PSII  
304 ( $\sigma_{PSII}'$  or  $\sigma_{PSII}$ ; nm<sup>2</sup> quanta<sup>-1</sup>) measured under Ex<sub>590nm</sub> (orange) excitation vs. the Phycobiliprotein  
305 to Chl *a* ratio (Table S14, S15).

306 Statistical differences for all analyses were determined at significance level  $\alpha = 0.05$ . The  
307 manuscript was prepared as a Rmarkdown document (Handel 2020) with figures prepared using  
308 the ggplot2 (Wickham 2016) and patchwork (Pedersen 2024) packages. All metadata, data and  
309 code is available on GitHub (<https://github.com/FundyPhytoPhys/BalticPhotoperiod>).  
310

## 311 **Results**

### 312 **Chlorophyll-specific exponential growth rate**

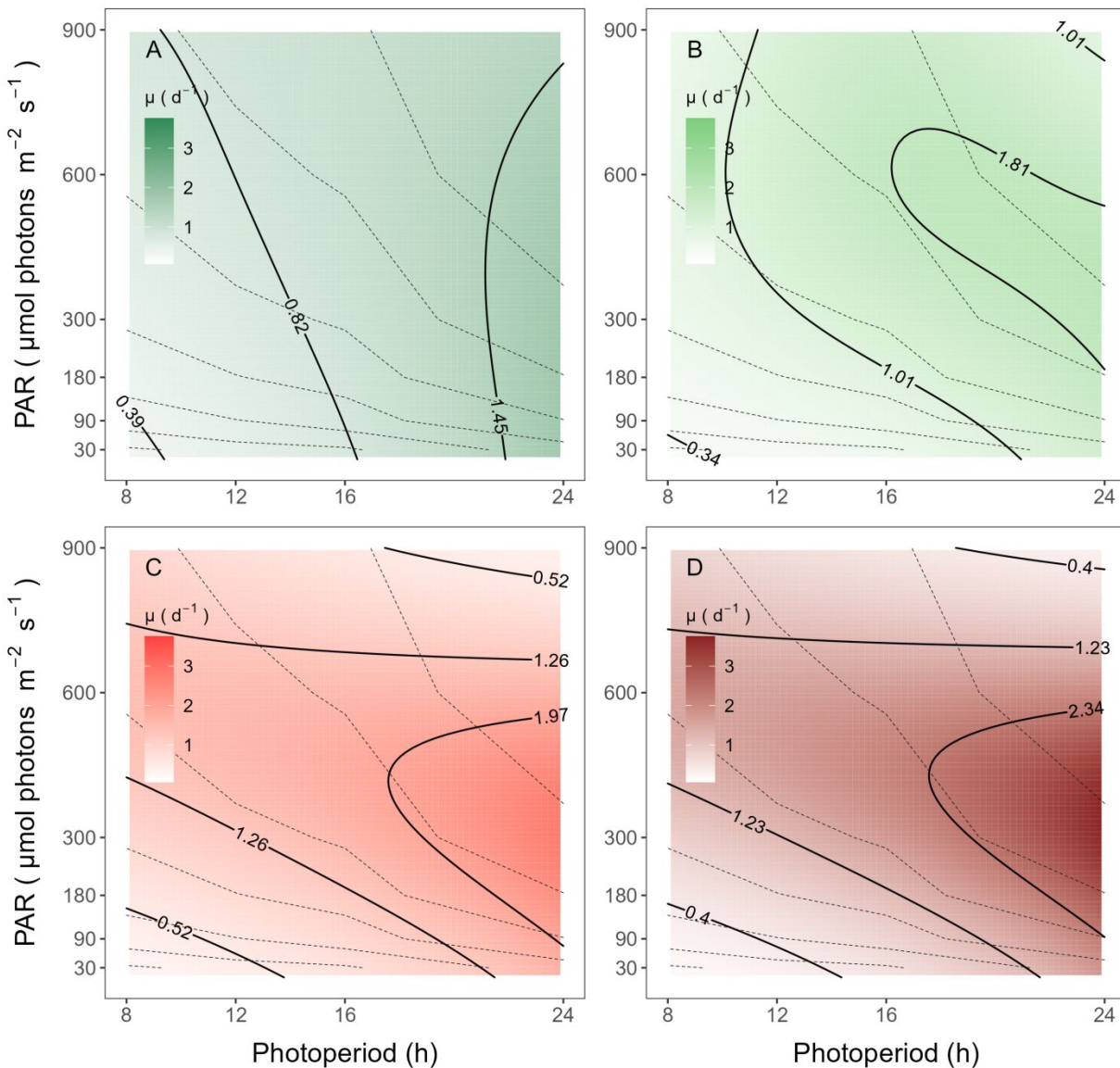
313 Not all cultures were grown long enough to reach full stationary phase, but onset of  
314 stationary phase, when determined, occurred fairly consistently when cultures reached  $\sim 0.5$   
315 OD<sub>720</sub> (PC-rich) or  $\sim 0.65$  OD<sub>720</sub> (PE-rich), no matter the level of culture PAR. It is therefore  
316 unlikely that an onset of light limitation imposed stationary phase on the cultures, which  
317 remained optically fairly thin, with even illumination to each tube from the PSI MultiCultivator

318 array of LED. Based upon parallel studies re-launching growth after stationary phase by dilution  
319 with fresh media, with the same strains, under the same growth conditions (unpub.), we  
320 hypothesize that nutrient limitation imposes the transition to stationary phase.

321 We used logistic curve fits (Fig. S3B) to determine chlorophyll-specific exponential  
322 growth rates ( $\mu$ ;  $d^{-1}$ ), for two PhycoCyanin(PC)-rich cultures (056, 077) and two  
323 PhycoErythrin(PE)-rich cultures (048, 127) of *Synechococcus* sp. grown at 30, 90, 180, 300, 600,  
324 or 900 peak PAR  $\mu\text{mol photons m}^{-2}\text{s}^{-1}$  ( $\mu\text{E}$ ); and photoperiods of 8, 12, 16, or 24 h. There were  
325 significant effects of all three independent variables on  $\mu$  as well as significant interactions  
326 between variables (ANOVA,  $p < 0.05$ ; Table S2). All tested strains, except PE-rich\_048, grew  
327 even under peak PAR 900  $\mu\text{mol photons m}^{-2}\text{s}^{-1}$  and 24 h photoperiod. The highest growth rate  
328 was recorded for *Synechococcus* sp. PE-rich\_127 ( $\mu = 4.5 \text{ d}^{-1}$ ; 3.7 h doubling time) and PC-  
329 rich\_056 ( $\mu = 3.4 \text{ d}^{-1}$ ; 4.9 h doubling time) at 180  $\mu\text{mol photons m}^{-2}\text{s}^{-1}$  peak PAR and  
330 photoperiod of 24 h.

331 The GAM model in Fig. 4 summarizes the growth responses of the PC-rich and PE-rich  
332 picocyanobacteria to peak PAR and photoperiod. PC-rich\_056 *Synechococcus* sp. showed  
333 highest growth rates under a photoperiod of 24 h, across a wide range of peak PAR indicated by  
334 the contour line labeled  $1.45 \text{ d}^{-1}$ , representing the 90<sup>th</sup> percentile of achieved growth rates for the  
335 strain. On the other hand, the other tested PC-rich strain (077) showed highest growth rates in the  
336 range of photoperiod 16–24 h and peak PAR between 300 – 700  $\mu\text{mol photons m}^{-2}\text{s}^{-1}$ , indicated  
337 by the  $1.81 \text{ d}^{-1}$  contour line again representing the 90<sup>th</sup> percentile of maximum achieved growth  
338 rates for the strain. For both PC-rich strains, growth was slowest under 30  $\mu\text{mol photons m}^{-2}\text{s}^{-1}$   
339 and a photoperiod of 8 h.

340 Both PE-rich strains achieved fastest growth rates above peak PAR of ~300  $\mu\text{mol}$  photons  
341  $\text{m}^{-2}\text{s}^{-1}$ , under the longest photoperiod of 24 h, indicated by the  $1.97 \text{ d}^{-1}$  for PE-rich\_048, and  
342  $2.34 \text{ d}^{-1}$  for PE-rich\_127, contour lines. For the PE-rich strains growth decreased with decreasing  
343 photoperiod and decreasing peak PAR. Moreover, PE-rich strains showed photoinhibition of  
344 growth at peak PAR of 900  $\mu\text{mol}$  photons  $\text{m}^{-2}\text{s}^{-1}$  and photoperiods of 16- 24 h. The growth rate  
345 contours for PC-rich and PE-rich *Synechococcus* sp. did not generally follow the isoclines of  
346 cumulative diel photon dose ( $\mu\text{mol}$  photons  $\text{m}^{-2}\text{d}^{-1}$ , dashed lines), showing that photoperiod, and  
347 peak PAR, influenced growth rates beyond cumulative diel photon dose.



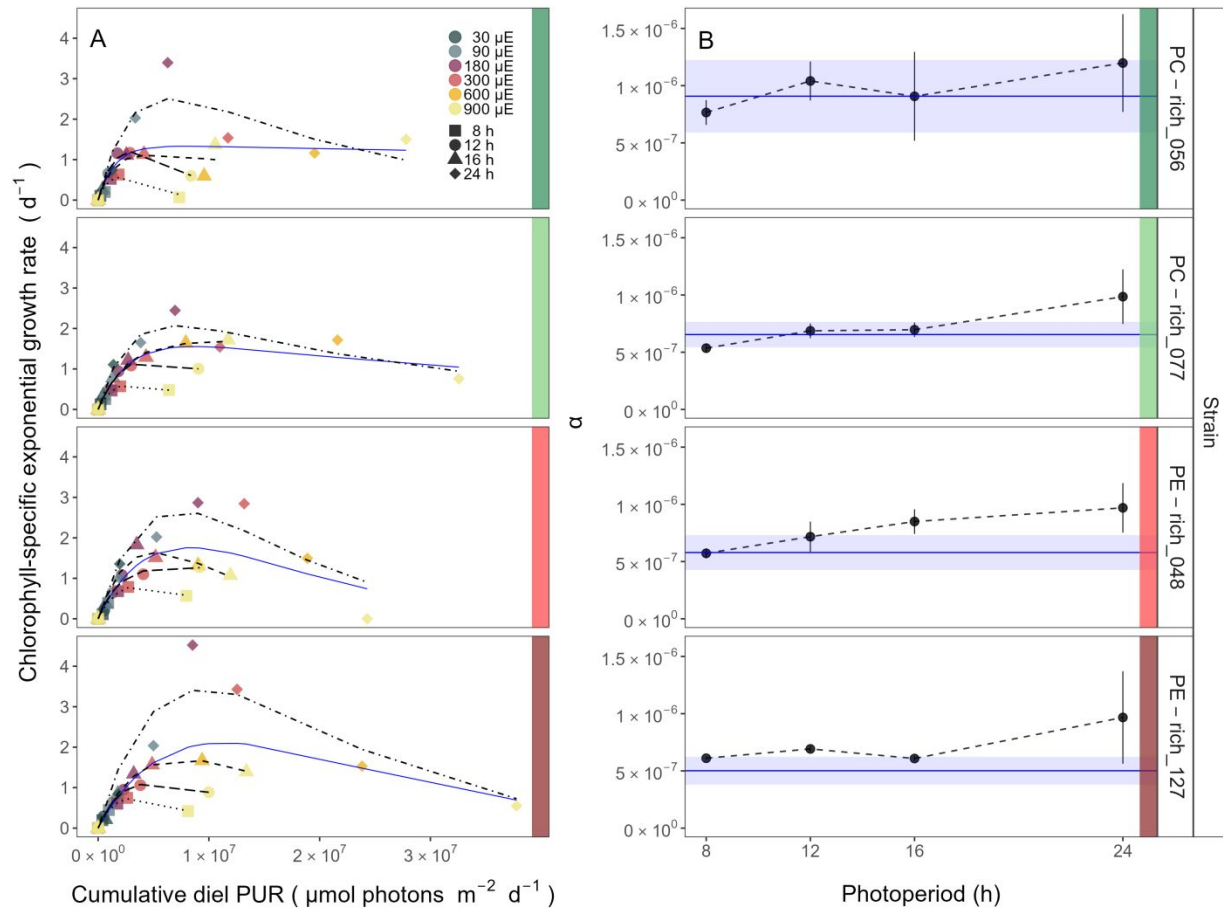
348

349 **Fig. 4.** A contour plot of a Generalized Additive Model (GAM) of chlorophyll-specific growth rates ( $d^{-1}$ ) for two  
 350 PC-rich cultures: **(A)** 056, **(B)** 077 and two PE-rich cultures: **(C)** 048, **(D)** 127 of *Synechococcus* sp. grown at 30, 90,  
 351 180, 300, 600, or 900 peak PAR  $\mu\text{mol photons m}^{-2}\text{s}^{-1}$ ; and photoperiods of 8, 12, 16, or 24 h. Legends show colour  
 352 gradients of growth rate ( $\mu$ ;  $d^{-1}$ ) from no growth (white) to 3.0  $d^{-1}$  (dark green for PC-rich\_056, light green for PC-  
 353 rich\_077, light red for PE-rich\_048 or dark red for PE-rich\_127 strains). Labeled contour lines indicate the 90%,  
 354 50%, and 10% quantiles for achieved growth rate. Dotted lines show isoclines of cumulative diel photon dose ( $\mu\text{mol}$   
 355  $\text{photons m}^{-2} d^{-1}$ ).

356

357 A three parameter light response model fit (Harrison and Platt 1986) of chlorophyll-  
358 specific exponential growth rates vs. cumulative diel PUR dose for two PC-rich and two PE-rich  
359 cultures of *Synechococcus* sp. showed significant differences between model fits of the pooled  
360 data vs. fits for all tested photoperiods (8, 12, 16, or 24 h; ANOVA,  $p < 0.05$ ; Fig. 5A, Table S3).  
361 The alpha parameters of the initial rise of growth rate ( $\alpha$ ) vs. cumulative diel PUR, estimated  
362 from data pooled for each photoperiod increased with increasing photoperiod for all strains. The  
363 highest increase (>2-fold) of  $\alpha$  with increasing photoperiod was recorded for PC-rich\_056 (Fig.  
364 5B). Strains also showed distinct growth rate responses to cumulative diel PUR, depending upon  
365 peak PAR (Fig. S4A, Table S4), that differ from a single light response model fit to the pooled  
366 data across all peak PAR from a strain. Exceptions were observed in the strains PC-rich\_077 and  
367 PE-rich\_048 with the peak PAR of 600 or 900  $\mu\text{mol photons m}^{-2}\text{s}^{-1}$ , which were not  
368 significantly different from the pooled data model. A caveat to these findings is that cumulative  
369 diel photon dose is a product of photoperiod and PAR, so the highest levels of cumulative PUR  
370 dose are only achieved under the 600 or 900  $\mu\text{mol photons m}^{-2}\text{s}^{-1}$ . The alpha parameters of the  
371 initial rise of growth rate ( $\alpha$ ) vs. cumulative diel PUR, estimated from data pooled for each peak  
372 PAR decreased across peak PAR for all tested strains (Fig. S4B).

373 Growth rate saturated under increasing cumulative diel PUR for all strains, however, the  
374 achieved estimates of  $\mu_{\max}$  varied depending upon photoperiod and peak diel PAR. Growth rates  
375 vs. cumulative diel PAR relationships, estimated for exponential phase cultures, followed similar  
376 patterns (Fig. S5, Fig. S6 and Table S5, S6 in Supporting Information).



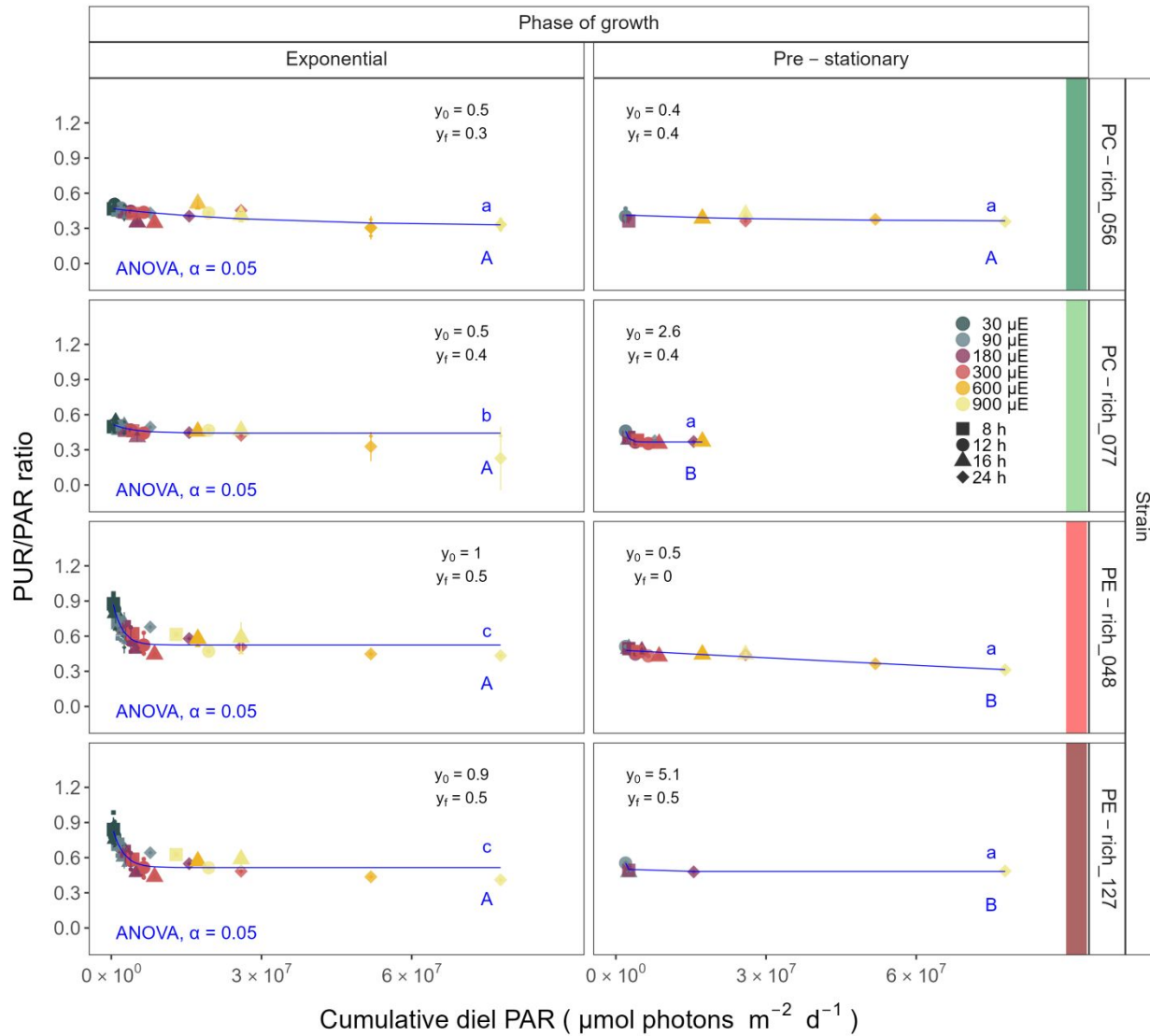
377

378 **Fig. 5.** (A) Chlorophyll-specific exponential growth rates ( $d^{-1}$ ) vs. cumulative diel Photosynthetically Usable  
 379 Radiation (PUR,  $\mu\text{mol photons m}^{-2}\text{d}^{-1}$ ). Growth rates ( $\pm$  SE falling within symbols) were estimated from logistic fits  
 380 of chlorophyll proxy  $\text{OD}_{680} - \text{OD}_{720}$  ( $\Delta\text{OD}$ ) vs. elapsed time (Fig. 1, Fig. S3B), for two PC-rich cultures (056; dark  
 381 green, 077; light green) and two PE-rich cultures (048; light red, 127; dark red) of *Synechococcus* sp. grown at 30  
 382 (dark gray), 90 (light gray), 180 (purple), 300 (red), 600 (orange), or 900 (yellow) peak PAR  $\mu\text{mol photons m}^{-2}\text{s}^{-1}$   
 383 ( $\mu\text{E}$ ); and photoperiods of 8 (square), 12 (circle), 16 (triangle), or 24 (diamond) h. Solid blue line shows a fit of the  
 384 pooled growth rates through photoperiods for each strain, with a three parameter model (Harrison and Platt 1986).  
 385 We also fit the same model separately for 8 (dotted line), 12 (long dash line), 16 (dashed line), or 24 (two dash line)  
 386 h photoperiods, since for all strains they were each significantly different (ANOVA,  $p < 0.05$ ) from the fit of pooled  
 387 data. (B) Alpha parameters of the initial rise of growth rate ( $\alpha$ ) vs. cumulative diel Photosynthetically Usable  
 388 Radiation (PUR), estimated from data pooled for each photoperiod (points ( $\pm$  SE) connected by dashed lines), and  
 389 estimated for all data across photoperiods (solid blue horizontal line  $\pm$  SE), for each strain.

390

391 **PUR/PAR ratio vs. cumulative diel PAR**

392 The PUR/PAR ratio is an index of the efficacy of light capture for a culture under a given  
393 growth condition; showing the fraction of PAR that can be captured by the absorbance of the  
394 cells (Fig. 6). For the two PC-rich and, particularly, for the two PE-rich cultures of  
395 *Synechococcus* sp. PUR/PAR decayed exponentially to a plateau, with increasing cumulative  
396 diel PAR, when pooling PUR/PAR data across different combinations of photoperiod and peak  
397 PAR. Although all strains followed a similar trend, the single phase exponential decay model fit  
398 parameters varied significantly among strains, during their exponential phase of growth  
399 (ANOVA,  $p < 0.05$ ), except the model fits from PE-rich\_048 and PE-rich\_127 (ANOVA,  $p >$   
400 0.05; Table S9). Moreover, the PUR/PAR ratio was higher in the PE-rich strains under low  
401 cumulative diel photon dose during their exponential phase of growth ( $y_0$  greater or equal to 0.9),  
402 but decayed towards a plateau close to the PC-rich strains as cumulative diel photon dose  
403 increases ( $y_f = 0.5$ ). On the other hand, the single phase exponential decay model fits did not  
404 differ significantly among strains, during their pre-stationary phase of growth (ANOVA,  $p >$   
405 0.05; Table S9). During this phase, response of PUR/PAR ratio to increasing cumulative diel  
406 PAR exhibits damping, maintaining a consistent trend across all strains within the  $y_f$  range of 0.4  
407 to 0.5, with the exception of the PE-rich\_048 strain. We also find that model fits from different  
408 phases of growth differed within a given strain, with the exception of PC-rich\_056 (ANOVA;  $p$   
409  $< 0.05$ , Table S9). A similar decay trend was observed for Phycobiliprotein to Chl *a* ratio  
410 ( $\mu\text{g}:\mu\text{g}$ ) across cumulative diel PAR (Fig. S7).



411

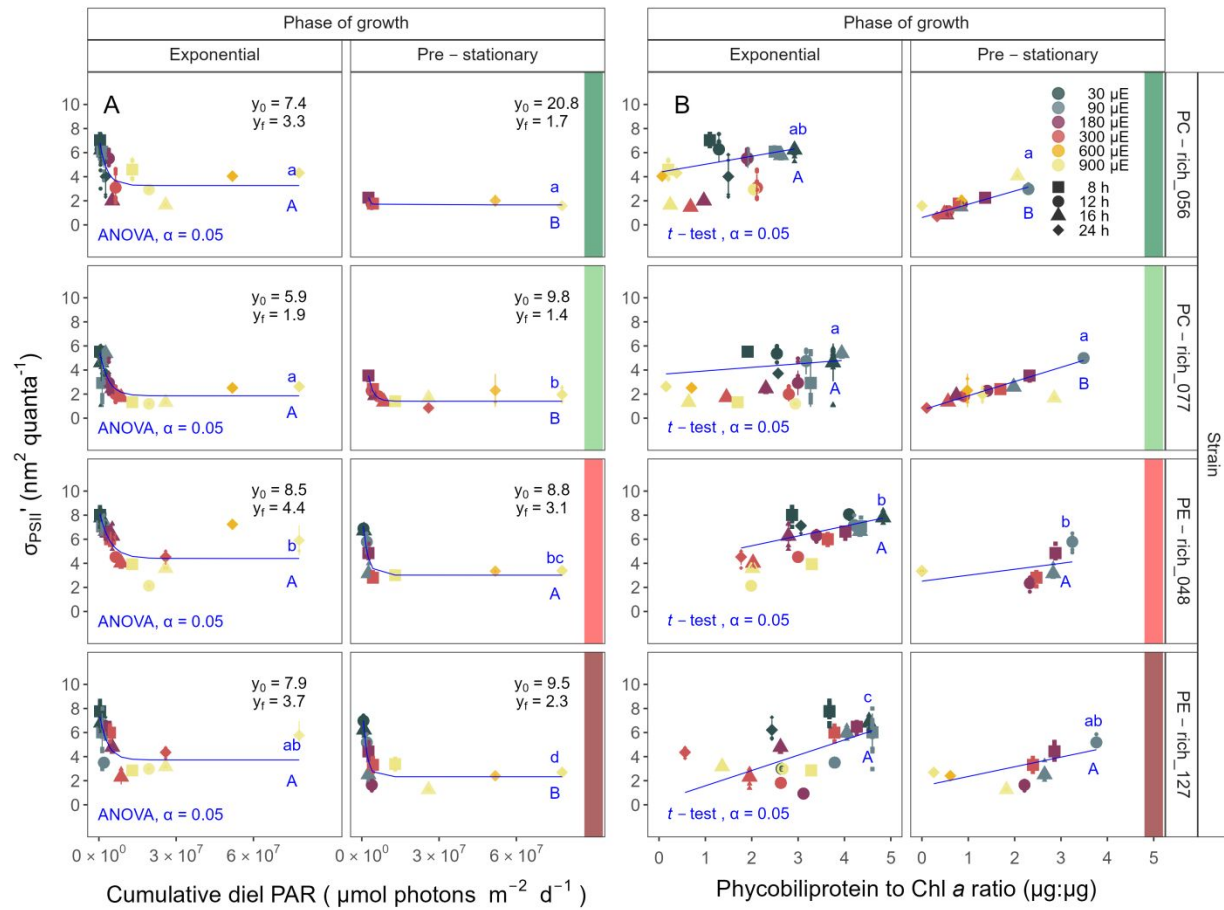
412 **Fig. 6.** Changes in PUR/PAR ratio vs. cumulative diel PAR ( $\mu\text{mol photons m}^{-2} \text{d}^{-1}$ ). PUR/PAR ratio was estimated  
 413 for two PC-rich cultures (056; dark green, 077; light green) and two PE-rich cultures (048; light red, 127; dark red)  
 414 of *Synechococcus* sp. grown at 30 (dark gray), 90 (light gray), 180 (purple), 300 (red), 600 (orange), or 900 (yellow)  
 415 peak PAR  $\mu\text{mol photons m}^{-2} \text{s}^{-1}$  ( $\mu\text{E}$ ); and photoperiods of 8 (square), 12 (circle), 16 (triangle), or 24 (diamond) h.  
 416 Figure presents data (smaller symbols) and means (bigger symbols) from exponential or pre-stationary phase of  
 417 growth. Blue solid line shows single phase exponential decay fit for data from each strain and growth phase, with fit  
 418 parameters presented. Different lowercase letters indicate statistically significant differences between the fit models  
 419 for different strains within a given phase of growth. Different uppercase letters indicate statistically significant  
 420 differences between the fit models for different phases of growth within a given strain (ANOVA;  $p < 0.05$ ).

421

422 **Effective absorption cross section of PSII of picocyanobacteria**

423 The effective absorption cross section of PSII ( $\sigma_{PSII}'$ ,  $\text{nm}^2 \text{ quanta}^{-1}$ ), was estimated using  
424 FRRf induction curves using  $\text{Ex}_{590\text{nm}}$  (orange) excitation, for two PC-rich (056, 077) and two PE-  
425 rich (048, 127) cultures of *Synechococcus* sp. grown at 30, 90, 180, 300, 600, or 900 peak PAR  
426  $\mu\text{mol photons m}^{-2}\text{s}^{-1}$  ( $\mu\text{E}$ ); and photoperiods of 8, 12, 16, or 24 h (Fig. 7). The  $\sigma_{PSII}'$  measured  
427 under diel peak PAR growth light under  $\text{Ex}_{445\text{nm}}$  (blue) excitation vs. cumulative diel photon  
428 dose is shown in Supporting Information (Fig. S8, Table S12).

429 All strains showed consistent patterns of sharp, exponential decay of effective absorption  
430 cross section for PSII photochemistry vs. cumulative diel photon doses, across different  
431 combinations of photoperiod and peak PAR (Fig. 7A). Although all strains showed this response  
432 pattern, the exponential decay fits differed significantly among two PC-rich strains and PE-  
433 rich\_048 strains during their exponential phase of growth (ANOVA,  $p < 0.05$ ; Table S11). PE-  
434 rich strains showed higher  $\sigma_{PSII}'$  under low cumulative diel photon dose ( $y_0$  about 0.8 and  $y_f$   
435 about 4) than did PC-rich strains. During pre-stationary phase this response dampens in the PC-  
436 rich strains but persists in the PE-rich strains (Table S11).  $\sigma_{PSII}'$  for the PE-rich strains during  
437 pre-stationary phase of growth still remain higher ( $y_f$  between 2.3 – 3.0) than in the PC-rich  
438 strains ( $y_f$  between 1.4 – 1.7) even as cumulative diel photon dose increases. Model fits from  
439 different phases of growth differed within a given strain, with the exception of PE-rich\_048  
440 (ANOVA;  $p < 0.05$ , Table S11).



441

442 **Fig. 7. (A)** Effective absorption cross section of PSII ( $\sigma_{\text{PSII}'}$ ;  $\text{nm}^2 \text{ quanta}^{-1}$ ) measured under diel peak PAR growth  
 443 light vs. cumulative diel PAR ( $\mu\text{mol photons m}^{-2} \text{ d}^{-1}$ ); blue solid line shows single phase exponential decay fit for  
 444 data from each strain and growth phase. **(B)** Changes of  $\sigma_{\text{PSII}'}$  measured under diel peak PAR growth light vs. the  
 445 ratio of sum of  $\mu\text{g}$  phycobilins (PE, PC, APC protein, Phycobiliprotein) to  $\mu\text{g}$  Chl *a*; blue solid line shows linear  
 446 model fit for data from each strain and growth phase.  $\sigma_{\text{PSII}'}$  was estimated using FRRf induction curves with  
 447 excitation of phycobilisomes (Ex<sub>590nm</sub>, orange), for two PC-rich cultures (056; dark green, 077; light green) and two  
 448 PE-rich cultures (048; light red, 127; dark red) of *Synechococcus* sp. grown at 30 (dark gray), 90 (light gray), 180  
 449 (purple), 300 (red), 600 (orange), or 900 (yellow) peak PAR  $\mu\text{mol photons m}^{-2} \text{ s}^{-1}$  ( $\mu\text{E}$ ); and photoperiods of 8  
 450 (square), 12 (circle), 16 (triangle), or 24 (diamond) h. Figure presents data (smaller symbols) and means (bigger  
 451 symbols) from exponential or pre-stationary phase of growth. Different lowercase letters indicate statistically  
 452 significant differences between the fit models for different strains within a given phase of growth. Different

453 uppercase letters indicate statistically significant differences between the fit models for different phases of growth  
454 within a given strain ( $p < 0.05$ ).

455

456 Effective absorption cross section of PSII ( $\sigma_{PSII}'$ ; nm<sup>2</sup> quanta<sup>-1</sup>), measured under diel peak  
457 PAR growth light with Ex<sub>590nm</sub> (orange) excitation through phycobilisome absorbance (Fig. 7B)  
458 shows positive linear correlations with the Phycobiliprotein to Chl *a* ratio, although strains in  
459 exponential growth show significant scatter around this positive relation, likely related to  
460 regulatory control of  $\sigma_{PSII}'$  under different measurement PAR, beyond pigment composition.  
461 Under pre-stationary phase the relationship between  $\sigma_{PSII}'$  and Phycobiliprotein to Chl *a* ratio  
462 was more consistent, suggesting increased reliance upon compositional regulation to control light  
463 delivery to PSII, as opposed to shorter-term physiological regulation under changing light. The  
464 linear fits of  $\sigma_{PSII}'$  vs. Phycobiliprotein to Chl *a* ratio also vary significantly between PC-  
465 rich\_077 and two PE-rich strains during their exponential phase of growth. During pre-stationary  
466 phase we noted significant differences between two PC-rich strains and PE-rich\_048. Moreover,  
467 significant differences between the fit models for varying phases of growth were noted for PC-  
468 rich strains 056 and 077 (*t*-test;  $p < 0.05$ , Table S14).

469 Changes in effective absorption cross section of PSII ( $\sigma_{PSII}$ ; nm<sup>2</sup> quanta<sup>-1</sup>) measured in the  
470 dark with Ex<sub>590nm</sub> (orange) excitation vs. Phycobiliprotein to Chl *a* ratio (Fig. S9A, Table S15)  
471 and  $\sigma_{PSII}'$  measured under diel peak PAR growth light under Ex<sub>445nm</sub> (blue) excitation  
472 vs. Phycobiliprotein to Chl *a* ratio (Fig. S9B and Table S13) are shown in Supporting  
473 Information.

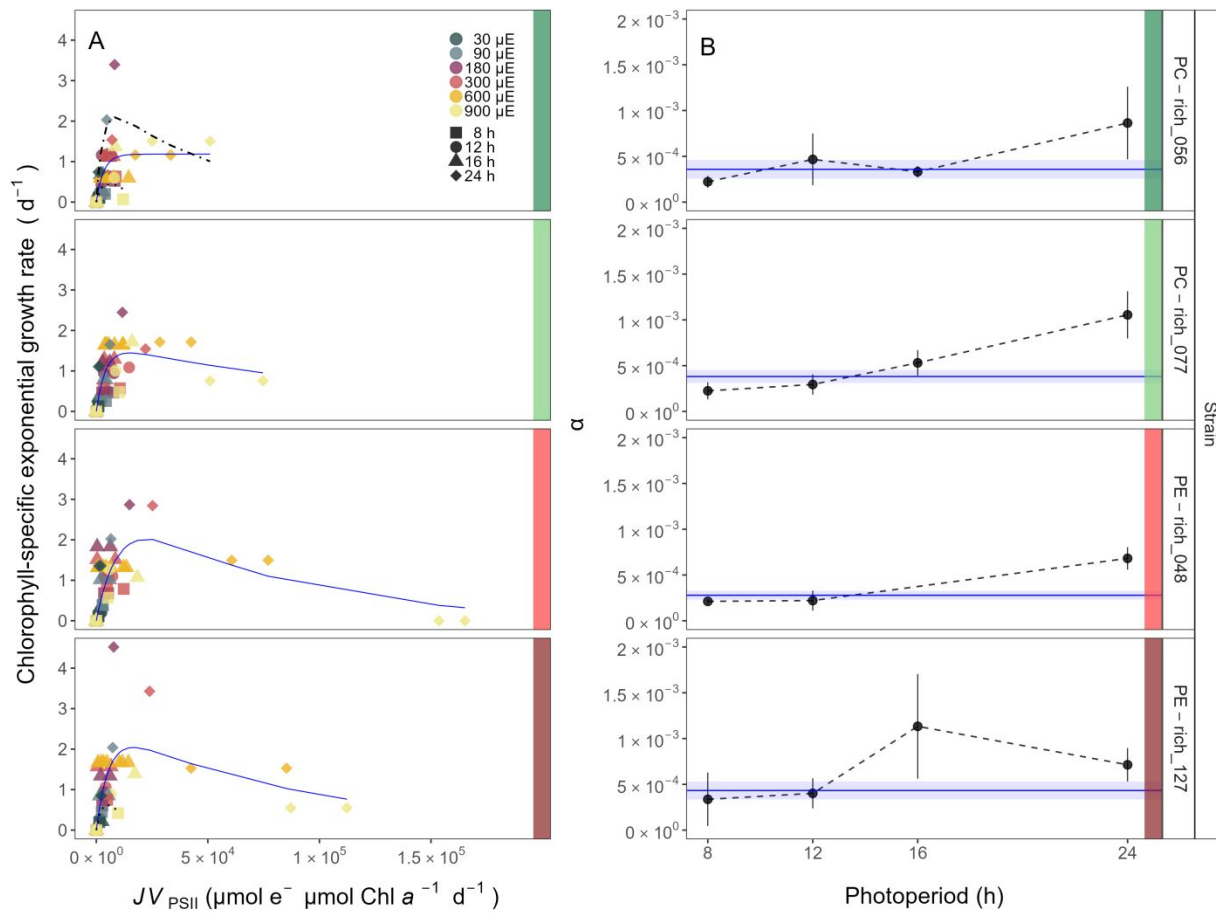
474

#### 475    **Growth rates vs. cumulative diel PSII electron flux**

476       Chlorophyll-specific exponential growth rates ( $d^{-1}$ ), within each strain, show fairly  
477       consistent saturating responses to increasing cumulative diel PSII electron flux ( $JV_{PSII}$ ;  $\mu\text{mol e}^-$   
478        $\mu\text{mol Chl } a^{-1} d^{-1}$ ) estimated under diel peak PAR growth light, and estimated using FRRf  
479       induction curves with excitation of chlorophyll (Ex<sub>445nm</sub>, blue), although photoperiod (Fig. 8A,  
480       Table S7) and peak PAR (Fig. S10, Table S8) retained a secondary influence on achieved growth  
481       responses for some growth conditions.

482       A three parameter model fit of (Harrison and Platt 1986) vs. cumulative diel PSII electron  
483       flux ( $JV_{PSII}$ ;  $\mu\text{mol e}^- \mu\text{mol Chl } a^{-1} d^{-1}$ ) for two PC-rich and two PE-rich cultures of  
484       *Synechococcus* sp. showed no significant differences between fits of the pooled data vs. fits for  
485       different photoperiods (8, 12, 16, or 24 h; ANOVA,  $p < 0.05$ ), with exception of 8 and 24 h  
486       photoperiod for PC-rich\_056 and 8 h photoperiod for PE-rich\_127 strains (ANOVA,  $p > 0.05$ ;  
487       Table S7).

488       Alpha parameters of the initial rise of growth rate ( $\alpha$ ) vs. cumulative diel  $JV_{PSII}$  reflect the  
489       yield of growth from electron transport. Alpha data pooled for each photoperiod showed an  
490       increase across increasing photoperiods for each strain except for PE-rich\_0127. The highest  
491       increase (>2-fold) of  $\alpha$  from the lowest to the highest photoperiod was recorded for PC-rich\_077  
492       (Fig. 8B).



493

494 **Fig. 8.** (A) Chlorophyll-specific exponential growth rates ( $d^{-1}$ ) vs. cumulative diel PSII electron flux ( $JV_{PSII}$ ;  $\mu\text{mol e}^-$   
 495  $\mu\text{mol Chl } a^{-1} d^{-1}$ ) measured under diel peak PAR growth light. Growth rates ( $\pm$  SE falling within symbols) were  
 496 estimated from logistic fits of chlorophyll proxy  $OD_{680} - OD_{720}$  ( $\Delta OD$ ) vs. elapsed time (Fig. S3B).  $JV_{PSII}$  was  
 497 estimated using FRRf induction curves with excitation of chlorophyll ( $Ex_{445\text{nm}}$ , blue), for two PC-rich cultures (056;  
 498 dark green, 077; light green) and two PE-rich cultures (048; light red, 127; dark red) of *Synechococcus* sp. grown at  
 499 30 (dark gray), 90 (light gray), 180 (purple), 300 (red), 600 (orange), or 900 (yellow) peak PAR  $\mu\text{mol photons}$   
 500  $\text{m}^{-2}\text{s}^{-1}$  ( $\mu\text{E}$ ); and photoperiods of 8 (square), 12 (circle), 16 (triangle), or 24 (diamond) h. Solid blue line shows a fit  
 501 of the pooled growth rates for each strain, with a three parameter model (Harrison and Platt 1986). We also fit the  
 502 same model separately for 8 (dotted line) and 24 (two dash line) h photoperiods, when they were significantly  
 503 different (ANOVA,  $p < 0.05$ ) from the fit of pooled data. (B) Alpha parameters of the initial rise of growth rate ( $\alpha$ )  
 504 vs. cumulative diel  $JV_{PSII}$ , estimated from data pooled for each photoperiod (points ( $\pm$  SE) connected by dashed  
 505 lines), and estimated for all data across photoperiods (horizontal line  $\pm$  SE), for each strain.

506

507 **Discussion**508 **Photic regimes - implications for picocyanobacteria growth and distribution**

509 Light regimes, including photoperiod, and peak PAR, are major factors affecting the  
510 distribution and seasonality of phytoplankters (Erga and Heimdal 1984). Changes in photoperiod  
511 trigger acclimation responses, shaping the temporal dynamics and community structure of  
512 phytoplankton (Theus et al. 2022; Longobardi et al. 2022). Each tested picocyanobacterial strain  
513 showed influences of photoperiod upon the responses of growth rate to cumulative diel PUR  
514 (Fig. 5) and PAR (Fig. S5). To our surprise, increasing photoperiod increased the ranges of  
515 responses to PAR and PUR. Both the PC-rich and the PE-rich strains of *Synechococcus* sp.  
516 exhibited their highest initial responses of growth to increasing PUR and PAR (alpha, (Fig. 5B),  
517 Fig. S5B), and their fastest growth rates under continuous light (24 h photoperiod), consistent  
518 with some other strains (Jacob-Lopes et al. 2009; Klepacz-Smólka et al. 2020). Yet, 24 h  
519 photoperiod also exacerbated eventual photoinhibition under excess cumulative diel PUR and  
520 PAR. Our four temperate strains do not currently experience direct selective pressures to exploit  
521 a continuous 24 photoperiod (Brand and Guillard 1981), so achieving maximum growth under a  
522 24 h photoperiod rather suggests lack of a requirement for a dark period, and lack of requirement  
523 for a regular photoperiod. Coastal phytoplankton strains are selected to exploit instantaneous  
524 light (Brand and Guillard 1981), of whatever duration, to cope with fluctuating light and  
525 nutrients in coastal environments (MacIntyre et al. 2000; Litchman et al. 2009), leading to a  
526 pleiotropic capacity for exploiting continuous light. *Synechococcus* assemblages in coastal areas  
527 would tend to be dominated by PC-rich strains by virtue of the higher turbidity of these areas  
528 relative to the open ocean, perhaps regardless of photoperiod. However, the ability of both PC-

529 rich and PE-rich coastal picocyanobacteria to exploit continuous light means they could,  
530 potentially, grow rapidly at higher latitudes, in future warmer polar summer water.

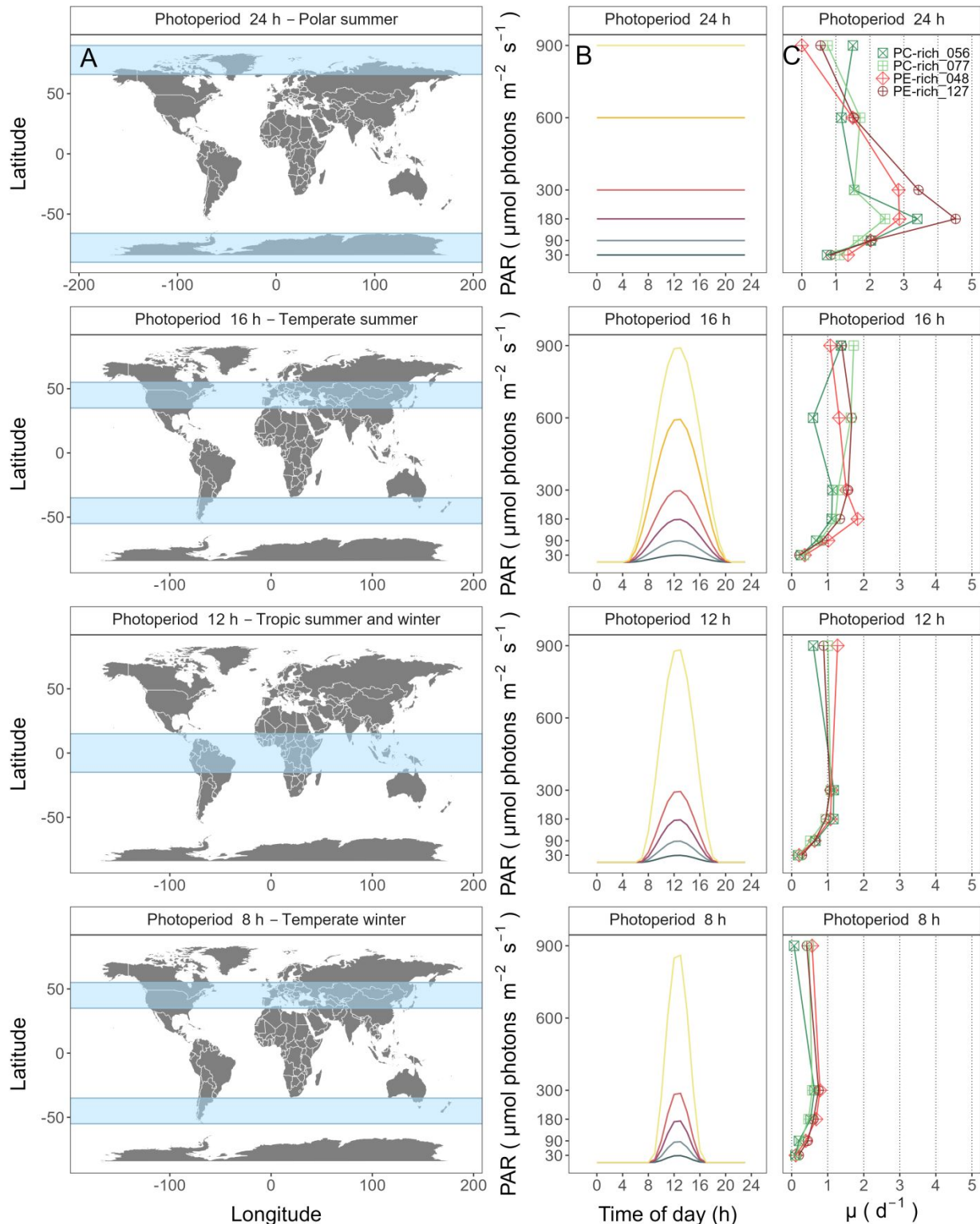
531 Light level is another key driver of picocyanobacteria productivity (Pick 1991; Six et al.  
532 2007; Aguilera et al. 2023). The spatial and temporal distribution of PAR within aquatic  
533 ecosystems is influenced by solar angle, water depth, water clarity, and the presence of light-  
534 absorbing substances such as dissolved organic matter (Morel 1978, 1988) and phytoplankton  
535 cells themselves. PUR then represents the light potentially available for phytoplankton to  
536 photosynthesize. PUR is always smaller than PAR ( $\text{PUR} < \text{PAR}$ ), and depends on the spectral  
537 composition of the PAR, versus the phytoplankton pigment composition, determining cellular  
538 spectral absorption (Morel 1978), which changes depending upon taxa, growth conditions and  
539 the phase of growth.

540 PE-rich and PC-rich *Synechococcus* sp. strains show distinct growth responses to  
541 cumulative diel photon dose, depending upon the peak PAR or PUR of the applied photoregime  
542 (Fig. 5). Chlorophyll-specific exponential growth rates of the PE-rich and PC-rich  
543 *Synechococcus* sp. strains increased with increasing light levels, to a plateau in the range of 180  
544 – 300  $\mu\text{mol photons m}^{-2}\text{s}^{-1}$ . Growth above 600  $\mu\text{mol photons m}^{-2}\text{s}^{-1}$  occurred with a growth  
545 yield per cumulative diel photon lower than under moderate light, particularly when combined  
546 with short 8 h or long 24 h photoperiods. Even though PE-rich *Synechococcus* sp. are more  
547 adapted to lower-light conditions deeper in the water column (Stomp et al. 2007), our findings  
548 show that PE-rich strains will grow under higher irradiance, which is generally contradictory to  
549 previous literature reports (Vörös et al. 1998; Moser et al. 2009). Observations that PE-rich  
550 picocyanobacteria may be better adapted for lower light may be more a consequence of light  
551 quality, rather than the light quantity (Hauschild et al. 1991; Pick 1991).

552        The maximum growth rate of *Synechococcus* sp. PE-rich\_127 strain under 22°C, 24 h  
553        photoperiod and peak PAR of 180  $\mu\text{mol photons m}^{-2}\text{s}^{-1}$  was  $4.5 \text{ d}^{-1}$  ( $\mu = 0.187 \text{ h}^{-1}$ ),  
554        corresponding to a doubling time of 3.7 h (Fig. 5); faster than previously reported for marine  
555        picocyanobacteria, and indeed faster than for the model freshwater cyanobacteria *Synechococcus*  
556        sp. PCC6301 (doubling time of 4.5-5 h under 38°C, constant illumination and 250  $\mu\text{mol photons}$   
557         $\text{m}^{-2}\text{s}^{-1}$ ) (Sakamoto and Bryant 1999), or *Synechocystis* sp. PCC 6803 (doubling time of 4.3 h  
558        under 30°C and 120  $\mu\text{mol photons m}^{-2}\text{s}^{-1}$ ) (van Alphen et al. 2018). The fastest growth rate as  
559        yet achieved for any phytoplankton was in a genetically modified green algae *Picochlorum celeri*,  
560        with a maximum of about  $6.7 \text{ d}^{-1}$  and ~2.5 h doubling time (under 30°C, constant illumination,  
561        and 900  $\mu\text{mol photons m}^{-2}\text{s}^{-1}$ ) (Weissman et al. 2018). The Baltic *Synechococcus* sp. strains, not  
562        genetically modified, preferred 24 h photoperiod and moderate peak PAR of 180  $\mu\text{mol photons}$   
563         $\text{m}^{-2}\text{s}^{-1}$ , suggesting they could, potentially, thrive in warming polar latitude waters.  
564        *Synechococcus* sp. strains indeed already occur across geographical regions (Śliwińska-  
565        Wilczewska et al. 2018b) with different photic regimes, including polar regions (reviewed by  
566        Velichko et al. (2021)), exceeding latitude 80°S and 80°N. The prolonged daylight hours of polar  
567        summers, coupled with nutrient-rich waters, promote growth of genetically diverse  
568        *Synechococcus* populations (Vincent et al. 2000), contributing significantly to primary  
569        productivity. Gradinger and Lenz (1989) suggested that *Synechococcus*-type picocyanobacteria  
570        may serve as indicator organisms for the advection of warm water masses into polar regions,  
571        important in the context of monitoring upcoming climate changes.

572        The coastal PC-rich and PE-rich strains of *Synechococcus* showed saturation, and then  
573        photoinhibition of growth rates under increasing cumulative diel PUR, although the achieved  
574        estimates of  $\mu_{\max}$ , and the onset of photoinhibition of growth, varied depending upon strain,

575 photoperiod and peak PAR (Fig. 4). The tested strains were generally opportunistic in exploiting  
576 longer photoperiods to achieve faster  $\mu$ , although PE-rich strains suffered strong photoinhibition  
577 of growth under peak PAR above 600  $\mu\text{mol photons m}^{-2}\text{s}^{-1}$  and 24 h photoperiod (Fig. 5),  
578 consistent with the PE-rich strains being better adapted to lower light and deeper parts of the  
579 water column. The least favorable growth conditions for both PE-rich and PC-rich strains of  
580 *Synechococcus* sp. were under high light ( $> 600 \mu\text{mol photons m}^{-2}\text{s}^{-1}$ ) and the shortest  
581 photoperiod (8 h), even though the cumulative diel PUR dose was equivalent to conditions where  
582 the light intensity was lower, and the photoperiod was longer. Thus, these Baltic  
583 picocyanobacteria are prone to photoinhibition under both the longest, and the shortest,  
584 photoperiod regimes, with flatter growth responses to light under intermediate photoperiods. In  
585 regions and periods with a longer photoperiod, both PC-rich and PE-rich *Synechococcus* sp.  
586 could become dominant species in surface waters but could suffer under shorter photoperiods  
587 (Fig. 9).



588

589 **Fig. 9.** Latitudinal bands, equivalent summer or winter photoperiods, and picocyanobacterial growth responses. **(A)**  
 590 Latitudinal bands corresponding to tested growth photoperiods. **(B)** Tested photoperiod and peak PAR regimes used

591 for growth experiments. (C) Chlorophyll specific exponential growth rates ( $\pm$  SE falling within symbols) for two  
592 PhycoCyanin(PC)-rich cultures (056; dark green, 077; light green) and two PhycoErythrin(PE)-rich cultures (048;  
593 light red, 127; dark red) of *Synechococcus* sp. under tested photoperiod and peak PAR regimes.

594

595 **Photic regimes and growth phase both influence cellular absorbance and light  
596 use**

597 Cyanobacteria growth includes lag, exponential growth, stationary, and death phases  
598 (Reynolds 2006). During the lag phase, cyanobacteria acclimate to the environment and prepare  
599 for active growth by synthesizing essential cellular components. Exponential growth phase is  
600 marked by cell division and biomass accumulation, fueled by nutrient and light availability. If  
601 growth is limited by declining nutrients, by light, or by accumulation of inhibitory factors, algae  
602 enter stationary phase, characterized by a balance between cell division and death, leading to a  
603 plateau in population. The death phase occurs when cyanobacteria cell death outruns division,  
604 leading to net decomposition, contributing to nutrient recycling in aquatic ecosystems (Reynolds  
605 2006). Moreover, Schuurmans et al. (2017) proposed an additional phase between the  
606 exponential and stationary phases of picocyanobacteria growth, which is often neglected in  
607 physiological studies. Herein, we summarize the results obtained both in the exponential phase  
608 of growth and after the transition to the pre-stationary and stationary growth phases.

609 Under nutrient replete exponential growth the picocyanobacterial strains show an  
610 exponential decline in PUR/PAR ratio versus cumulative diel photon doses. Thus, under nutrient  
611 repletion the picocyanobacteria adjust pigment composition to match light conditions (Fig. 6). In  
612 addition to chlorophyll *a*, picocyanobacteria use phycobilins, including phycocyanin (harvesting  
613 red light at 620 nm) and phycoerythrin (harvesting yellow light at 570 nm), as accessory  
614 pigments to enhance light harvesting efficiency. Picocyanobacteria enhance phycobilin

615 production to compensate for limited irradiance, thereby optimizing their photosynthetic  
616 capabilities (Śliwińska-Wilczewska et al. 2018a) and increasing their PUR/PAR. During the pre-  
617 stationary phase, the PE-rich strains lose these capabilities and the relative absorbance of PE  
618 peak was much lower, which would not be expected if light was limiting, as cell density  
619 increased, again suggesting that nitrogen could be the limiting factor leading to entry into pre-  
620 stationary and stationary phase.

621 The effective absorption cross section for photochemistry of PSII in the light ( $\sigma_{PSII}'$ )  
622 comprises the probability of light capture by PSII and the quantum yield for subsequent  
623 photochemistry. PC-rich and PE-rich strains of *Synechococcus* again show consistent patterns of  
624 an exponential decay to a plateau with increasing cumulative diel PAR doses, for  $\sigma_{PSII}'$  ( $\text{nm}^2$   
625 quanta $^{-1}$ , measured under diel peak PAR growth light under Ex<sub>590nm</sub> (orange) excitation), without  
626 detectable influences of photoperiod, nor of peak PAR (Fig. 7A).  $\sigma_{PSII}'$  excited through  
627 chlorophyll absorbance at 445 nm was, in contrast, consistently small across strains and growth  
628 conditions (Fig. S8, Fig. S9), since in cyanobacteria the number of chlorophyll serving each PSII  
629 is nearly fixed (Xu et al. 2018).  $\sigma_{PSII}'$  excited through phycobilisome absorbance at 590 nm  
630 shows, as expected, a positive correlation with Phycobiliprotein:Chl *a*. Growth under low  
631 cumulative diel PAR results in an increased Phycobiliprotein:Chl *a*, as the picocyanobacteria  
632 allocate protein resources towards phycobiliprotein-mediated light capture (Beale 1994;  
633 Stadnichuk et al. 2015; Chakdar and Pabbi 2016). PC-rich and PE-rich strains of *Synechococcus*  
634 sp. in exponential growth nonetheless show significant scatter around this pattern, likely related  
635 to regulatory control of  $\sigma_{PSII}'$ , beyond pigment composition. In pre-stationary phase  $\sigma_{PSII}'$   
636 vs. Phycobiliprotein:Chl *a* was better aligned, suggesting reliance upon fixed compositional

637 regulation of phycobiliprotein content to control light delivery to PSII, as opposed to shorter-  
638 term regulation.

639 A 16S rRNA gene phylogeny (amplicon average 1385 bp) placed the tested strains in order  
640 Synechococcales and family Synechoccaceae, within the cluster 5 picocyanobacterial lineage, in  
641 sub-cluster 5.2 together with other freshwater, brackish and halotolerant strains, separate from  
642 marine sub-clusters 5.1 and 5.3 (Fig. 1S). The 16S rRNA of the strains showed ~100% identity  
643 with strains assigned to *Synechococcus* spp. or to *Cyanobium* spp. It is worth emphasizing that  
644 light capture and light absorption abilities differed significantly among these tested strains (Six et  
645 al. 2021). The PE-rich strains show a much higher PUR/PAR ratio under low cumulative diel  
646 photon doses during exponential phase, but decay towards a plateau and reach a similar value to  
647 the PC-rich strains as cumulative diel photon dose increases. Thus, the PE-rich strains in  
648 exponential phase demonstrated higher ability to modulate light absorbance capacity, whereas  
649 PC-rich strains retained a more stable PUR/PAR across cumulative diel photon doses. What is  
650 more, during exponential phase, the PE-rich strains show a much higher  $\sigma_{PSII}'$  under low  
651 cumulative diel photon dose, and their  $\sigma_{PSII}'$  remains higher than the PC-rich strains, even as  
652 cumulative diel photon dose increases. Hence, PE-rich strains exhibit higher light harvesting  
653 efficiency, at the expense of susceptibility to higher light levels, particularly under the shortest  
654 (8h) and longest (24h) photoperiods.

655 *Synechococcus* exhibits remarkable acclimation even within a given strain to different  
656 environmental conditions (Śliwińska-Wilczewska et al. 2018a, 2020; Aguilera et al. 2023).  
657 Under high cumulative diel photon dose, *Synechococcus* employs photoprotective mechanisms  
658 to prevent the harmful effects of excess light energy. These include the dissipation of excess  
659 energy as heat via non-photochemical quenching (NPQ) and the regulation of phycobilisome

660 antenna pigments, to balance light absorption and energy transfer. In contrast, under conditions  
661 of low cumulative diel PAR dose, *Synechococcus* sp. increases the expression of light-harvesting  
662 complexes to enhance light absorption (Fig. 6) and capture (Fig. 7).

663 Available photic regimes, combining photoperiod and peak PAR, may influence the  
664 occurrences of PC-rich and PE-rich picocyanobacterial phenotypes. Nitrogen (N) is an essential  
665 element for cyanobacteria, while the N costs to produce photosynthetic pigments varies. The  
666 molecular weight of the two phycoerythrin (PE; phycoerythrobilin) subunits is about 20,000 and  
667 18,300 g mol<sup>-1</sup>, while the two phycocyanin (PC; phycocyanobilin) subunits are about 17,600 and  
668 16,300 g mol<sup>-1</sup>, and allophycocyanin (APC) is lower still, about 16,000 g mol<sup>-1</sup> (Bennett and  
669 Bogorad 1971). It follows that N-cost of producing PE is higher than that of PC, even though  
670 PE-rich picocyanobacteria capture light better than PC-rich phenotypes (Fig. 6; Fig. 7. Our  
671 results confirm that PE-rich strains are stronger light-harvesting competitors, while the PC-rich  
672 strains have lower N-quotients for their phycobilin light capture system.

673

#### 674 **Photic regimes - implications for cumulative diel PSII electron flux**

675 Algal dynamics respond rapidly to changes in environmental conditions (Connor 2018).  
676 We used Fast Repetition Rate fluorometry (FRRf; Fig. 3) (Kolber et al. 1998) to generate an  
677 index of PSII electron transport rate per unit volume ( $JV_{PSII}$ ) (Oxborough et al. 2012; Tortell and  
678 Suggett 2021; Berman-Frank et al. 2023), calibrated to absolute rates of electron transport  
679 through parallel measures of oxygen evolution. Across different photic regimes the growth rates,  
680  $\mu$ , of PC-rich and PE-rich picocyanobacteria show fairly consistent saturating responses to  
681 increasing cumulative diel PSII electron flux ( $JV_{PSII}$ ;  $\mu\text{mol e}^- \mu\text{mol Chl } a^{-1} d^{-1}$ ; Fig. 8). As  
682 previously found for diatoms (Li et al. 2017) cumulative diel reductant generation was indeed a

683 better predictor of  $\mu$  than was cumulative diel PUR, although photoperiod and peak PAR retain  
684 some secondary influence on achieved growth responses of the picocyanobacteria to  $JV_{PSII}$ .

685

## 686 **Conclusions**

687 Coastal picocyanobacteria show differing growth responses to photoperiod and light level,  
688 even under combinations giving equivalent cumulative diel PUR. Both PE-rich and PC-rich  
689 strains of *Synechococcus* sp., grew fastest under moderate light and a 24 h photoperiod.  
690 Consequently, these coastal strains from *Synechococcus* cluster 5.2 show potential to emerge as  
691 components of the phytoplankton during the Arctic or Antarctic summer under future, warmed,  
692 polar regions. In optimal conditions (24 h of photoperiod and a peak PAR of 180  $\mu\text{mol photons}$   
693  $\text{m}^{-2}\text{s}^{-1}$  and only 22°C), one of the PE-rich *Synechococcus* sp., reached a chlorophyll-specific  
694 exponential growth rate of 4.5  $\text{d}^{-1}$  (3.7 h doubling time), a record for a cyanobacteria. PE-rich  
695 strains in the exponential phase of growth also demonstrated high ability to modulate their  
696 PUR/PAR ratio by adjusting pigment composition, giving an advantage in the competition for  
697 light. However, based on the present study the PE-rich strains are more susceptible to  
698 photoinhibition of growth. We determined that growth yields of PC-rich and PE-rich  
699 picocyanobacteria are well predicted by cumulative diel PSII electron fluxes, across different  
700 photic regimes. PE-rich phenotypes of picocyanobacteria currently predominate in abundance  
701 and genetic diversity in the Baltic Sea (Aguilera et al. 2023). This dominance may be the result  
702 of eutrophication in the Baltic Sea, providing higher nitrogen for phycobiliprotein synthesis, and  
703 leading to lower light even in near-surface waters. Our results suggest possible expansion of the  
704 range of picocyanobacteria to new photic regimes in a warmed future and indicate that PE-rich

705 *Synechococcus* sp. may be a dominant component of picophytoplankton in nutrient-rich  
706 environments.

707

708 **Additional Supporting Information may be found in the online version of this article.**

709

710 **Authors Contribution Statement:** S.S-W. designed the study with input from D.A.C. M.K.  
711 estimated the transition point between exponential and pre-stationary phase of growth. M.S.  
712 ensured the proper operation of the photobioreactors. A.A. conducted genetic analysis. N.M.O.  
713 solved technical problems related to computer operation and software. S.S-W., M.S., N.M.O.,  
714 D.A.C. contributed to R coding and data analysis. S.S-W. conducted the experiments, created  
715 plots and wrote the manuscript, with support from D.A.C. All authors contributed to the  
716 discussion of the results, supported manuscript preparation, and approved the final submitted  
717 manuscript.

718

719 **Data availability statement**

720 Data supporting this study is available on:

721 <https://github.com/FundyPhytoPhys/BalticPhotoperiod> (public GitHub Repository) and  
722 [https://docs.google.com/spreadsheets/d/1ZXpwR7Gfto-uRzVdXzMpQF4frbrvMLH\\_IyLqonFZRSw/edit#gid=0](https://docs.google.com/spreadsheets/d/1ZXpwR7Gfto-uRzVdXzMpQF4frbrvMLH_IyLqonFZRSw/edit#gid=0) (URL for MetaDataCatalog).

724 Code to perform data processing and analyses is available at

725 <https://github.com/FundyPhytoPhys/BalticPhotoperiod>.

726 16S rRNA sequences used in this study are available in GenBank under the accession  
727 numbers PP034393, PP034394, PP034396 and PP034403.

728

729 **Acknowledgements**

730 We would like to express our sincere gratitude to the two Editors, Ilana Berman-Frank and Elisa  
731 Schaum, and two Reviewers for their efforts reviewing and improving this manuscript. We thank  
732 Maximilian Berthold for the code for the GAM model; Miranda Corkum who maintained  
733 cultures and trained personnel in culture handling; Laurel Genge, and Carlie Barnhill (Mount  
734 Allison students) who assisted with R code. This work was supported by Canada Research Chair  
735 in Phytoplankton Ecophysiology (D.A.C) and Latitude & Light; NSERC of Canada Discovery  
736 Grant (D.A.C).

737

738 **Conflict of Interest**

739 None declared.

740

741 **References**

- 742 Aguilera, A., J. Alegria Zufia, L. Bas Conn, and others. 2023. Ecophysiological analysis reveals  
743 distinct environmental preferences in closely related Baltic Sea picocyanobacteria.  
744 Environmental Microbiology **25**: 1674–1695. doi:10.1111/1462-2920.16384
- 745 Arrigo, K. R. 2014. Sea ice ecosystems. Annual Review of Marine Science **6**: 439–467.  
746 doi:10.1146/annurev-marine-010213-135103
- 747 Beale, S. I. 1994. Biosynthesis of cyanobacterial tetrapyrrole pigments: Hemes, chlorophylls,  
748 and phycobilins, p. 519–558. In D.A. Bryant [ed.], The Molecular Biology of Cyanobacteria.  
749 Springer Netherlands.

- 750 Behrenfeld, M. J., R. T. O'Malley, D. A. Siegel, and others. 2006. Climate-driven trends in  
751 contemporary ocean productivity. *Nature* **444**: 752–755. doi:10.1038/nature05317
- 752 Bennett, A., and L. Bogorad. 1971. Properties of subunits and aggregates of blue-green algal  
753 biliproteins. *Biochemistry* **10**: 3625–3634. doi:10.1021/bi00795a022
- 754 Bennett, A., and L. Bogorad. 1973. Complementary Chromatic Adaptation in a filamentous blue-  
755 green alga. *Journal of Cell Biology* **58**: 419–435. doi:10.1083/jcb.58.2.419
- 756 Berman-Frank, I., D. Campbell, A. Ciotti, and others. 2023. Application of Single Turnover  
757 Active Chlorophyll Fluorescence for Phytoplankton Productivity Measurements. Version 2.0,  
758 June, 26, 2023. Report Scientific Committee on Oceanic Research (SCOR) Working Group 156.
- 759 Boatman, T. G., R. J. Geider, and K. Oxborough. 2019. Improving the accuracy of Single  
760 Turnover Active Fluorometry (STAF) for the estimation of Phytoplankton Primary Productivity  
761 (PhytoPP). *Frontiers in Marine Science* **6**. doi:10.3389/fmars.2019.00319
- 762 Brand, L. E., and R. R. L. Guillard. 1981. The effects of continuous light and light intensity on  
763 the reproduction rates of twenty-two species of marine phytoplankton. *Journal of Experimental  
764 Marine Biology and Ecology* **50**: 119–132. doi:10.1016/0022-0981(81)90045-9
- 765 Chakdar, H., and S. Pabbi. 2016. Cyanobacterial phycobilins: Production, purification, and  
766 regulation, p. 45–69. In P. Shukla [ed.], *Frontier Discoveries and Innovations in Interdisciplinary  
767 Microbiology*. Springer India.
- 768 Christaki, U., S. Jacquet, J. R. Dolan, D. Vaulot, and F. Rassoulzadegan. 1999. Growth and  
769 grazing on *Prochlorococcus* and *Synechococcus* by two marine ciliates. *Limnology and  
770 Oceanography* **44**: 52–61. doi:10.4319/lo.1999.44.1.0052

- 771 Connor, D. 2018. Investigating the use of fast repetition rate fluorometry in understanding algal  
772 physiology in optically complex oceans.
- 773 Elzhov, T. V., K. M. Mullen, A.-N. Spiess, and B. Bolker. 2023. Minpack.lm: R Interface to the  
774 Levenberg-Marquardt Nonlinear Least-Squares Algorithm Found in MINPACK, Plus Support  
775 for Bounds.
- 776 Erga, S. R., and B. R. Heimdal. 1984. Ecological studies on the phytoplankton of Korsfjorden,  
777 western Norway. The dynamics of a spring bloom seen in relation to hydrographical conditions  
778 and light regime. *Journal of Plankton Research* **6**: 67–90. doi:10.1093/plankt/6.1.67
- 779 Falkowski, P., and Z. Kolber. 1993. Estimation of phytoplankton photosynthesis by active  
780 fluorescence. *ICES Marine Science Symposium* **197**: 92–103.
- 781 Field, C. B., M. J. Behrenfeld, J. T. Randerson, and P. Falkowski. 1998. Primary production of  
782 the biosphere: Integrating terrestrial and oceanic components. *Science* **281**: 237–240.  
783 doi:10.1126/science.281.5374.237
- 784 Flombaum, P., J. L. Gallegos, R. A. Gordillo, and others. 2013. Present and future global  
785 distributions of the marine Cyanobacteria *Prochlorococcus* and *Synechococcus*. *Proceedings of*  
786 *the National Academy of Sciences* **110**: 9824–9829. doi:10.1073/pnas.1307701110
- 787 Gradinger, R., and J. Lenz. 1989. Picocyanobacteria in the high Arctic. *Marine Ecology Progress Series*  
788 **52**: 99–101. doi:10.3354/meps052099
- 789 Guillard, R. R. L. 1975. Culture of phytoplankton for feeding marine invertebrates, p. 29–60. *In*  
790 W.L. Smith and M.H. Chanley [eds.], *Culture of Marine Invertebrate Animals: Proceedings —*  
791 *1st Conference on Culture of Marine Invertebrate Animals* Greenport. Springer US.

- 792 Handel, A. 2020. Andreas Handel - Custom Word formatting using R Markdown.
- 793 Harrison, W. G., and T. Platt. 1986. Photosynthesis-irradiance relationships in polar and  
794 temperate phytoplankton populations. *Polar biology* **5**: 153–164.
- 795 Hauschild, C. A., H. J. G. McMurter, and F. R. Pick. 1991. Effect of Spectral Quality on Growth  
796 and Pigmentation of Picocyanobacteria1. *Journal of Phycology* **27**: 698–702. doi:10.1111/j.0022-  
797 3646.1991.00698.x
- 798 Haverkamp, T. H. A., D. Schouten, M. Doeleman, U. Wollenzien, J. Huisman, and L. J. Stal.  
799 2009. Colorful microdiversity of *Synechococcus* strains (picocyanobacteria) isolated from the  
800 Baltic Sea. *The ISME Journal* **3**: 397–408. doi:10.1038/ismej.2008.118
- 801 Hirata, T., N. J. Hardman-Mountford, R. J. W. Brewin, and others. 2011. Synoptic relationships  
802 between surface Chlorophyll-*a* and diagnostic pigments specific to phytoplankton functional  
803 types. *Biogeosciences* **8**: 311–327. doi:10.5194/bg-8-311-2011
- 804 Holtrop, T., J. Huisman, M. Stomp, and others. 2021. Vibrational modes of water predict spectral  
805 niches for photosynthesis in lakes and oceans. *Nature Ecology & Evolution* **5**: 55–66.  
806 doi:10.1038/s41559-020-01330-x
- 807 Huisman, J., M. Arrayás, U. Ebert, and B. Sommeijer. 2002. How do sinking phytoplankton  
808 species manage to persist? *The American Naturalist* **159**: 245–254. doi:10.1086/338511
- 809 Jacob-Lopes, E., C. H. G. Scoparo, L. M. C. F. Lacerda, and T. T. Franco. 2009. Effect of light  
810 cycles (night/day) on CO<sub>2</sub> fixation and biomass production by microalgae in photobioreactors.  
811 *Chemical Engineering and Processing: Process Intensification* **48**: 306–310.  
812 doi:10.1016/j.cep.2008.04.007

- 813 Jávorfi, T., J. Erostyák, J. Gál, A. Buzády, L. Menczel, G. Garab, and K. Razi Naqvi. 2006.
- 814 Quantitative spectrophotometry using integrating cavities. Journal of Photochemistry and
- 815 Photobiology B: Biology **82**: 127–131. doi:10.1016/j.jphotobiol.2005.10.002
- 816 Katoh, K., J. Rozewicki, and K. D. Yamada. 2019. MAFFT online service: Multiple sequence
- 817 alignment, interactive sequence choice and visualization. Briefings in Bioinformatics **20**: 1160–
- 818 1166. doi:10.1093/bib/bbx108
- 819 Klepacz-Smólka, A., D. Pietrzyk, R. Szeląg, P. Głuscz, M. Daroch, J. Tang, and S. Ledakowicz.
- 820 2020. Effect of light colour and photoperiod on biomass growth and phycocyanin production by
- 821 *Synechococcus* PCC 6715. Bioresource Technology **313**: 123700.
- 822 doi:10.1016/j.biortech.2020.123700
- 823 Kolber, Z. S., O. Prášil, and P. G. Falkowski. 1998. Measurements of variable chlorophyll
- 824 fluorescence using fast repetition rate techniques: Defining methodology and experimental
- 825 protocols. Biochimica et Biophysica Acta (BBA) - Bioenergetics **1367**: 88–106.
- 826 doi:10.1016/S0005-2728(98)00135-2
- 827 Lane, D. J. 1991. 16S/23S rRNA sequencing. Nucleic acid techniques in bacterial systematics
- 828 115–175.
- 829 LaRoche, J., and B. M. Robicheau. 2022. The Pelagic Light-Dependent Microbiome, p. 395–
- 830 423. In L.J. Stal and M.S. Cretoiu [eds.], The Marine Microbiome. Springer International
- 831 Publishing.

- 832 Li, G., D. Talmy, and D. A. Campbell. 2017. Diatom growth responses to photoperiod and light  
833 are predictable from diel reductant generation. *Journal of Phycology* **53**: 95–107.  
834 doi:10.1111/jpy.12483
- 835 Li, Q., L. Legendre, and N. Jiao. 2015. Phytoplankton responses to nitrogen and iron limitation  
836 in the tropical and subtropical Pacific Ocean. *Journal of Plankton Research* **37**: 306–319.  
837 doi:10.1093/plankt/fbv008
- 838 Li, W. K. W. 1995. Composition of ultraphytoplankton in the central North Atlantic. *Marine  
839 Ecology Progress Series* **122**: 1–8.
- 840 Ligges, U., T. Short, P. Kienzle, and others. 2024. Signal: Signal Processing.
- 841 Litchman, E., C. A. Klausmeier, and K. Yoshiyama. 2009. Contrasting size evolution in marine  
842 and freshwater diatoms. *Proceedings of the National Academy of Sciences* **106**: 2665–2670.  
843 doi:10.1073/pnas.0810891106
- 844 Longobardi, L., L. Dubroca, F. Margiotta, D. Sarno, and A. Zingone. 2022. Photoperiod-driven  
845 rhythms reveal multi-decadal stability of phytoplankton communities in a highly fluctuating  
846 coastal environment. *Scientific Reports* **12**: 3908. doi:10.1038/s41598-022-07009-6
- 847 MacIntyre, H. L., T. M. Kana, R. J. Geider, H. L. MacIntyre, T. M. Kana, and R. J. Geider. 2000.  
848 The effect of water motion on short-term rates of photosynthesis by marine phytoplankton.  
849 *Trends in Plant Science* **5**: 12–17. doi:10.1016/S1360-1385(99)01504-6
- 850 Moejes, F. W., A. Matuszyńska, K. Adhikari, and others. 2017. A systems-wide understanding  
851 of photosynthetic acclimation in algae and higher plants. *Journal of Experimental Botany* **68**:  
852 2667–2681. doi:10.1093/jxb/erx137

- 853 Morel, A. 1978. Available, usable, and stored radiant energy in relation to marine  
854 photosynthesis. Deep Sea Research **25**: 673–688. doi:10.1016/0146-6291(78)90623-9
- 855 Morel, A. 1988. Optical modeling of the upper ocean in relation to its biogenous matter content  
856 (case I waters). Journal of Geophysical Research: Oceans **93**: 10749–10768.  
857 doi:10.1029/JC093iC09p10749
- 858 Moser, M., C. Callieri, and T. Weisse. 2009. Photosynthetic and growth response of freshwater  
859 picocyanobacteria are strain-specific and sensitive to photoacclimation. Journal of Plankton  
860 Research **31**: 349–357. doi:10.1093/plankt/fbn123
- 861 Nedbal, L., M. Trtílek, J. Červený, O. Komárek, and H. B. Pakrasi. 2008. A photobioreactor  
862 system for precision cultivation of photoautotrophic microorganisms and for high-content  
863 analysis of suspension dynamics. Biotechnology and Bioengineering **100**: 902–910.  
864 doi:10.1002/bit.21833
- 865 Ortmann, A. C., J. E. Lawrence, and C. A. Suttle. 2002. Lysogeny and Lytic Viral Production  
866 during a Bloom of the Cyanobacterium *Synechococcus* spp. Microbial Ecology **43**: 225–231.
- 867 Oxborough, K., and N. R. Baker. 1997. Resolving chlorophyll *a* fluorescence images of  
868 photosynthetic efficiency into photochemical and non-photochemical components – calculation  
869 of qP and Fv-/Fm-; without measuring Fo-; Photosynthesis Research **54**: 135–142.  
870 doi:10.1023/A:1005936823310
- 871 Oxborough, K., C. M. Moore, D. J. Suggett, T. Lawson, H. G. Chan, and R. J. Geider. 2012.  
872 Direct estimation of functional PSII reaction center concentration and PSII electron flux on a

- 873 volume basis: A new approach to the analysis of Fast Repetition Rate fluorometry (FRRf) data.
- 874 Limnology and Oceanography: Methods **10**: 142–154. doi:10.4319/lom.2012.10.142
- 875 Pedersen, T. L. 2024. Patchwork: The Composer of Plots.
- 876 Pick, F. R. 1991. The abundance and composition of freshwater picocyanobacteria in relation to  
877 light penetration. Limnology and Oceanography **36**: 1457–1462. doi:10.4319/lo.1991.36.7.1457
- 878 Posit team. 2022. RStudio: Integrated development environment for r, Posit Software, PBC.
- 879 R Core Team. 2023. R: A language and environment for statistical computing, R Foundation for  
880 Statistical Computing.
- 881 Reynolds, C. S. 2006. The Ecology of Phytoplankton, Cambridge University Press.
- 882 Ryan, J. A., J. M. Ulrich, R. Bennett, and C. Joy. 2024. Xts: eXtensible Time Series.
- 883 Sakamoto, T., and D. A. Bryant. 1999. Nitrate transport and not photoinhibition limits growth of  
884 the freshwater cyanobacterium *Synechococcus* species PCC 6301 at low temperature. Plant  
885 Physiology **119**: 785–794. doi:10.1104/pp.119.2.785
- 886 Schuurmans, R. M., J. C. P. Matthijs, and K. J. Hellingwerf. 2017. Transition from exponential  
887 to linear photoautotrophic growth changes the physiology of *Synechocystis* sp. PCC 6803.  
888 Photosynthesis Research **132**: 69–82. doi:10.1007/s11120-016-0329-8
- 889 Serway, R. A., C. J. Moses, and C. A. Moyer. 2004. Modern Physics, Cengage Learning.
- 890 Six, C., Z. V. Finkel, A. J. Irwin, and D. A. Campbell. 2007. Light variability illuminates niche-  
891 partitioning among marine picocyanobacteria. PLOS ONE **2**: e1341.  
892 doi:10.1371/journal.pone.0001341

- 893 Six, C., M. Ratin, D. Marie, and E. Corre. 2021. Marine *Synechococcus* picocyanobacteria: Light  
894 utilization across latitudes. Proceedings of the National Academy of Sciences **118**: e2111300118.  
895 doi:10.1073/pnas.2111300118
- 896 Śliwińska-Wilczewska, S., A. Cieszyńska, J. Maculewicz, and A. Latała. 2018a.  
897 Ecophysiological characteristics of red, green, and brown strains of the Baltic  
898 picocyanobacterium *Synechococcus* sp. – a laboratory study. Biogeosciences **15**: 6257–6276.  
899 doi:10.5194/bg-15-6257-2018
- 900 Śliwińska-Wilczewska, S., Z. Konarzewska, K. Wiśniewska, and M. Konik. 2020.  
901 Photosynthetic pigments changes of three phenotypes of picocyanobacteria *Synechococcus* sp.  
902 Under different light and temperature conditions. Cells **9**: 2030. doi:10.3390/cells9092030
- 903 Śliwińska-Wilczewska, S., J. Maculewicz, A. Barreiro Felpeto, and A. Latała. 2018b.  
904 Allelopathic and bloom-forming picocyanobacteria in a changing world. Toxins **10**: 48.  
905 doi:10.3390/toxins10010048
- 906 Stadnichuk, I. N., P. M. Krasilnikov, and D. V. Zlenko. 2015. Cyanobacterial phycobilisomes  
907 and phycobiliproteins. Microbiology **84**: 101–111. doi:10.1134/S0026261715020150
- 908 Stomp, M., J. Huisman, L. Vörös, F. R. Pick, M. Laamanen, T. Haverkamp, and L. J. Stal. 2007.  
909 Colourful coexistence of red and green picocyanobacteria in lakes and seas. Ecology Letters **10**:  
910 290–298. doi:10.1111/j.1461-0248.2007.01026.x
- 911 Strickland, J. D., and T. R. Parsons. 1972. Practical Hand Book of Seawater Analysis. Fisheries  
912 Research Board of Canada **167 (2nd edition)**: 1–311. doi:DOI: <http://dx.doi.org/10.25607/OBP-1791>

- 914 Theus, M. E., T. J. Layden, N. McWilliams, S. Crafton-Tempel, C. T. Kremer, and S. B. Fey.  
915 2022. Photoperiod influences the shape and scaling of freshwater phytoplankton responses to  
916 light and temperature. *Oikos* **2022**: e08839. doi:10.1111/oik.08839
- 917 Torremorell, A., M. E. Llames, G. L. Pérez, R. Escaray, J. Bustingorry, and H. Zagarese. 2009.  
918 Annual patterns of phytoplankton density and primary production in a large, shallow lake: The  
919 central role of light. *Freshwater Biology* **54**: 437–449. doi:10.1111/j.1365-2427.2008.02119.x
- 920 Tortell, P., and D. J. Suggett. 2021. A user guide for the application of Single Turnover active  
921 chlorophyll fluorescence for phytoplankton productivity measurements. Version 1. Report  
922 Scientific Committee on Oceanic Research (SCOR) Working Group 156.
- 923 van Alphen, P., H. Abedini Najafabadi, F. Branco dos Santos, and K. J. Hellingwerf. 2018.  
924 Increasing the photoautotrophic growth rate of *Synechocystis* sp. PCC 6803 by identifying the  
925 limitations of its cultivation. *Biotechnology Journal* **13**: 1700764. doi:10.1002/biot.201700764
- 926 Velichko, N., S. Smirnova, S. Averina, and A. Pinevich. 2021. A survey of Antarctic  
927 cyanobacteria. *Hydrobiologia* **848**: 2627–2653.
- 928 Vincent, W. F., J. P. Bowman, L. M. Rankin, and T. A. McMeekin. 2000. Phylogenetic diversity  
929 of picocyanobacteria in Arctic and Antarctic ecosystems. *Microbial biosystems: new frontiers.*  
930 Proceedings of the 8th International Symposium on Microbial Ecology 317–322.
- 931 Vörös, L., C. Callieri, K. V.-Balogh, and R. Bertoni. 1998. Freshwater picocyanobacteria along a  
932 trophic gradient and light quality range. *Phytoplankton and Trophic Gradients*. Springer  
933 Netherlands. 117–125.

- 934 Weissman, J. C., M. Likhogrud, D. C. Thomas, W. Fang, D. A. J. Karns, J. W. Chung, R.  
935 Nielsen, and M. C. Posewitz. 2018. High-light selection produces a fast-growing *Picochlorum*  
936 *Celeri*. Algal Research **36**: 17–28. doi:10.1016/j.algal.2018.09.024
- 937 Wickham, H. 2016. Data Analysis, p. 189–201. In H. Wickham [ed.], Ggplot2: Elegant Graphics  
938 for Data Analysis. Springer International Publishing.
- 939 Wood, S. N. 2017. Generalized Additive Models: An Introduction with R, Second Edition, 2nd  
940 ed. Chapman and Hall/CRC.
- 941 Xi, H., S. N. Losa, A. Mangin, and others. 2020. Global retrieval of phytoplankton functional  
942 types based on empirical orthogonal functions using CMEMS GlobColour merged products and  
943 further extension to OLCI data. Remote Sensing of Environment **240**: 111704.  
944 doi:10.1016/j.rse.2020.111704
- 945 Xu, K., J. L. Grant-Burt, N. Donaher, and D. A. Campbell. 2017. Connectivity among  
946 Photosystem II centers in phytoplankters: Patterns and responses. Biochimica et Biophysica Acta  
947 (BBA) - Bioenergetics **1858**: 459–474. doi:10.1016/j.bbabi.2017.03.003
- 948 Xu, K., J. Lavaud, R. Perkins, E. Austen, M. Bonnanfant, and D. A. Campbell. 2018.  
949 Phytoplankton  $\sigma$ PSII and excitation dissipation; implications for estimates of primary  
950 productivity. Frontiers in Marine Science **5**. doi:10.3389/fmars.2018.00281

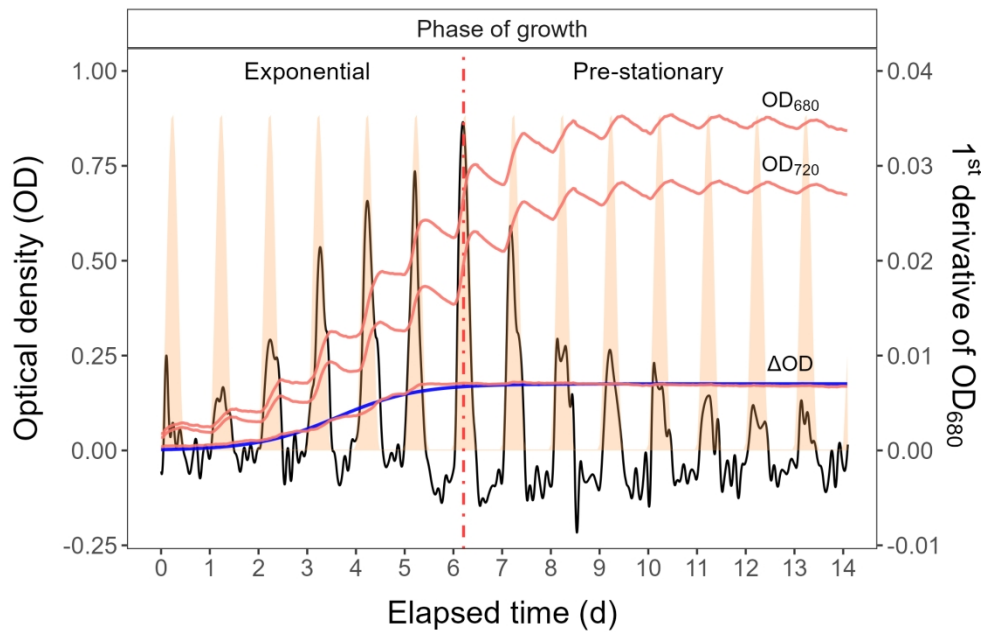


Fig. 1. Example of a growth curve (tracked as OD<sub>720</sub>, OD<sub>680</sub>, or  $\Delta$ OD; red solid lines, left y-axis) of PE-rich culture of *Synechococcus* sp. (048; grown at 180 peak PAR  $\mu\text{mol photons m}^{-2}\text{s}^{-1}$ ; and photoperiods of 12 h) vs. elapsed time (d, x-axis). 1<sup>st</sup> derivative of OD<sub>680</sub> taken over 1 h increments (black solid line, right y-axis); solid blue line shows logistic fits of chlorophyll proxy OD<sub>680</sub> – OD<sub>720</sub> ( $\Delta$ OD) vs. elapsed time. The vertical red dot dash line represents the time when the culture reached the maximum of the 1<sup>st</sup> derivative of OD<sub>680</sub>, or maximum absolute hourly growth (tMaxAHG), taken as the time of transition from exponential to pre-stationary growth phases.

452x290mm (118 x 118 DPI)

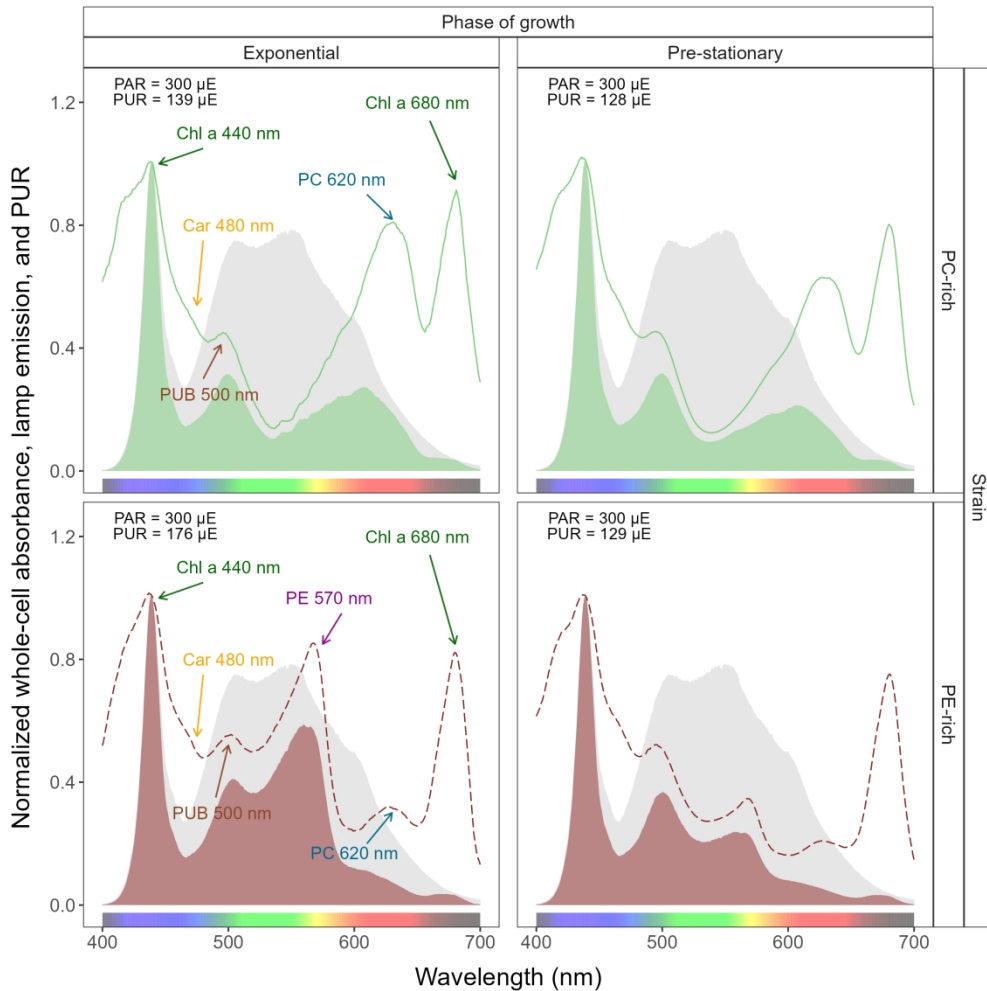


Fig. 2. Whole-cell absorbance spectra of PC-rich (077; solid light green lines) or PE-rich (127; dashed dark red lines) cultures of *Synechococcus* sp. Representative absorbance spectra, normalized to 440 nm (NormA440), were measured from the exponential or pre-stationary phases of growth, together with emission spectra of the white LED lamp used for PAR, normalized to emission at 440 nm (NormEm440, light gray area), in this example PAR was 300  $\mu\text{mol photons m}^{-2}\text{s}^{-1}$ . Estimated Photosynthetically Usable Radiation (PUR) is shown as a darker green area for the PC-rich strain and a darker red area for the PE-rich strain, with PUR given for each culture ( $\mu\text{E} = \mu\text{mol photons m}^{-2}\text{s}^{-1}$ ). Peaks characteristic of known pigments are labeled; Chl a, chlorophyll a; PC, phycocyanin; PE, phycoerythrin; PUB, phycourobilin; Car, carotenoids.

581x581mm (118 x 118 DPI)

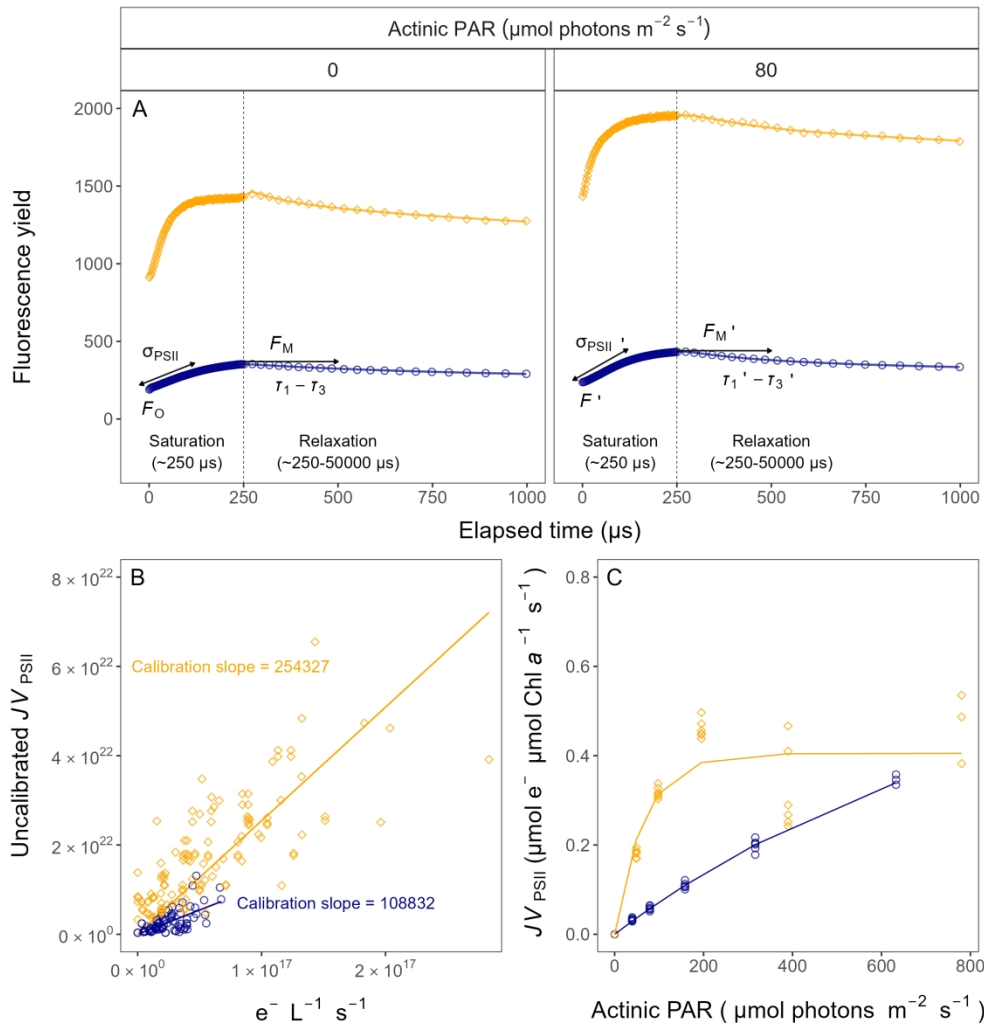


Fig. 3. Single turnover (ST) fluorescence induction by Fast Repetition Rate fluorometry (FRRf). (A) Examples of fluorescence yield vs. elapsed time ( $\mu\text{s}$ ) for PE-rich culture of *Synechococcus* sp. (048) in the dark (dark-relaxed; 0  $\mu\text{mol photons m}^{-2}\text{s}^{-1}$ ) and under actinic PAR (in this example 80  $\mu\text{mol photons m}^{-2}\text{s}^{-1}$ ) using blue LED (Ex445nm; open blue circles) or orange (Ex590nm; open orange diamonds) excitation. The ST technique delivers a series of flashlets for non-intrusive, repeated monitoring of chlorophyll fluorescence parameters (including  $F_0$ ,  $F'$ ,  $F_M$ ,  $F'_M$ ,  $\tau_1 - \tau_3$ ,  $\tau'_1 - \tau'_3$ ,  $\sigma_{\text{PSII}}$ , and  $\sigma_{\text{PSII}'}$ ). (B) Linear regressions of uncalibrated PSII electron flux ( $JV_{\text{PSII}}$ ) vs.  $e^- \text{ L}^{-1} \text{ s}^{-1}$  derived from simultaneously measured oxygen evolution Light Response Curves (LRC) under blue LED (Ex445nm; open blue circles) or orange (Ex590nm; open orange diamonds) excitation. (C) Rapid Light Curve (RLC), fit with a three parameter model (Harrison and Platt 1986), for PSII electron flux ( $JV_{\text{PSII}}$ ;  $\mu\text{mol e}^- \mu\text{mol Chl } a^{-1} \text{ s}^{-1}$ ) vs. actinic PAR measured under blue LED (Ex445nm; open blue circles) or orange (Ex590nm; open orange diamonds) excitation.

613x645mm (118 x 118 DPI)

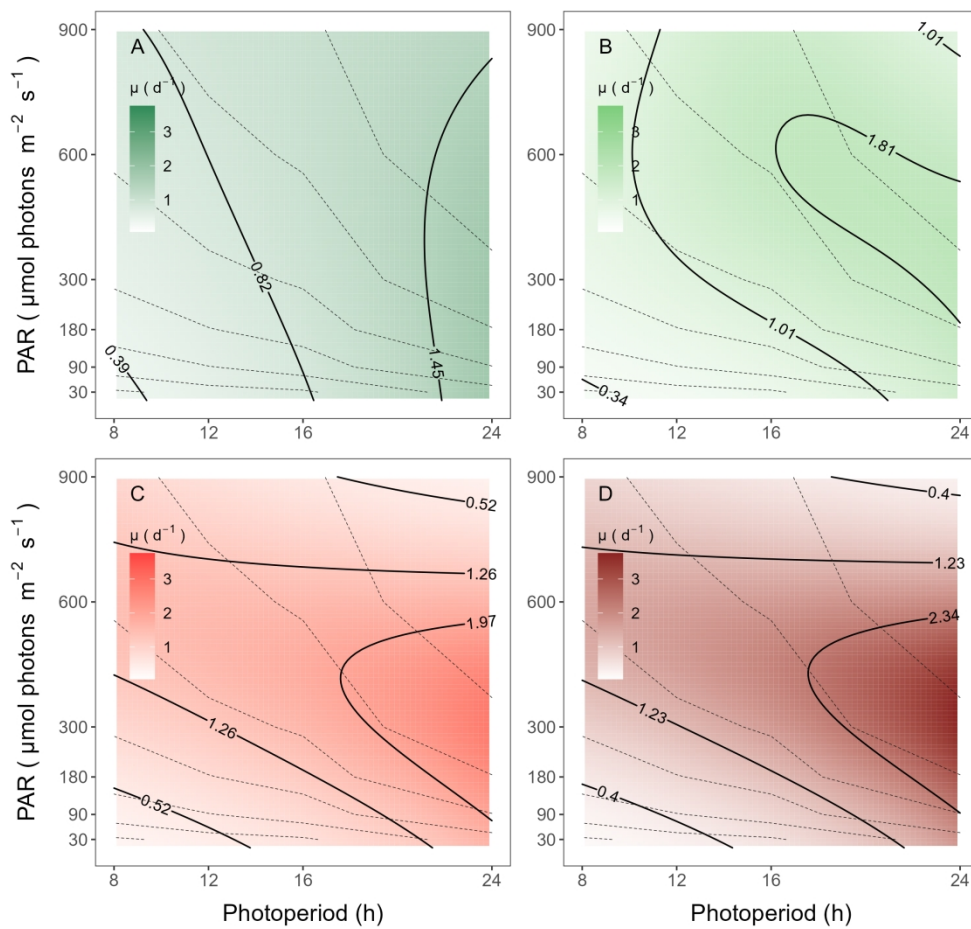


Fig. 4. A contour plot of a Generalized Additive Model (GAM) of chlorophyll-specific growth rates ( $d^{-1}$ ) for two PC-rich cultures: (A) 056, (B) 077 and two PE-rich cultures: (C) 048, (D) 127 of *Synechococcus* sp. grown at 30, 90, 180, 300, 600, or 900 peak PAR  $\mu\text{mol photons m}^{-2}\text{s}^{-1}$ ; and photoperiods of 8, 12, 16, or 24 h. Legends show colour gradients of growth rate ( $\mu; d^{-1}$ ) from no growth (white) to 3.0  $d^{-1}$  (dark green for PC-rich\_056, light green for PC-rich\_077, light red for PE-rich\_048 or dark red for PE-rich\_127 strains). Labeled contour lines indicate the 90%, 50%, and 10% quantiles for achieved growth rate. Dotted lines show isoclines of cumulative diel photon dose ( $\mu\text{mol photons m}^{-2}\text{d}^{-1}$ ).

613x581mm (118 x 118 DPI)

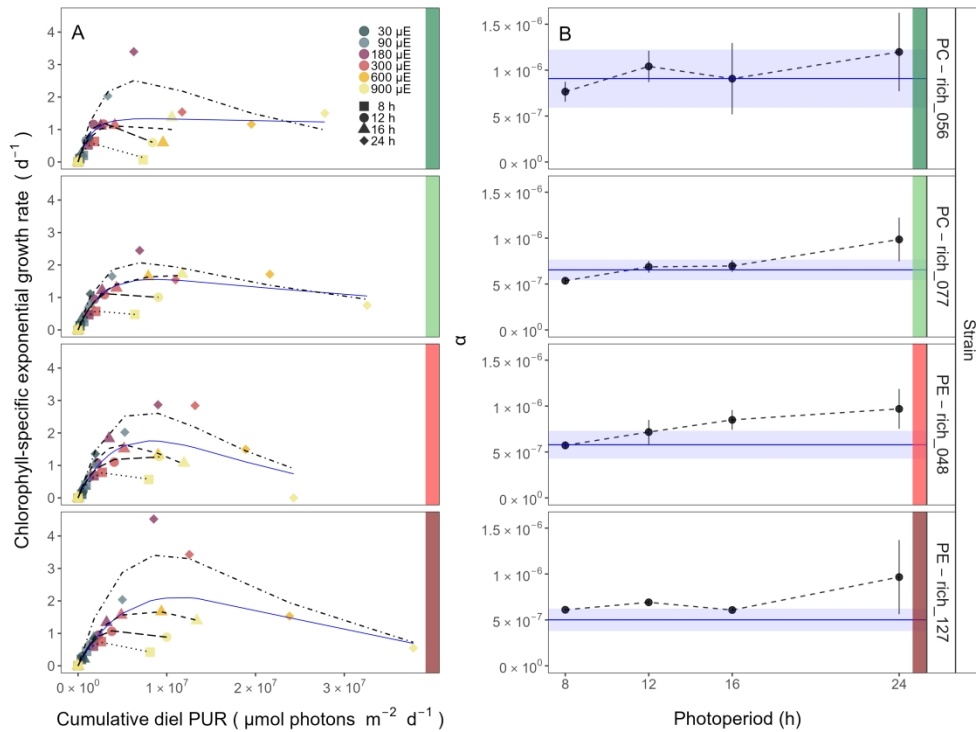


Fig. 5. (A) Chlorophyll-specific exponential growth rates ( $d^{-1}$ ) vs. cumulative diel Photosynthetically Usable Radiation (PUR,  $\mu\text{mol photons m}^{-2} \text{d}^{-1}$ ). Growth rates ( $\pm$  SE falling within symbols) were estimated from logistic fits of chlorophyll proxy OD<sub>680</sub> – OD<sub>720</sub> ( $\Delta$ O<sub>D</sub>) vs. elapsed time (Fig. 1, Fig. S3B), for two PC-rich cultures (056; dark green, 077; light green) and two PE-rich cultures (048; light red, 127; dark red) of *Synechococcus* sp. grown at 30 (dark gray), 90 (light gray), 180 (purple), 300 (red), 600 (orange), or 900 (yellow) peak PAR  $\mu\text{mol photons m}^{-2} \text{s}^{-1}$  ( $\mu\text{E}$ ); and photoperiods of 8 (square), 12 (circle), 16 (triangle), or 24 (diamond) h. Solid blue line shows a fit of the pooled growth rates through photoperiods for each strain, with a three parameter model (Harrison and Platt 1986). We also fit the same model separately for 8 (dotted line), 12 (long dash line), 16 (dashed line), or 24 (two dash line) h photoperiods, since for all strains they were each significantly different (ANOVA,  $p < 0.05$ ) from the fit of pooled data. (B) Alpha parameters of the initial rise of growth rate ( $\alpha$ ) vs. cumulative diel Photosynthetically Usable Radiation (PUR), estimated from data pooled for each photoperiod (points ( $\pm$  SE) connected by dashed lines), and estimated for all data across photoperiods (solid blue horizontal line  $\pm$  SE), for each strain.

774x581mm (118 x 118 DPI)

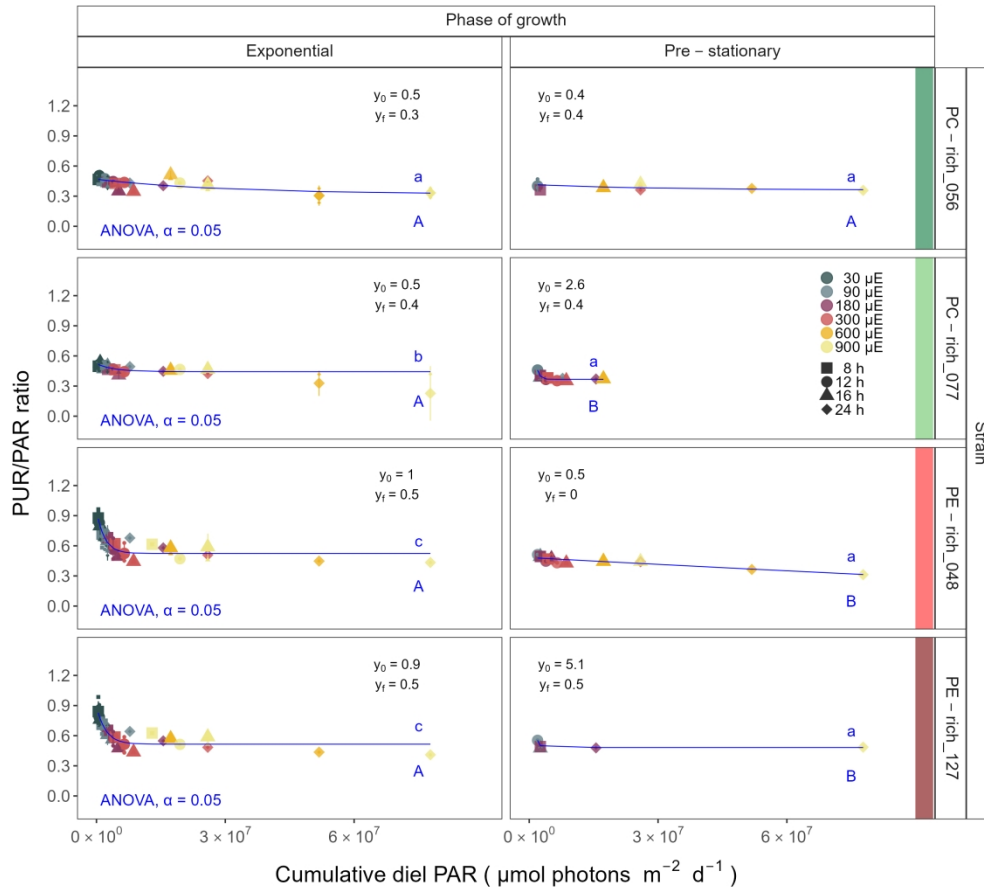


Fig. 6. Changes in PUR/PAR ratio vs. cumulative diel PAR ( $\mu\text{mol photons m}^{-2}\text{d}^{-1}$ ). PUR/PAR ratio was estimated for two PC-rich cultures (056; dark green, 077; light green) and two PE-rich cultures (048; light red, 127; dark red) of *Synechococcus* sp. grown at 30 (dark gray), 90 (light gray), 180 (purple), 300 (red), 600 (orange), or 900 (yellow) peak PAR  $\mu\text{mol photons m}^{-2}\text{s}^{-1}$  ( $\mu\text{E}$ ); and photoperiods of 8 (square), 12 (circle), 16 (triangle), or 24 (diamond) h. Figure presents data (smaller symbols) and means (bigger symbols) from exponential or pre-stationary phase of growth. Blue solid line shows single phase exponential decay fit for data from each strain and growth phase, with fit parameters presented. Different lowercase letters indicate statistically significant differences between the fit models for different strains within a given phase of growth. Different uppercase letters indicate statistically significant differences between the fit models for different phases of growth within a given strain (ANOVA;  $p < 0.05$ ).

645x581mm (118 x 118 DPI)

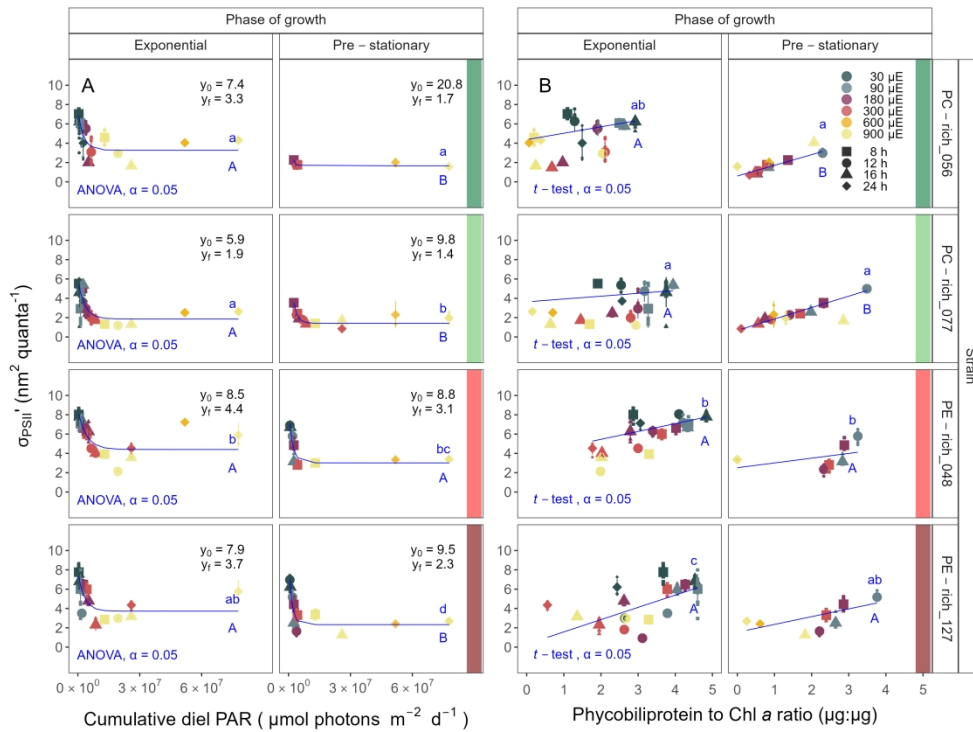


Fig. 7. (A) Effective absorption cross section of PSII ( $\sigma_{\text{PSII}'}$ ; nm<sup>2</sup> quanta<sup>-1</sup>) measured under diel peak PAR growth light vs. cumulative diel PAR ( $\mu\text{mol photons m}^{-2}\text{d}^{-1}$ ); blue solid line shows single phase exponential decay fit for data from each strain and growth phase. (B) Changes of  $\sigma_{\text{PSII}'}$  measured under diel peak PAR growth light vs. the ratio of sum of  $\mu\text{g}$  phycobilins (PE, PC, APC protein, Phycobiliprotein) to  $\mu\text{g}$  Chl a; blue solid line shows linear model fit for data from each strain and growth phase.  $\sigma_{\text{PSII}'}$  was estimated using FRRF induction curves with excitation of phycobilisomes (Ex590nm, orange), for two PC-rich cultures (056; dark green, 077; light green) and two PE-rich cultures (048; light red, 127; dark red) of *Synechococcus* sp. grown at 30 (dark gray), 90 (light gray), 180 (purple), 300 (red), 600 (orange), or 900 (yellow) peak PAR  $\mu\text{mol photons m}^{-2}\text{s}^{-1}$  ( $\mu\text{E}$ ); and photoperiods of 8 (square), 12 (circle), 16 (triangle), or 24 (diamond) h. Figure presents data (smaller symbols) and means (bigger symbols) from exponential or pre-stationary phase of growth. Different lowercase letters indicate statistically significant differences between the fit models for different strains within a given phase of growth. Different uppercase letters indicate statistically significant differences between the fit models for different phases of growth within a given strain ( $p < 0.05$ ).

774x581mm (118 x 118 DPI)

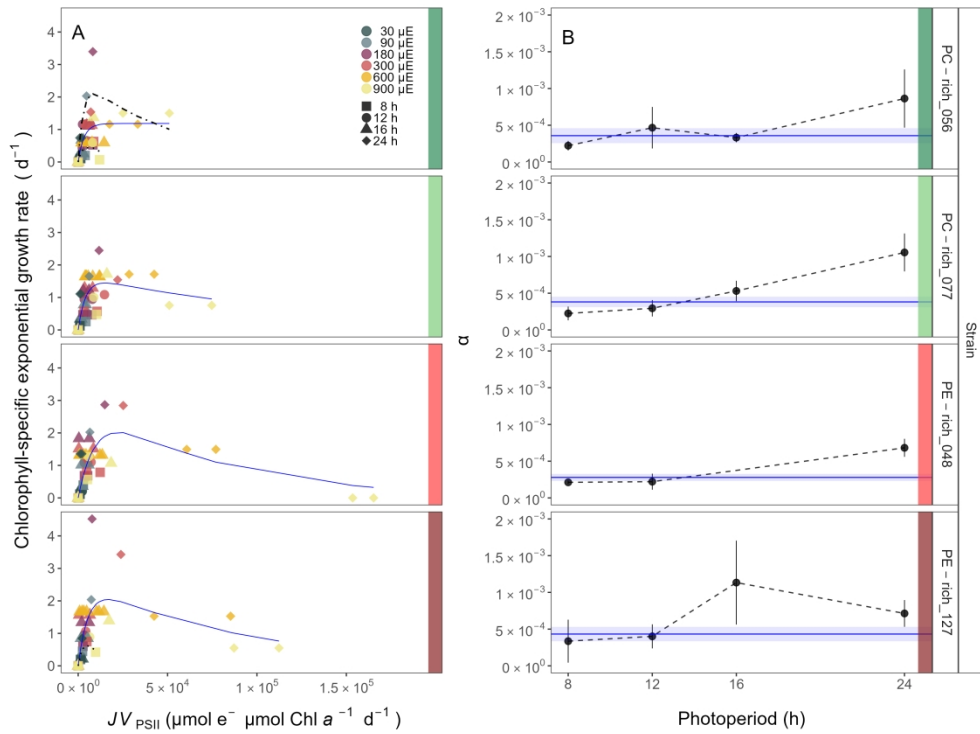


Fig. 8. (A) Chlorophyll-specific exponential growth rates ( $d^{-1}$ ) vs. cumulative diel PSII electron flux ( $JV_{PSII}$ ;  $\mu\text{mol e}^- \mu\text{mol Chl } a^{-1} d^{-1}$ ) measured under diel peak PAR growth light. Growth rates ( $\pm$  SE falling within symbols) were estimated from logistic fits of chlorophyll proxy OD<sub>680</sub> - OD<sub>720</sub> ( $\Delta$ OD) vs. elapsed time (Fig. S3B).  $JV_{PSII}$  was estimated using FRRF induction curves with excitation of chlorophyll (Ex445nm, blue), for two PC-rich cultures (056; dark green, 077; light green) and two PE-rich cultures (048; light red, 127; dark red) of *Synechococcus* sp. grown at 30 (dark gray), 90 (light gray), 180 (purple), 300 (red), 600 (orange), or 900 (yellow) peak PAR  $\mu\text{mol photons m}^{-2}\text{s}^{-1}$  ( $\mu\text{E}$ ); and photoperiods of 8 (square), 12 (circle), 16 (triangle), or 24 (diamond) h. Solid blue line shows a fit of the pooled growth rates for each strain, with a three parameter model (Harrison and Platt 1986). We also fit the same model separately for 8 (dotted line) and 24 (two dash line) h photoperiods, when they were significantly different (ANOVA,  $p < 0.05$ ) from the fit of pooled data. (B) Alpha parameters of the initial rise of growth rate ( $\alpha$ ) vs. cumulative diel  $JV_{PSII}$ , estimated from data pooled for each photoperiod (points ( $\pm$  SE) connected by dashed lines), and estimated for all data across photoperiods (horizontal line  $\pm$  SE), for each strain.

774x581mm (118 x 118 DPI)

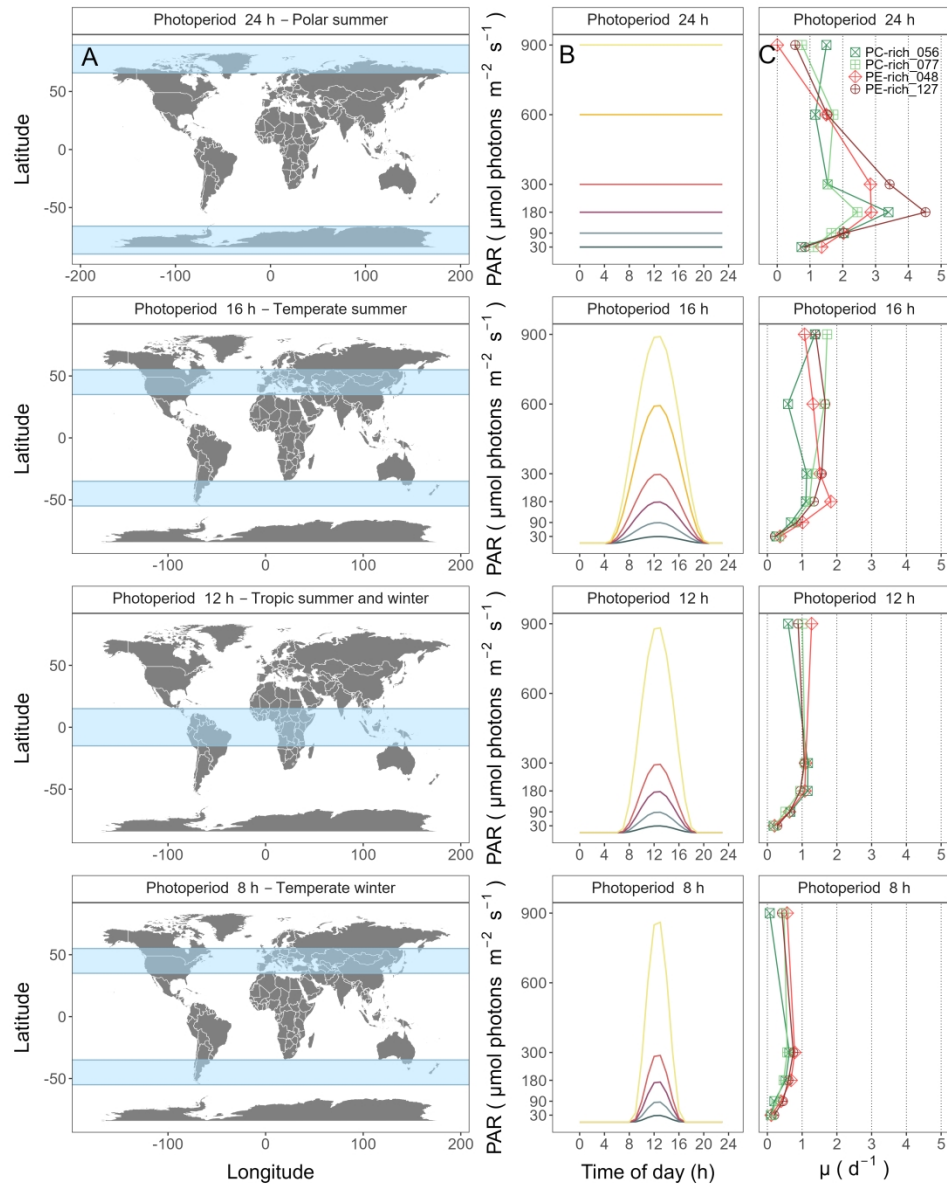


Fig. 9. Latitudinal bands, equivalent summer or winter photoperiods, and picocyanobacterial growth responses. (A) Latitudinal bands corresponding to tested growth photoperiods. (B) Tested photoperiod and peak PAR regimes used for growth experiments. (C) Chlorophyll specific exponential growth rates ( $\pm$  SE falling within symbols) for two PhycoCyanin(PC)-rich cultures (056; dark green, 077; light green) and two PhycoErythrin(PE)-rich cultures (048; light red, 127; dark red) of *Synechococcus* sp. under tested photoperiod and peak PAR regimes.

774x968mm (118 x 118 DPI)

1   **Long & low; or short & high; photoperiods and light**  
2   **differentially influence growth and potential niches of**  
3   **PhycoCyanin and PhycoErythrin-rich picocyanobacteria**

4

5   **Sylwia Śliwińska-Wilczewska<sup>1,2</sup>, Marta Konik<sup>3,4</sup>, Mireille Savoie<sup>1</sup>, Anabella**  
6   **Aguilera<sup>5,6§</sup>, Naaman M. Omar<sup>1</sup>, and Douglas A. Campbell<sup>1,\*</sup>**

7

8   <sup>1</sup> Department of Biology, Mount Allison University, 53 York St., Sackville, NB, E4L 1C9,  
9   Canada

10   <sup>2</sup> Institute of Oceanography, University of Gdańsk, 46 Piłsudskiego St, 81-378, Gdynia, Poland

11   <sup>3</sup> Department of Geography, University of Victoria, Victoria, BC, V8P 5C2, Canada

12   <sup>4</sup> Institute of Oceanology, Polish Academy of Sciences, 81-712 Sopot, Poland

13   <sup>5</sup> Department of Biology and Environmental Science, Centre for Ecology and Evolution in  
14   Microbial Model Systems (EEMiS), Linnaeus University, Kalmar, Sweden

15   <sup>6§</sup> Department of Aquatic Sciences and Assessment, Swedish University of Agricultural  
16   Sciences, Uppsala, Sweden

17   \* Correspondence: Douglas A. Campbell: dubhglascambeuil@gmail.com

18

19   **Running head:** *Picocyanobacteria across photic regimes*

20   **Keywords:** Cumulative diel photon dose; Light-capture, PAR; Photic regime; Phase of growth;  
21   Photoperiod; Picocyanobacteria; PUR

22 ***Supporting Information***

23

For Review Only

25 **Tab. S1.** Linear regression, coefficient of determination (R square), Pearson correlation coefficients (R), and *p*-value  
 26 used to calculate the pigment content ( $\mu\text{g mL}^{-1}$ ) of two PhycoCyanin(PC)-rich cultures (056, 077) and two  
 27 PhycoErythrin(PE)-rich cultures (048, 127) (Culture Collection of Baltic Algae) of *Synechococcus* sp. based on  
 28 absorbance (A) measurements.  
 29

Pigment	Abs	Linear_regression	R_square	R	<i>p</i> _value
Chl a	665	Chl a $\mu\text{g/mL} = (\text{Abs}_{665} * 13.411029) + 0.154793$	0.865	0.930	$2.2 \times 10^{-16}$
Car	480	Car $\mu\text{g/mL} = (\text{Abs}_{480} * 5.469880) + 0.089971$	0.791	0.890	$2.2 \times 10^{-16}$
PE	565	PE $\mu\text{g/mL} = (\text{Abs}_{565} * 26.760737) - 0.143872$	0.698	0.840	$2.2 \times 10^{-16}$
PC	620	PC $\mu\text{g/mL} = (\text{Abs}_{620} * 29.979866) - 0.182611$	0.807	0.900	$2.2 \times 10^{-16}$
APC	650	APC $\mu\text{g/mL} = (\text{Abs}_{650} * 3.873803) + 0.021964$	0.087	0.300	$2.8 \times 10^{-6}$

30  
 31 **Tab. S2.** Three-way factorial ANOVA testing whether peak PAR, photoperiod, strain, and their interactions  
 32 (Source\_of\_variation), significantly influence the chlorophyll specific exponential growth rate ( $\mu; \text{d}^{-1}$ ), estimated  
 33 from logistic fits of chlorophyll proxy OD<sub>680</sub> – OD<sub>720</sub> vs. cumulative diel PUR, for two PhycoCyanin(PC)-rich  
 34 cultures (056, 077) and two PhycoErythrin(PE)-rich cultures (048, 127) (Culture Collection of Baltic Algae) of  
 35 *Synechococcus* sp., grown at 30, 90, 180, 300, 600, or 900 peak PAR  $\mu\text{mol photons m}^{-2}\text{s}^{-1}$ ; and photoperiods of 8,  
 36 12, 16, or 24 h. Df – degrees of freedom; Sum Sq – sum of squares; Mean Sq – mean sum of squares; *F*\_value –  
 37 Fisher's *F*-test statistic; *p*\_value - level of significance.  
 38

Source_of_variation	Df	Sum Sq	Mean Sq	<i>F</i> _value	<i>p</i> _value
Par_ue	5	0.049	0.010	$3.2 \times 10^{30}$	$2.2 \times 10^{-16}$
Photoperiod	3	0.076	0.025	$8.3 \times 10^{30}$	$2.2 \times 10^{-16}$
Strain	3	0.003	0.001	$3.1 \times 10^{29}$	$2.2 \times 10^{-16}$
Par_ue:Photoperiod	13	0.040	0.003	$1.0 \times 10^{30}$	$2.2 \times 10^{-16}$
Par_ue:Strain	15	0.007	0.000	$1.5 \times 10^{29}$	$2.2 \times 10^{-16}$
Photoperiod:Strain	9	0.004	0.000	$1.3 \times 10^{29}$	$2.2 \times 10^{-16}$
Par_ue:Photoperiod:Strain	39	0.017	0.000	$1.4 \times 10^{29}$	$2.2 \times 10^{-16}$
Residuals	88	0.000	0.000	NA	N/A

39

41   **Tab. S3.** One-way ANOVA of a three parameter model (Harrison and Platt 1986) from pooled data (All) and data fit  
 42   across different photoperiods (8, 12, 16, or 24) from chlorophyll specific exponential growth rate vs. cumulative diel  
 43   PUR (Fit\_model), for two PhycoCyanin(PC)-rich cultures (056, 077) and two PhycoErythrin(PE)-rich cultures (048,  
 44   127) of *Synechococcus* sp., grown at 30, 90, 180, 300, 600, or 900 peak PAR  $\mu\text{mol photons m}^{-2}\text{s}^{-1}$ ; and  
 45   photoperiods of 8, 12, 16, or 24 h. Res.Df - residual degrees of freedom for each model; Res.Sum Sq - residual sum  
 46   of squares for each model;  $F$ \_value – Fisher's  $F$ -test statistic;  $p$ \_value - level of significance.  
 47

Strain	Fit_model	Res.Df	Res.Sum Sq	$F$ _value	$p$ _value
PC-rich_056	8_All	41	8.063	$1.8 \times 10^3$	$2.3 \times 10^{-8}$
PC-rich_056	12_All	41	8.063	$2.8 \times 10^1$	$7.2 \times 10^{-4}$
PC-rich_056	16_All	41	8.063	$8.5 \times 10^0$	$1.2 \times 10^{-2}$
PC-rich_056	24_All	41	8.063	$2.3 \times 10^1$	$1.1 \times 10^{-3}$
PC-rich_077	8_All	41	3.015	$6.1 \times 10^1$	$1.0 \times 10^{-4}$
PC-rich_077	12_All	41	3.015	$2.4 \times 10^1$	$9.9 \times 10^{-4}$
PC-rich_077	16_All	41	3.015	$1.8 \times 10^1$	$1.9 \times 10^{-3}$
PC-rich_077	24_All	41	3.015	$1.0 \times 10^1$	$7.2 \times 10^{-3}$
PE-rich_048	8_All	41	6.731	$1.4 \times 10^1$	$3.6 \times 10^{-3}$
PE-rich_048	12_All	41	6.731	$8.3 \times 10^1$	$5.0 \times 10^{-5}$
PE-rich_048	16_All	41	6.731	$8.4 \times 10^0$	$1.2 \times 10^{-2}$
PE-rich_048	24_All	41	6.731	$8.2 \times 10^1$	$5.2 \times 10^{-5}$
PE-rich_127	8_All	41	13.016	$1.4 \times 10^2$	$1.2 \times 10^{-5}$
PE-rich_127	12_All	41	13.016	$2.0 \times 10^3$	$1.7 \times 10^{-8}$
PE-rich_127	16_All	41	13.016	$6.9 \times 10^0$	$1.9 \times 10^{-2}$
PE-rich_127	24_All	41	13.016	$7.8 \times 10^1$	$5.9 \times 10^{-5}$



48  
 49  
 50  
 51  
 52  
 53  
 54  
 55  
 56  
 57  
 58

60 **Tab. S4.** One-way ANOVA of a three parameter model (Harrison and Platt 1986) from pooled data (All) and data fit  
 61 across different peak PAR (30, 90, 180, 300, 600 together with 900) from chlorophyll specific exponential growth  
 62 rate vs. cumulative diel PUR (Fit\_model), for two PhycoCyanin(PC)-rich cultures (056, 077) and two  
 63 PhycoErythrin(PE)-rich cultures (048, 127) of *Synechococcus* sp., grown at 30, 90, 180, 300, 600, or 900 peak PAR  
 64  $\mu\text{mol photons m}^{-2}\text{s}^{-1}$ ; and photoperiods of 8, 12, 16, or 24 h. Res.Df - residual degrees of freedom for each model;  
 65 Res.Sum Sq - residual sum of squares for each model;  $F_{\text{value}}$  – Fisher's  $F$ -test statistic;  $p_{\text{value}}$  - level of  
 66 significance.  
 67

Strain	Fit_model	Res.Df	Res.Sum Sq	$F_{\text{value}}$	$p_{\text{value}}$
PC-rich_056	30_All	41	8.063	$1.8 \times 10^3$	$2.3 \times 10^{-8}$
PC-rich_056	90_All	41	8.063	$2.8 \times 10^1$	$7.2 \times 10^{-4}$
PC-rich_056	180_All	41	8.063	$8.5 \times 10^0$	$1.2 \times 10^{-2}$
PC-rich_056	300_All	41	8.063	$2.3 \times 10^1$	$1.1 \times 10^{-3}$
PC-rich_056	900_All	41	8.063	$3.3 \times 10^0$	$2.9 \times 10^{-2}$
PC-rich_077	30_All	41	3.015	$6.1 \times 10^1$	$1.0 \times 10^{-4}$
PC-rich_077	90_All	41	3.015	$2.4 \times 10^1$	$9.9 \times 10^{-4}$
PC-rich_077	180_All	41	3.015	$1.8 \times 10^1$	$1.9 \times 10^{-3}$
PC-rich_077	300_All	41	3.015	$1.0 \times 10^1$	$7.2 \times 10^{-3}$
PC-rich_077	900_All	41	3.015	$6.5 \times 10^{-1}$	$8.2 \times 10^{-1}$
PE-rich_048	30_All	41	6.731	$1.4 \times 10^1$	$3.6 \times 10^{-3}$
PE-rich_048	90_All	41	6.731	$8.3 \times 10^1$	$5.0 \times 10^{-5}$
PE-rich_048	180_All	41	6.731	$8.4 \times 10^0$	$1.2 \times 10^{-2}$
PE-rich_048	300_All	41	6.731	$8.2 \times 10^1$	$5.2 \times 10^{-5}$
PE-rich_048	900_All	41	6.731	$1.3 \times 10^0$	$3.2 \times 10^{-1}$
PE-rich_127	30_All	41	13.016	$1.4 \times 10^2$	$1.2 \times 10^{-5}$
PE-rich_127	90_All	41	13.016	$2.0 \times 10^3$	$1.7 \times 10^{-8}$
PE-rich_127	180_All	41	13.016	$6.9 \times 10^0$	$1.9 \times 10^{-2}$
PE-rich_127	300_All	41	13.016	$7.8 \times 10^1$	$5.9 \times 10^{-5}$
PE-rich_127	900_All	41	13.016	$3.5 \times 10^0$	$2.5 \times 10^{-2}$

68

69

71 **Tab. S5.** One-way ANOVA of a three parameter model (Harrison and Platt 1986) from pooled data (All) and data fit  
 72 across different photoperiods (8, 12, 16, or 24) from chlorophyll specific exponential growth rate vs. cumulative diel  
 73 PAR (Fit\_model), for two PhycoCyanin(PC)-rich cultures (056, 077) and two PhycoErythrin(PE)-rich cultures (048,  
 74 127) of *Synechococcus* sp., grown at 30, 90, 180, 300, 600, or 900 peak PAR  $\mu\text{mol photons m}^{-2}\text{s}^{-1}$ ; and  
 75 photoperiods of 8, 12, 16, or 24 h. Res.Df - residual degrees of freedom for each model; Res.Sum Sq - residual sum  
 76 of squares for each model;  $F$ \_value – Fisher's  $F$ -test statistic;  $p$ \_value - level of significance.  
 77

Strain	Fit_model	Res.Df	Res.Sum Sq	$F$ _value	$p$ _value
PC-rich_056	8_All	135	18.854	$1.0 \times 10^3$	$2.0 \times 10^{-32}$
PC-rich_056	12_All	135	18.854	$1.4 \times 10^1$	$3.5 \times 10^{-10}$
PC-rich_056	16_All	135	18.854	$7.4 \times 10^0$	$3.4 \times 10^{-7}$
PC-rich_056	24_All	135	18.854	$1.2 \times 10^1$	$1.0 \times 10^{-9}$
PC-rich_077	8_All	131	5.672	$2.7 \times 10^1$	$1.9 \times 10^{-13}$
PC-rich_077	12_All	131	5.672	$8.9 \times 10^0$	$4.9 \times 10^{-8}$
PC-rich_077	16_All	131	5.672	$5.6 \times 10^0$	$5.4 \times 10^{-6}$
PC-rich_077	24_All	131	5.672	$4.0 \times 10^0$	$1.2 \times 10^{-4}$
PE-rich_048	8_All	133	16.660	$2.1 \times 10^1$	$3.6 \times 10^{-12}$
PE-rich_048	12_All	133	16.660	$1.9 \times 10^1$	$7.3 \times 10^{-12}$
PE-rich_048	16_All	133	16.660	$3.5 \times 10^0$	$3.5 \times 10^{-4}$
PE-rich_048	24_All	133	16.660	$8.0 \times 10^1$	$6.4 \times 10^{-19}$
PE-rich_127	8_All	133	26.508	$6.5 \times 10^1$	$7.3 \times 10^{-18}$
PE-rich_127	12_All	133	26.508	$6.7 \times 10^3$	$6.3 \times 10^{-42}$
PE-rich_127	16_All	133	26.508	$1.5 \times 10^1$	$1.6 \times 10^{-10}$
PE-rich_127	24_All	133	26.508	$5.2 \times 10^1$	$1.1 \times 10^{-16}$



78

79

81   **Tab. S6.** One-way ANOVA of a three parameter model (Harrison and Platt 1986) from pooled data (All) and data fit  
 82 across different peak PAR (30, 90, 180, 300, 600 together with 900) from chlorophyll specific exponential growth  
 83 rate vs. cumulative diel PAR (Fit\_model), for two PhycoCyanin(PC)-rich cultures (056, 077) and two  
 84 PhycoErythrin(PE)-rich cultures (048, 127) of *Synechococcus* sp., grown at 30, 90, 180, 300, 600, or 900 peak PAR  
 85  $\mu\text{mol photons m}^{-2}\text{s}^{-1}$ ; and photoperiods of 8, 12, 16, or 24 h. Res.Df - residual degrees of freedom for each model;  
 86 Res.Sum Sq - residual sum of squares for each model;  $F_{\text{value}}$  – Fisher's  $F$ -test statistic;  $p_{\text{value}}$  - level of  
 87 significance.  
 88

Strain	Fit_model	Res.Df	Res.Sum Sq	$F_{\text{value}}$	$p_{\text{value}}$
PC-rich_056	30_All	135	18.854	$1.0 \times 10^3$	$2.0 \times 10^{-32}$
PC-rich_056	90_All	135	18.854	$1.4 \times 10^1$	$3.5 \times 10^{-10}$
PC-rich_056	180_All	135	18.854	$7.4 \times 10^0$	$3.4 \times 10^{-7}$
PC-rich_056	300_All	135	18.854	$1.2 \times 10^1$	$1.0 \times 10^{-9}$
PC-rich_056	900_All	135	18.854	$2.5 \times 10^0$	$3.0 \times 10^{-3}$
PC-rich_077	30_All	131	5.672	$2.7 \times 10^1$	$1.9 \times 10^{-13}$
PC-rich_077	90_All	131	5.672	$8.9 \times 10^0$	$4.9 \times 10^{-8}$
PC-rich_077	180_All	131	5.672	$5.6 \times 10^0$	$5.4 \times 10^{-6}$
PC-rich_077	300_All	131	5.672	$4.0 \times 10^0$	$1.2 \times 10^{-4}$
PC-rich_077	900_All	131	5.672	$7.4 \times 10^{-1}$	$8.4 \times 10^{-1}$
PE-rich_048	30_All	133	16.660	$2.1 \times 10^1$	$3.6 \times 10^{-12}$
PE-rich_048	90_All	133	16.660	$1.9 \times 10^1$	$7.3 \times 10^{-12}$
PE-rich_048	180_All	133	16.660	$3.5 \times 10^0$	$3.5 \times 10^{-4}$
PE-rich_048	300_All	133	16.660	$8.0 \times 10^1$	$6.4 \times 10^{-19}$
PE-rich_048	900_All	133	16.660	$1.8 \times 10^0$	$3.4 \times 10^{-2}$
PE-rich_127	30_All	133	26.508	$6.5 \times 10^1$	$7.3 \times 10^{-18}$
PE-rich_127	90_All	133	26.508	$6.7 \times 10^3$	$6.3 \times 10^{-42}$
PE-rich_127	180_All	133	26.508	$1.5 \times 10^1$	$1.6 \times 10^{-10}$
PE-rich_127	300_All	133	26.508	$5.2 \times 10^1$	$1.1 \times 10^{-16}$
PE-rich_127	900_All	133	26.508	$2.8 \times 10^0$	$2.1 \times 10^{-3}$

89  
 90

92 **Tab. S7.** One-way ANOVA of a three parameter model (Harrison and Platt 1986) from pooled data (All) and data fit  
 93 across different photoperiods (8, 12, 16, or 24) from chlorophyll specific exponential growth rate vs. PSII electron  
 94 flux ( $JV_{PSII}$ ;  $\mu\text{mol e}^- \mu\text{mol Chl } a^{-1} d^{-1}$ ) (Fit\_model), for two PhycoCyanin(PC)-rich cultures (056, 077) and two  
 95 PhycoErythrin(PE)-rich cultures (048, 127) of *Synechococcus* sp., grown at 30, 90, 180, 300, 600, or 900 peak PAR  
 96  $\mu\text{mol photons m}^{-2}\text{s}^{-1}$ ; and photoperiods of 8, 12, 16, or 24 h. Res.Df - residual degrees of freedom for each model;  
 97 Res.Sum Sq - residual sum of squares for each model;  $F$ \_value – Fisher's  $F$ -test statistic;  $p$ \_value - level of  
 98 significance.  
 99

Strain	Fit_model	Res.Df	Res.Sum Sq	$F$ _value	$p$ _value
PC-rich_056	8_All	61	11.802	$3.9 \times 10^0$	0.016
PC-rich_056	12_All	61	11.802	$7.7 \times 10^{-1}$	0.730
PC-rich_056	16_All	61	11.802	$2.2 \times 10^{-1}$	1.000
PC-rich_056	24_All	61	11.802	$3.3 \times 10^0$	0.037
PC-rich_077	8_All	61	9.014	$1.1 \times 10^0$	0.459
PC-rich_077	12_All	61	9.014	$1.3 \times 10^0$	0.350
PC-rich_077	16_All	61	9.014	$6.1 \times 10^{-1}$	0.861
PC-rich_077	24_All	61	9.014	$1.5 \times 10^0$	0.260
PE-rich_048	8_All	61	16.583	$1.3 \times 10^0$	0.339
PE-rich_048	12_All	61	16.583	$1.9 \times 10^0$	0.174
PE-rich_048	16_All	61	16.583	$5.5 \times 10^{-1}$	0.903
PE-rich_048	24_All	61	16.583	$6.7 \times 10^{-1}$	0.817
PE-rich_127	8_All	53	21.117	$7.9 \times 10^0$	0.004
PE-rich_127	12_All	53	21.117	$4.1 \times 10^0$	0.057
PE-rich_127	16_All	53	21.117	$5.5 \times 10^{-1}$	0.882
PE-rich_127	24_All	53	21.117	$1.1 \times 10^0$	0.504

100

101

103 **Tab. S8.** One-way ANOVA of a three parameter model (Harrison and Platt 1986) from pooled data (All) and data fit  
 104 across different peak PAR (30, 90, 180, 300, 600 together with 900) from chlorophyll specific exponential growth  
 105 rate vs. PSII electron flux ( $JV_{PSII}$ ;  $\mu\text{mol e}^- \mu\text{mol Chl } a^{-1} d^{-1}$ ) (Fit\_model), for two PhycoCyanin(PC)-rich cultures  
 106 (056, 077) and two PhycoErythrin(PE)-rich cultures (048, 127) of *Synechococcus* sp., grown at 30, 90, 180, 300,  
 107 600, or 900 peak PAR  $\mu\text{mol photons m}^{-2}\text{s}^{-1}$ ; and photoperiods of 8, 12, 16, or 24 h. Res.Df - residual degrees of  
 108 freedom for each model; Res.Sum Sq - residual sum of squares for each model;  $F\_value$  – Fisher's  $F$ -test statistic;  
 109  $p\_value$  - level of significance.  
 110

Strain	Fit_model	Res.Df	Res.Sum Sq	$F\_value$	$p\_value$
PC-rich_056	30_All	61	11.802	$3.9 \times 10^0$	0.016
PC-rich_056	90_All	61	11.802	$7.7 \times 10^{-1}$	0.730
PC-rich_056	180_All	61	11.802	$2.2 \times 10^{-1}$	1.000
PC-rich_056	300_All	61	11.802	$3.3 \times 10^0$	0.037
PC-rich_056	900_All	61	11.802	$2.1 \times 10^0$	0.044
PC-rich_077	30_All	61	9.014	$1.1 \times 10^0$	0.459
PC-rich_077	90_All	61	9.014	$1.3 \times 10^0$	0.350
PC-rich_077	180_All	61	9.014	$6.1 \times 10^{-1}$	0.861
PC-rich_077	300_All	61	9.014	$1.5 \times 10^0$	0.260
PC-rich_077	900_All	61	9.014	$1.2 \times 10^0$	0.287
PE-rich_048	30_All	61	16.583	$1.3 \times 10^0$	0.339
PE-rich_048	90_All	61	16.583	$1.9 \times 10^0$	0.174
PE-rich_048	180_All	61	16.583	$5.5 \times 10^{-1}$	0.903
PE-rich_048	300_All	61	16.583	$6.7 \times 10^{-1}$	0.817
PE-rich_048	900_All	61	16.583	$3.1 \times 10^0$	0.007
PE-rich_127	30_All	53	21.117	$7.9 \times 10^0$	0.004
PE-rich_127	90_All	53	21.117	$4.1 \times 10^0$	0.057
PE-rich_127	180_All	53	21.117	$5.5 \times 10^{-1}$	0.882
PE-rich_127	300_All	53	21.117	$1.1 \times 10^0$	0.504
PE-rich_127	900_All	53	21.117	$3.7 \times 10^0$	0.002

111

112

114 **Tab. S9.** One-way ANOVA of single phase exponential decay fit model (Fit\_model) of pooled data across different  
 115 strains for a given phase of growth (exponential; \_Exp, pre-stationary; \_St) and across different phase of growth for  
 116 a given strain (\_Exp\_St) from PUR/PAR ratio in relation to the cumulative diel PAR ( $\mu\text{mol photons m}^{-2}\text{d}^{-1}$ ), for two  
 117 PhycoCyanin(PC)-rich cultures (056, 077) and two PhycoErythrin(PE)-rich cultures (048, 127) of *Synechococcus*  
 118 sp., grown at 30, 90, 180, 300, 600, or 900 peak PAR  $\mu\text{mol photons m}^{-2}\text{s}^{-1}$ ; and photoperiods of 8, 12, 16, or 24 h.  
 119 Res.Df - residual degrees of freedom for each model; Res.Sum Sq - residual sum of squares for each model;  $F_{\text{value}}$   
 120 – Fisher's  $F$ -test statistic;  $p_{\text{value}}$  - level of significance.

121

Fit_model	Res.Df	Res.Sum Sq	$F_{\text{value}}$	$p_{\text{value}}$
056_077_Exp	43	0.025	$2.8 \times 10^1$	$1.6 \times 10^{-11}$
048_127_Exp	51	0.217	NA	N/A
056_048_Exp	51	0.307	$2.7 \times 10^1$	$7.9 \times 10^{-12}$
077_048_Exp	51	0.307	$5.9 \times 10^1$	$8.5 \times 10^{-21}$
056_127_Exp	51	0.217	$1.6 \times 10^1$	$2.3 \times 10^{-8}$
077_127_Exp	51	0.217	$4.0 \times 10^1$	$1.3 \times 10^{-17}$
056_077_St	20	0.006	$-1.4 \times 10^{-1}$	$1.0 \times 10^0$
048_127_St	2	0.000	$5.3 \times 10^0$	$1.6 \times 10^{-1}$
056_048_St	17	0.009	$9.6 \times 10^{-2}$	$9.9 \times 10^{-1}$
077_048_St	17	0.009	$-2.0 \times 10^0$	$1.0 \times 10^0$
056_127_St	2	0.000	$1.4 \times 10^1$	$6.7 \times 10^{-2}$
077_127_St	2	0.000	$2.8 \times 10^0$	$2.9 \times 10^{-1}$
056_Exp_St	7	0.008	$1.8 \times 10^0$	$1.9 \times 10^{-1}$
077_Exp_St	20	0.006	$3.0 \times 10^0$	$7.3 \times 10^{-3}$
048_Exp_St	17	0.009	$1.6 \times 10^1$	$6.7 \times 10^{-8}$
127_Exp_St	2	0.000	$4.1 \times 10^1$	$2.3 \times 10^{-2}$

122

123

125 **Tab. S10.** One-way ANOVA of single phase exponential decay fit model (Fit\_model) of pooled data across  
 126 different strains for a given phase of growth (exponential; \_Exp, pre-stationary; \_St) and across different phase of  
 127 growth for a given strain (\_Exp\_St) from Phycobiliprotein to Chl *a* ratio in relation to the cumulative diel PAR  
 128 ( $\mu\text{mol photons m}^{-2}\text{d}^{-1}$ ), for two PhycoCyanin(PC)-rich cultures (056, 077) and two PhycoErythrin(PE)-rich  
 129 cultures (048, 127) of *Synechococcus* sp., grown at 30, 90, 180, 300, 600, or 900 peak PAR  $\mu\text{mol photons m}^{-2}\text{s}^{-1}$ ;  
 130 and photoperiods of 8, 12, 16, or 24 h. Res.Df - residual degrees of freedom for each model; Res.Sum Sq - residual  
 131 sum of squares for each model;  $F$ \_value – Fisher's  $F$ -test statistic;  $p$ \_value - level of significance.  
 132

Fit_model	Res.Df	Res.Sum Sq	$F$ _value	$p$ _value
056_077_Exp	49	38.089	$1.5 \times 10^1$	$2.8 \times 10^{-4}$
048_127_Exp	52	54.559	NA	N/A
056_048_Exp	52	39.302	$4.3 \times 10^0$	$4.5 \times 10^{-3}$
077_048_Exp	52	39.302	$5.2 \times 10^{-1}$	$6.7 \times 10^{-1}$
056_127_Exp	52	54.559	$1.0 \times 10^1$	$2.8 \times 10^{-6}$
077_127_Exp	52	54.559	$7.0 \times 10^0$	$4.8 \times 10^{-4}$
056_077_St	24	3.580	$-1.0 \times 10^1$	$1.0 \times 10^0$
048_127_St	19	3.343	NA	N/A
056_048_St	19	2.239	$-2.2 \times 10^{-1}$	$1.0 \times 10^0$
077_048_St	19	2.239	$2.2 \times 10^0$	$8.8 \times 10^{-2}$
056_127_St	19	3.343	$-1.1 \times 10^0$	$1.0 \times 10^0$
077_127_St	19	3.343	$2.6 \times 10^{-1}$	$9.2 \times 10^{-1}$
056_Exp_St	25	2.081	$1.3 \times 10^1$	$3.2 \times 10^{-9}$
077_Exp_St	24	3.580	$9.2 \times 10^0$	$3.2 \times 10^{-7}$
048_Exp_St	19	2.239	$9.5 \times 10^0$	$1.7 \times 10^{-6}$
127_Exp_St	19	3.343	$8.8 \times 10^0$	$3.2 \times 10^{-6}$

133

134

136 **Tab. S11.** One-way ANOVA of single phase exponential decay fit model (Fit\_model) of pooled data across  
 137 different strains for a given phase of growth (exponential; \_Exp, pre-stationary; \_St) and across different phase of  
 138 growth for a given strain (\_Exp\_St) from effective absorption cross section of PSII ( $\sigma_{PSII}'$ ; nm<sup>2</sup> quanta<sup>-1</sup>) measured  
 139 under diel peak PAR growth light under Ex590nm (orange) excitation in relation to the cumulative diel PAR ( $\mu\text{mol}$   
 140 photons m<sup>-2</sup>d<sup>-1</sup>), for two PhycoCyanin(PC)-rich cultures (056, 077) and two PhycoErythrin(PE)-rich cultures (048,  
 141 127) of *Synechococcus* sp., grown at 30, 90, 180, 300, 600, or 900 peak PAR  $\mu\text{mol}$  photons m<sup>-2</sup>s<sup>-1</sup>; and  
 142 photoperiods of 8, 12, 16, or 24 h. Res.Df - residual degrees of freedom for each model; Res.Sum Sq - residual sum  
 143 of squares for each model; F\_value – Fisher's F-test statistic; p\_value - level of significance.

144

Fit_model	Res.Df	Res.Sum Sq	F_value	p_value
056_077_Exp	97	116.359	$9.9 \times 10^{-1}$	$4.6 \times 10^{-1}$
048_127_Exp	72	106.728	$-1.6 \times 10^0$	$1.0 \times 10^0$
056_048_Exp	97	116.359	$3.7 \times 10^1$	$4.5 \times 10^{-16}$
077_048_Exp	112	134.219	$8.0 \times 10^0$	$2.3 \times 10^{-12}$
056_127_Exp	72	106.728	$2.5 \times 10^{-1}$	$9.9 \times 10^{-1}$
077_127_Exp	72	106.728	$4.6 \times 10^{-1}$	$9.9 \times 10^{-1}$
056_077_St	41	3.366	$1.5 \times 10^1$	$2.3 \times 10^{-7}$
048_127_St	45	38.775	$3.7 \times 10^0$	$1.4 \times 10^{-3}$
056_048_St	34	17.489	$1.1 \times 10^2$	$3.1 \times 10^{-14}$
077_048_St	34	17.489	$-3.9 \times 10^0$	$1.0 \times 10^0$
056_127_St	45	38.775	$1.5 \times 10^2$	$9.4 \times 10^{-16}$
077_127_St	45	38.775	$1.0 \times 10^2$	$3.4 \times 10^{-21}$
056_Exp_St	17	0.150	$1.6 \times 10^2$	$1.8 \times 10^{-16}$
077_Exp_St	41	3.366	$2.2 \times 10^1$	$4.3 \times 10^{-19}$
048_Exp_St	34	17.489	$1.1 \times 10^0$	$3.3 \times 10^{-1}$
127_Exp_St	45	38.775	$2.9 \times 10^0$	$7.1 \times 10^{-4}$

145

146

148 **Tab. S12.** *T*-test of linear fit model (Fit\_model) of pooled data across different strains for a given phase of growth  
 149 (exponential; \_Exp, pre-stationary; \_St) and across different phase of growth for a given strain (\_Exp\_St) from  
 150 effective absorption cross section of PSII ( $\sigma_{PSII}'$ ; nm<sup>2</sup> quanta<sup>-1</sup>) measured under diel peak PAR growth light under  
 151 Ex<sub>445nm</sub> (blue) excitation in relation to the cumulative diel PAR ( $\mu\text{mol photons m}^{-2}\text{d}^{-1}$ , for two PhycoCyanin(PC)-  
 152 rich cultures (056, 077) and two PhycoErythrin(PE)-rich cultures (048, 127) of *Synechococcus* sp., grown at 30, 90,  
 153 180, 300, 600, or 900 peak PAR  $\mu\text{mol photons m}^{-2}\text{s}^{-1}$ ; and photoperiods of 8, 12, 16, or 24 h. Estimate - estimation  
 154 statistics; Std.Error - standard error of the estimate; *t*\_value – *t*-test statistic; *p*\_value - level of significance.  
 155

Fit_model	Estimate	Std.Error	<i>t</i> _value	<i>p</i> _value
056_077_Exp	$-1.4 \times 10^{-9}$	$1.0 \times 10^{-9}$	-1.372	$1.7 \times 10^{-1}$
056_048_Exp	$-2.1 \times 10^{-9}$	$1.3 \times 10^{-9}$	-1.666	$9.6 \times 10^{-2}$
056_127_Exp	$-8.2 \times 10^{-10}$	$1.4 \times 10^{-9}$	-0.583	$5.6 \times 10^{-1}$
048_127_Exp	$1.3 \times 10^{-9}$	$1.6 \times 10^{-9}$	0.851	$3.9 \times 10^{-1}$
077_048_Exp	$-7.3 \times 10^{-10}$	$1.2 \times 10^{-9}$	-0.598	$5.5 \times 10^{-1}$
077_127_Exp	$6.2 \times 10^{-10}$	$1.3 \times 10^{-9}$	0.470	$6.3 \times 10^{-1}$
056_077_St	$2.4 \times 10^{-9}$	$1.3 \times 10^{-9}$	1.818	$7.0 \times 10^{-2}$
056_048_St	$5.2 \times 10^{-9}$	$2.0 \times 10^{-9}$	2.505	$1.3 \times 10^{-2}$
056_127_St	$1.7 \times 10^{-9}$	$1.8 \times 10^{-9}$	0.937	$3.4 \times 10^{-1}$
048_127_St	$-3.5 \times 10^{-9}$	$1.6 \times 10^{-9}$	-2.116	$3.5 \times 10^{-2}$
077_048_St	$2.8 \times 10^{-9}$	$1.2 \times 10^{-9}$	2.217	$2.7 \times 10^{-2}$
077_127_St	$-7.0 \times 10^{-10}$	$1.2 \times 10^{-9}$	-0.586	$5.5 \times 10^{-1}$
056_Exp_St	$2.4 \times 10^{-9}$	$1.6 \times 10^{-9}$	1.514	$1.3 \times 10^{-1}$
077_Exp_St	$6.3 \times 10^{-9}$	$9.1 \times 10^{-10}$	6.973	$2.4 \times 10^{-11}$
048_Exp_St	$9.9 \times 10^{-9}$	$1.6 \times 10^{-9}$	5.860	$1.7 \times 10^{-8}$
127_Exp_St	$5.0 \times 10^{-9}$	$1.6 \times 10^{-9}$	3.120	$2.0 \times 10^{-3}$

156

157

159 **Tab. S13.** *T*-test of linear fit model (Fit\_model) of pooled data across different strains for a given phase of growth  
 160 (exponential; \_Exp, pre-stationary; \_St) and across different phase of growth for a given strain (\_Exp\_St) from  
 161 effective absorption cross section of PSII ( $\sigma_{PSII}'$ ; nm<sup>2</sup> quanta<sup>-1</sup>) measured under diel peak PAR growth light under  
 162 Ex<sub>445nm</sub> (blue) excitation in relation to Phycobiliprotein to Chl *a* ratio, for two PhycoCyanin(PC)-rich cultures (056,  
 163 077) and two PhycoErythrin(PE)-rich cultures (048, 127) of *Synechococcus* sp., grown at 30, 90, 180, 300, 600, or  
 164 900 peak PAR  $\mu\text{mol photons m}^{-2}\text{s}^{-1}$ ; and photoperiods of 8, 12, 16, or 24 h. Estimate - estimation statistics;  
 165 Std.Error - standard error of the estimate; *t*\_value - *t*-test statistic; *p*\_value - level of significance.  
 166

Fit_model	Estimate	Std.Error	<i>t</i> _value	<i>p</i> _value
056_077_Exp	0.003	0.008	0.424	$6.7 \times 10^{-1}$
056_048_Exp	0.078	0.009	9.082	$2.1 \times 10^{-19}$
056_127_Exp	0.039	0.009	4.382	$1.2 \times 10^{-5}$
048_127_Exp	-0.039	0.009	-4.416	$1.0 \times 10^{-5}$
077_048_Exp	0.075	0.008	8.954	$6.6 \times 10^{-19}$
077_127_Exp	0.036	0.009	4.117	$3.9 \times 10^{-5}$
056_077_St	-0.023	0.007	-3.495	$4.9 \times 10^{-4}$
056_048_St	-0.062	0.016	-3.788	$1.6 \times 10^{-4}$
056_127_St	-0.037	0.014	-2.606	$9.3 \times 10^{-3}$
048_127_St	0.026	0.023	1.143	$2.5 \times 10^{-1}$
077_048_St	-0.039	0.014	-2.823	$4.8 \times 10^{-3}$
077_127_St	-0.013	0.012	-1.117	$2.6 \times 10^{-1}$
056_Exp_St	0.083	0.013	6.327	$3.2 \times 10^{-10}$
077_Exp_St	0.057	0.009	6.590	$5.9 \times 10^{-11}$
048_Exp_St	-0.057	0.018	-3.217	$1.3 \times 10^{-3}$
127_Exp_St	0.008	0.020	0.389	$6.9 \times 10^{-1}$

167

168

170 **Tab. S14.** *T*-test of linear fit model (Fit\_model) of pooled data across different strains for a given phase of growth  
 171 (exponential; \_Exp, pre-stationary; \_St) and across different phase of growth for a given strain (\_Exp\_St) from  
 172 effective absorption cross section of PSII ( $\sigma_{PSII}'$ ; nm<sup>2</sup> quanta<sup>-1</sup>) measured under Ex<sub>590nm</sub> (orange) excitation in  
 173 relation to the Phycobiliprotein to Chl *a* ratio, for two PhycoCyanin(PC)-rich cultures (056, 077) and two  
 174 PhycoErythrin(PE)-rich cultures (048, 127) of *Synechococcus* sp., grown at 30, 90, 180, 300, 600, or 900 peak PAR  
 175 μmol photons m<sup>-2</sup>s<sup>-1</sup>; and photoperiods of 8, 12, 16, or 24 h. Estimate - estimation statistics; Std.Error - standard  
 176 error of the estimate; *t*\_value – *t*-test statistic; *p*\_value - level of significance.  
 177

Fit_model	Estimate	Std.Error	<i>t</i> _value	<i>p</i> _value
056_077_Exp	-0.369	0.092	-4.000	$6.6 \times 10^{-5}$
056_048_Exp	0.149	0.082	1.812	$7.0 \times 10^{-2}$
056_127_Exp	0.606	0.099	6.122	$1.1 \times 10^{-9}$
048_127_Exp	0.457	0.090	5.084	$4.1 \times 10^{-7}$
077_048_Exp	0.518	0.083	6.267	$4.6 \times 10^{-10}$
077_127_Exp	0.976	0.097	10.089	$2.7 \times 10^{-23}$
056_077_St	0.077	0.029	2.669	$7.7 \times 10^{-3}$
056_048_St	-0.610	0.079	-7.751	$4.7 \times 10^{-14}$
056_127_St	-0.299	0.071	-4.191	$3.2 \times 10^{-5}$
048_127_St	0.311	0.177	1.759	$8.0 \times 10^{-2}$
077_048_St	-0.688	0.076	-9.099	$2.1 \times 10^{-18}$
077_127_St	-0.377	0.070	-5.371	$1.2 \times 10^{-7}$
056_Exp_St	0.440	0.117	3.761	$1.7 \times 10^{-4}$
077_Exp_St	0.887	0.091	9.780	$7.6 \times 10^{-22}$
048_Exp_St	-0.319	0.148	-2.164	$3.0 \times 10^{-2}$
127_Exp_St	-0.465	0.247	-1.882	$6.0 \times 10^{-2}$

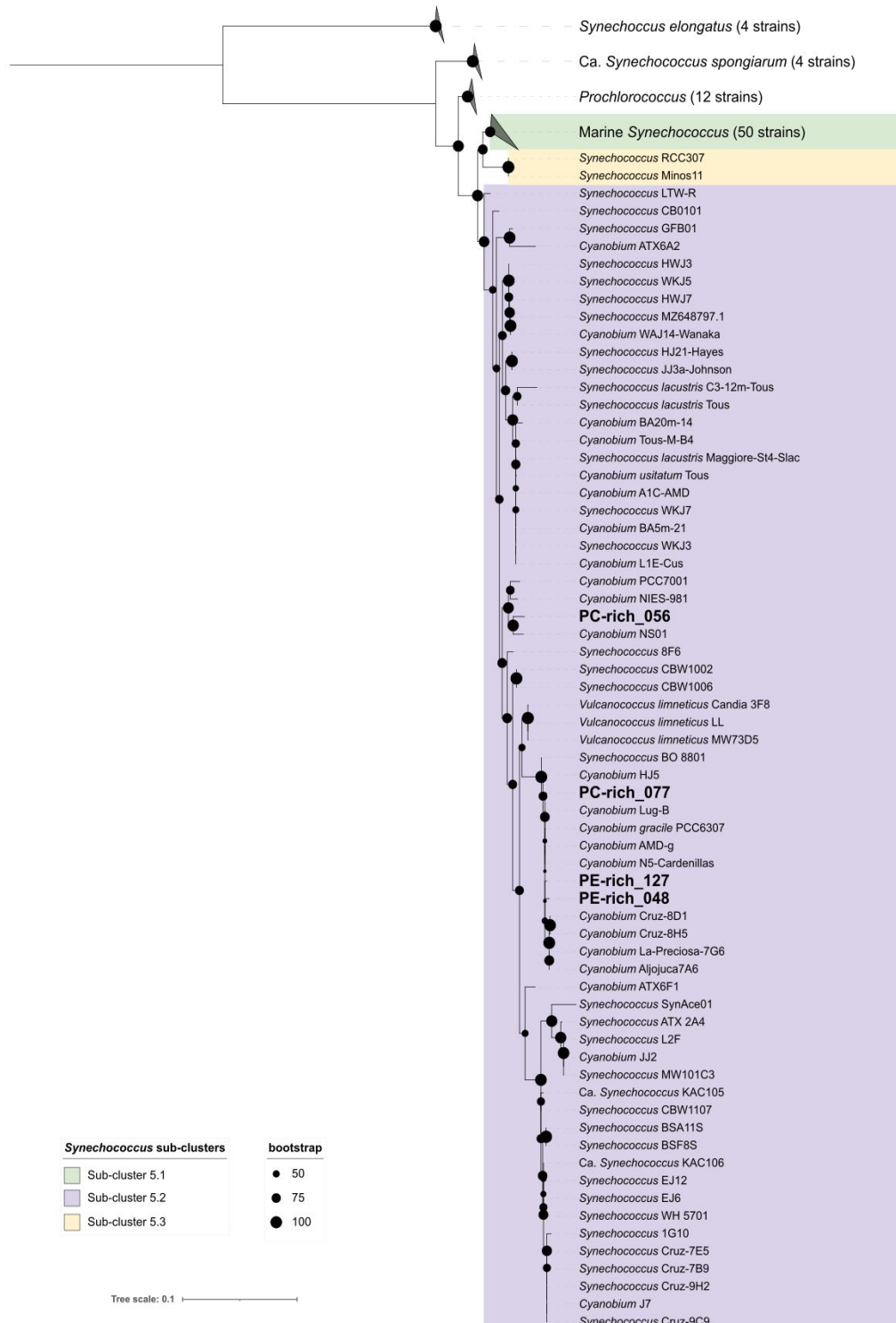
178

179

181 **Tab. S15.** *T*-test of linear fit model (Fit\_model) of pooled data across different strains for a given phase of growth  
 182 (exponential; \_Exp, pre-stationary; \_St) and across different phase of growth for a given strain (\_Exp\_St) from  
 183 effective absorption cross section of PSII ( $\sigma_{PSII}$ ; nm<sup>2</sup> quanta<sup>-1</sup>) measured under Ex590nm (orange) excitation in  
 184 relation to the Phycobiliprotein to Chl *a* ratio, for two PhycoCyanin(PC)-rich cultures (056, 077) and two  
 185 PhycoErythrin(PE)-rich cultures (048, 127) of *Synechococcus* sp., grown at 30, 90, 180, 300, 600, or 900 peak PAR  
 186 μmol photons m<sup>-2</sup>s<sup>-1</sup>; and photoperiods of 8, 12, 16, or 24 h. Estimate - estimation statistics; Std.Error - standard  
 187 error of the estimate; *t*\_value – *t*-test statistic; *p*\_value - level of significance.  
 188

Fit_model	Estimate	Std.Error	<i>t</i> _value	<i>p</i> _value
056_077_Exp	-0.118	0.060	-1.962	$4.9 \times 10^{-2}$
056_048_Exp	0.216	0.058	3.693	$2.2 \times 10^{-4}$
056_127_Exp	0.841	0.076	11.067	$1.8 \times 10^{-27}$
048_127_Exp	0.625	0.076	8.187	$5.5 \times 10^{-16}$
077_048_Exp	0.334	0.060	5.526	$3.8 \times 10^{-8}$
077_127_Exp	0.959	0.075	12.806	$6.7 \times 10^{-36}$
056_077_St	0.397	0.027	14.566	$6.5 \times 10^{-43}$
056_048_St	-0.120	0.064	-1.873	$6.1 \times 10^{-2}$
056_127_St	0.086	0.061	1.411	$1.5 \times 10^{-1}$
048_127_St	0.206	0.114	1.801	$7.3 \times 10^{-2}$
077_048_St	-0.516	0.048	-10.776	$1.7 \times 10^{-24}$
077_127_St	-0.310	0.044	-7.121	$3.7 \times 10^{-12}$
056_Exp_St	0.317	0.075	4.234	$2.4 \times 10^{-5}$
077_Exp_St	0.831	0.061	13.656	$8.9 \times 10^{-40}$
048_Exp_St	-0.019	0.122	-0.155	$8.7 \times 10^{-1}$
127_Exp_St	-0.438	0.209	-2.099	$3.6 \times 10^{-2}$

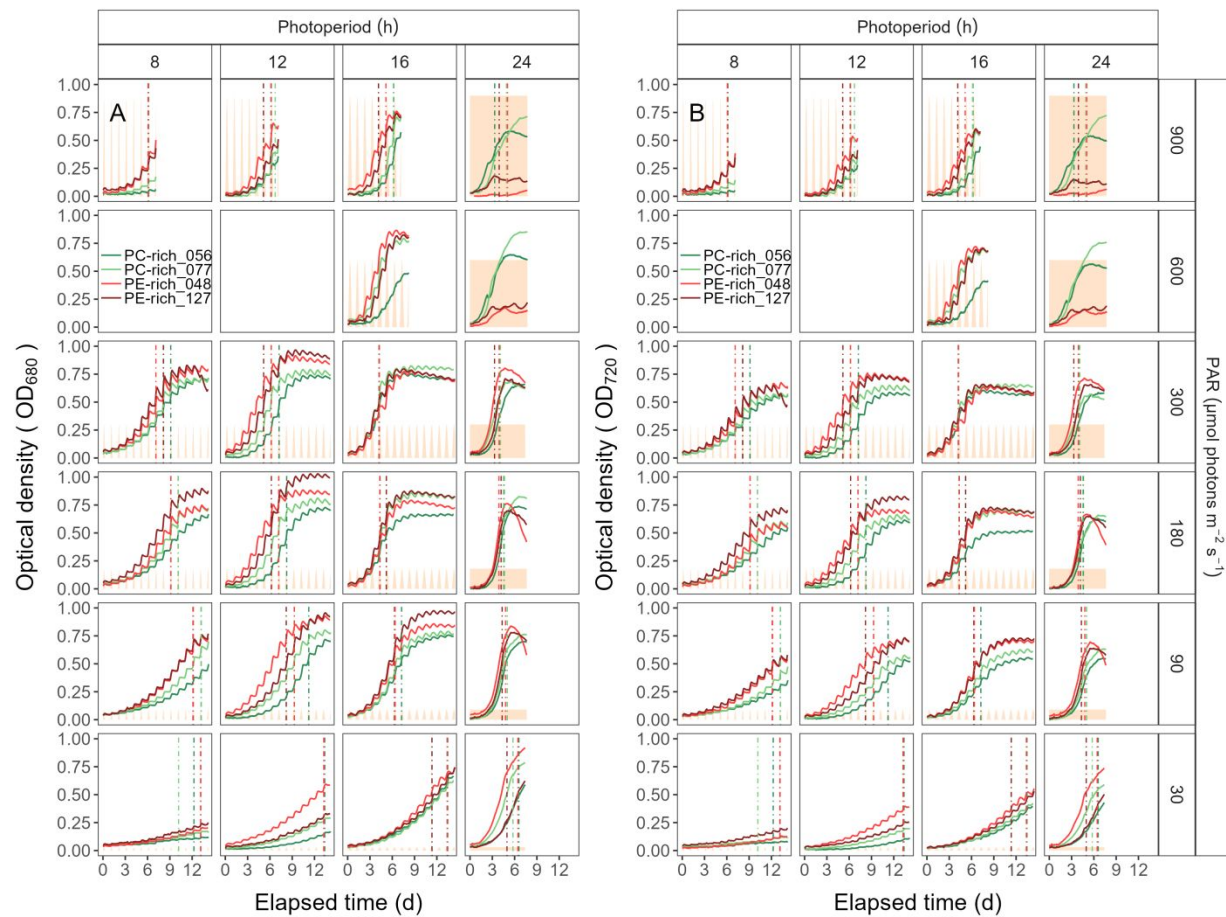
189  
 190  
 191  
 192  
 193  
 194  
 195  
 196  
 197  
 198



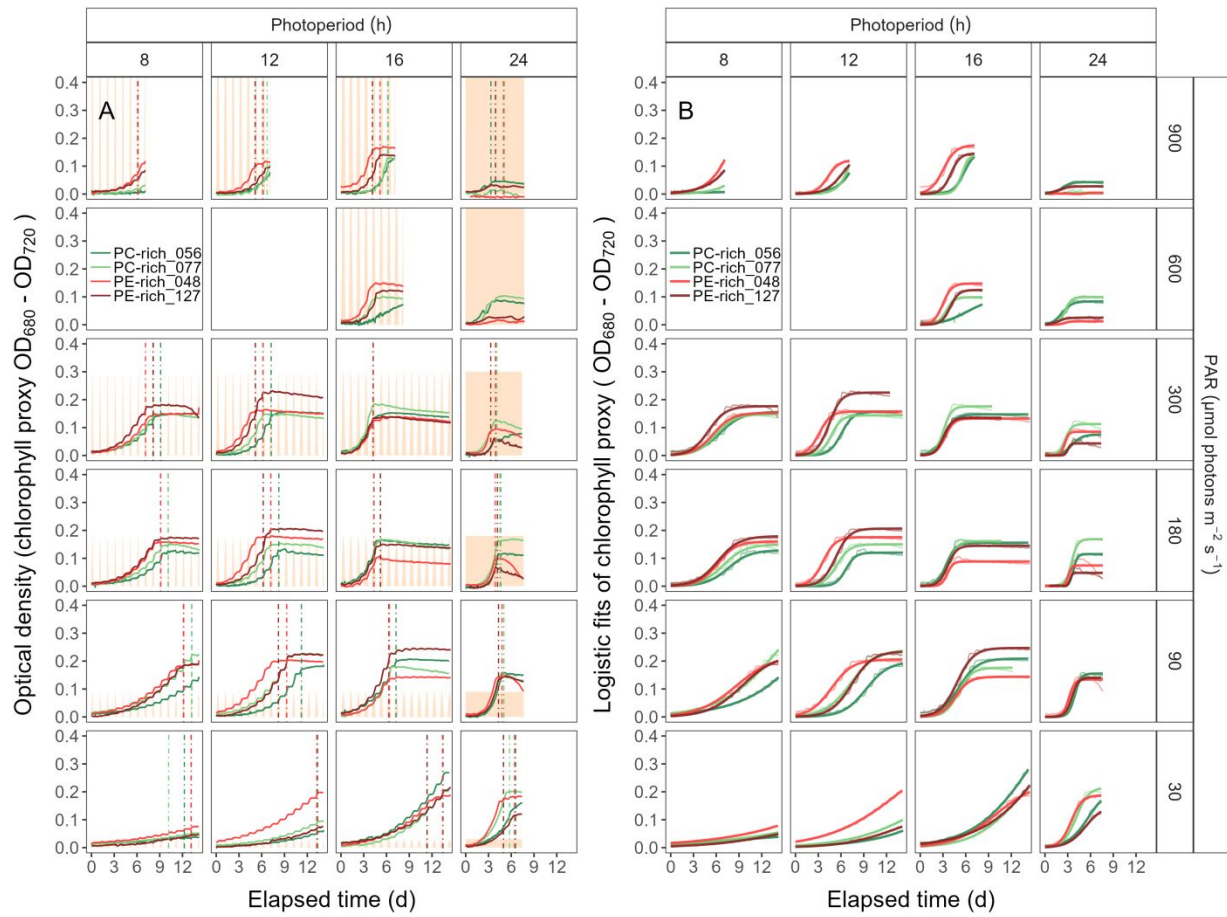
199

200 **Fig. S1.** Phylogenetic tree derived from partial 16S rRNA gene sequences using topology given by Maximum  
 201 Likelihood (1000 bootstraps). Support values are indicated by the size of internal nodes. Strains used in this study  
 202 are shown in bold. Phylogenetic trees were created using IQ-TREE v. 1.6.12 (Hoang et al. 2018), using  
 203 GTR+F+I+R3 model determined by ModelFinder (Kalyaanamoorthy et al. 2017). Samples for total genomic

204 DNA were collected by harvesting 10 mL of each culture and centrifuging for 8 minutes at 8,000 x g. DNA was  
 205 extracted using the FastDNA<sup>TM</sup> SPIN Kit for Soil (MP Biomedicals) with Matrix E columns following manufacturer  
 206 instructions with the addition of an incubation with proteinase-K (1% final concentration) at 55°C for one hour.  
 207 DNA concentration was measured using an Invitrogen Qubit 2.0 fluorometer (Thermo Fisher Scientific Inc.) and  
 208 purity was assessed using a Thermo Scientific<sup>TM</sup> NanoDrop 2000 spectrophotometer (Thermo Fisher Scientific Inc.).  
 209

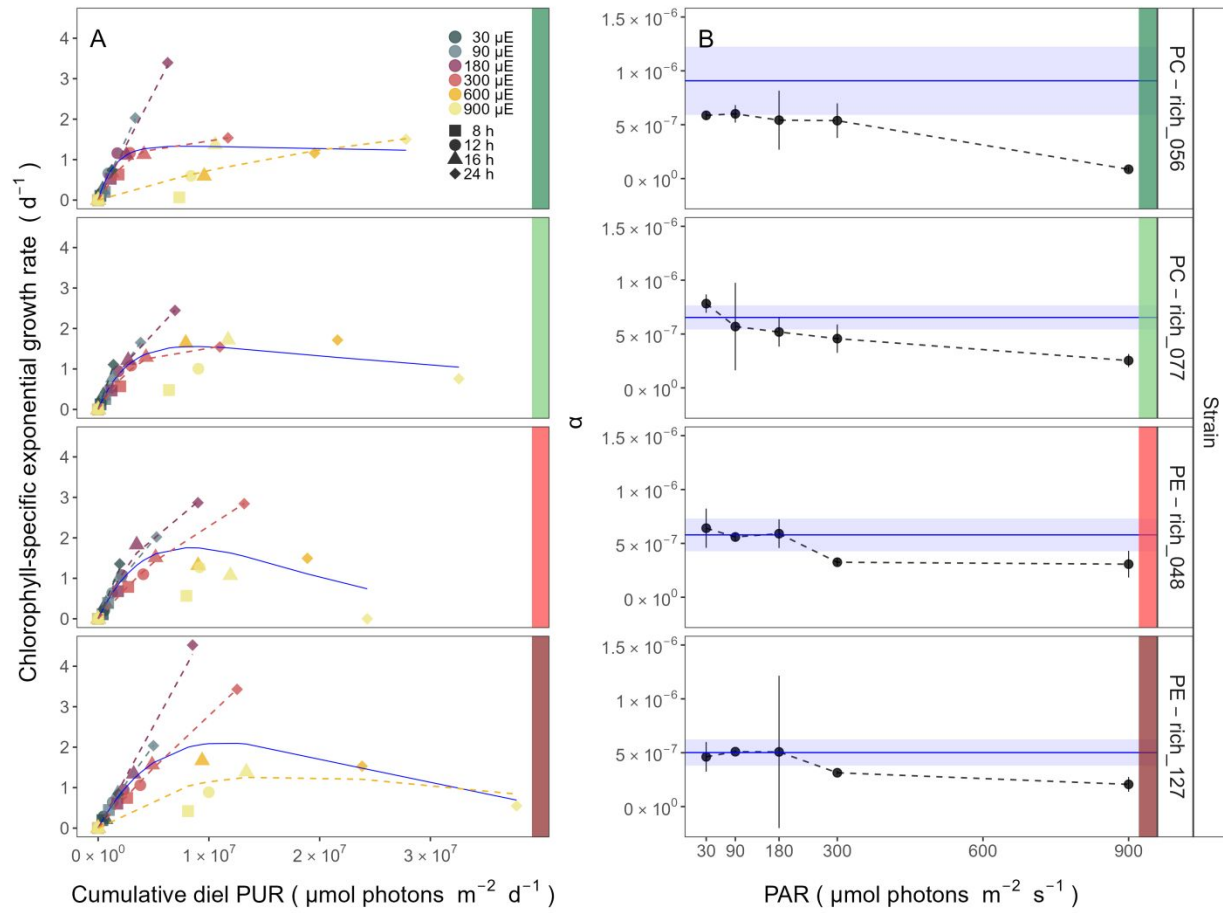


210  
 211 **Fig. S2.** Growth curves, tracked as OD<sub>680</sub> (**A**) and OD<sub>720</sub> (**B**) vs. elapsed time (d). Growth curves were estimated  
 212 over 5-min intervals for two PC-rich cultures (056; dark green, 077; light green) and two PE-rich cultures (048; light  
 213 red, 127; dark red) of *Synechococcus* sp. grown at 30, 90, 180, 300, 600, or 900 peak PAR  $\mu\text{mol photons m}^{-2}\text{s}^{-1}$ ; and  
 214 photoperiods of 8, 12, 16, or 24 h. The vertical lines represent the time when the cultures reached the maximum of  
 215 the 1<sup>st</sup> derivative of OD<sub>680</sub>, or maximum absolute hourly growth (tMaxAHG), taken as an index of transition from  
 216 exponential to pre-stationary growth phases. The orange area represents the photoperiods, with peak PAR x 1/1000  
 217 to scale to the Y axis.  
 218



219

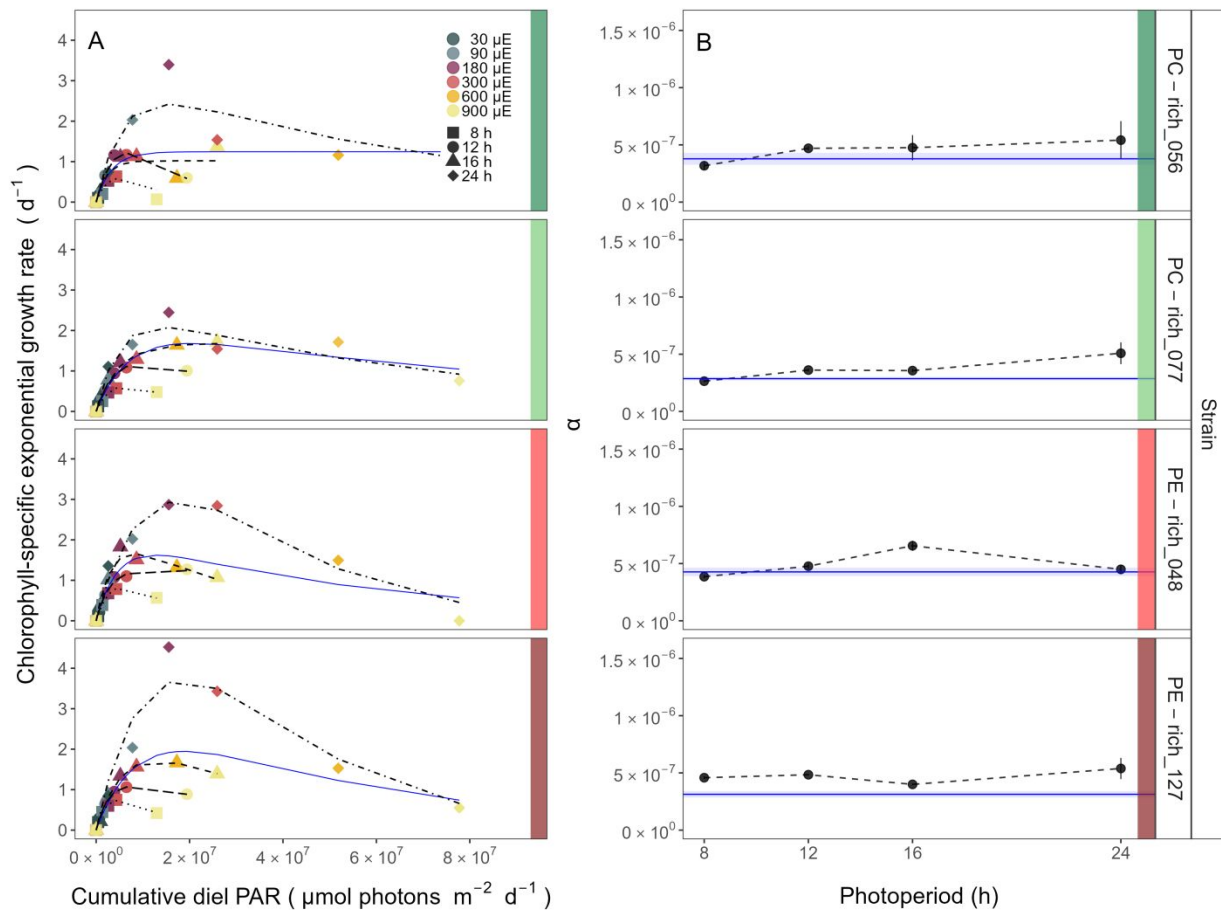
220 **Fig. S3.** (A) Growth curves (tracked as chlorophyll proxy  $\text{OD}_{680}-\text{OD}_{720}; \Delta \text{OD}$ ) vs. elapsed time (d). Growth curves  
 221 were estimated over 5-min intervals for two PC-rich cultures (056; dark green, 077; light green) and two PE-rich  
 222 cultures (048; light red, 127; dark red) of *Synechococcus* sp. grown at 30, 90, 180, 300, 600, or 900 peak PAR  $\mu\text{mol}$   
 223 photons  $\text{m}^{-2}\text{s}^{-1}$ ; and photoperiods of 8, 12, 16, or 24 h. The vertical lines represent the time when the cultures  
 224 reached the maximum of the 1<sup>st</sup> derivative of  $\text{OD}_{680}$ , or maximum absolute hourly growth (tMaxAHG), taken as an  
 225 index of transition from exponential to pre-stationary growth phases. The orange area represents the photoperiods,  
 226 with peak PAR  $\times 1/2000$  to scale to the Y axis. (B) Logistic fits (thick lines) of chlorophyll proxy  $\text{OD}_{680}-\text{OD}_{720} (\Delta$   
 227  $\text{OD})$  vs. elapsed time (d). Growth curves (thin line) measured over 5-min intervals for each strain were also  
 228 presented.  
 229



230

231 **Fig. S4.** (A) Chlorophyll-specific exponential growth rates ( $d^{-1}$ ) vs. cumulative diel Photosynthetically Usable  
 232 Radiation (PUR,  $\mu\text{mol photons m}^{-2}\text{d}^{-1}$ ). Growth rates ( $\pm \text{SE}$  falling within symbols) were estimated from logistic fits  
 233 of chlorophyll proxy  $\text{OD}_{680} - \text{OD}_{720}$  ( $\Delta\text{OD}$ ) vs. elapsed time (Fig. 1, Fig. S3B), for two PC-rich cultures (056; dark  
 234 green, 077; light green) and two PE-rich cultures (048; light red, 127; dark red) of *Synechococcus* sp. grown at 30  
 235 (dark gray), 90 (light gray), 180 (purple), 300 (red), 600 (orange), or 900 (yellow) peak PAR  $\mu\text{mol photons m}^{-2}\text{s}^{-1}$   
 236 ( $\mu\text{E}$ ); and photoperiods of 8 (square), 12 (circle), 16 (triangle), or 24 (diamond) h. Solid blue line shows a fit of the  
 237 pooled growth rates through peak PAR for each strain, with a three parameter model (Harrison and Platt, 1986). We  
 238 also fit the same model separately for 30 (dark gray), 90 (light gray), 180 (purple), 300 (red), 600 together with 900  
 239 (orange) peak PAR  $\mu\text{mol photons m}^{-2}\text{s}^{-1}$ , only when they were each significantly different (ANOVA,  $p < 0.05$ ) from  
 240 the fit of pooled data. (B) Alpha parameters of the initial rise of growth rate ( $\alpha$ ) vs. cumulative diel  
 241 Photosynthetically Usable Radiation (PUR), estimated from data pooled for each peak PAR (points ( $\pm \text{SE}$ )  
 242 connected by dashed lines), and estimated for all data across all peak PAR, for each strain (solid blue horizontal line  
 243  $\pm \text{SE}$ ).

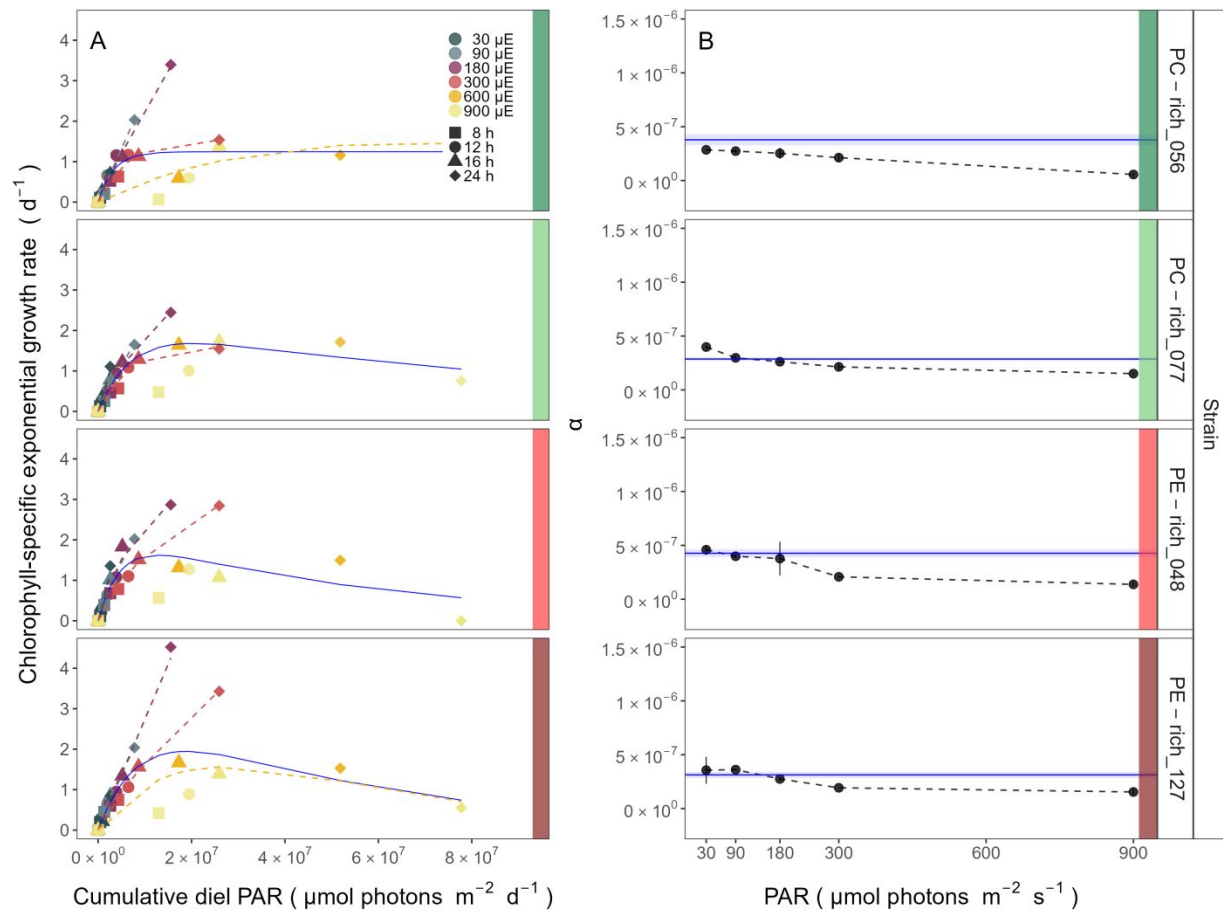
244



245

**Fig. S5.** (A) Chlorophyll-specific exponential growth rates ( $d^{-1}$ ) vs. cumulative diel PAR ( $\mu\text{mol photons m}^{-2} \text{d}^{-1}$ ). Growth rates ( $\pm \text{SE}$  falling within symbols) were estimated from logistic fits of chlorophyll proxy OD<sub>680</sub> – OD<sub>720</sub> ( $\Delta\text{OD}$ ) vs. elapsed time (Fig. 1, Fig. S3B), for two PC-rich cultures (056; dark green, 077; light green) and two PE-rich cultures (048; light red, 127; dark red) of *Synechococcus* sp. grown at 30 (dark gray), 90 (light gray), 180 (purple), 300 (red), 600 (orange), or 900 (yellow) peak PAR  $\mu\text{mol photons m}^{-2}\text{s}^{-1}$  ( $\mu\text{E}$ ); and photoperiods of 8 (square), 12 (circle), 16 (triangle), or 24 (diamond) h. Solid blue line shows a fit of the pooled growth rates through photoperiod (h) for each strain, with a three parameter model (Harrison and Platt 1986). We also fit the same model separately for 8 (dotted line), 12 (long dash line), 16 (dashed line), or 24 (two dash line) h photoperiods, since for all strains they were each significantly different (ANOVA,  $p < 0.05$ ) from the fit of pooled data. (B) Alpha parameters of the initial rise of growth rate ( $\alpha$ ) vs. cumulative diel PAR, estimated from data pooled for each photoperiod (points ( $\pm \text{SE}$ ) connected by dashed lines), and estimated for all data across photoperiods (solid blue horizontal line  $\pm \text{SE}$ ), for each strain.

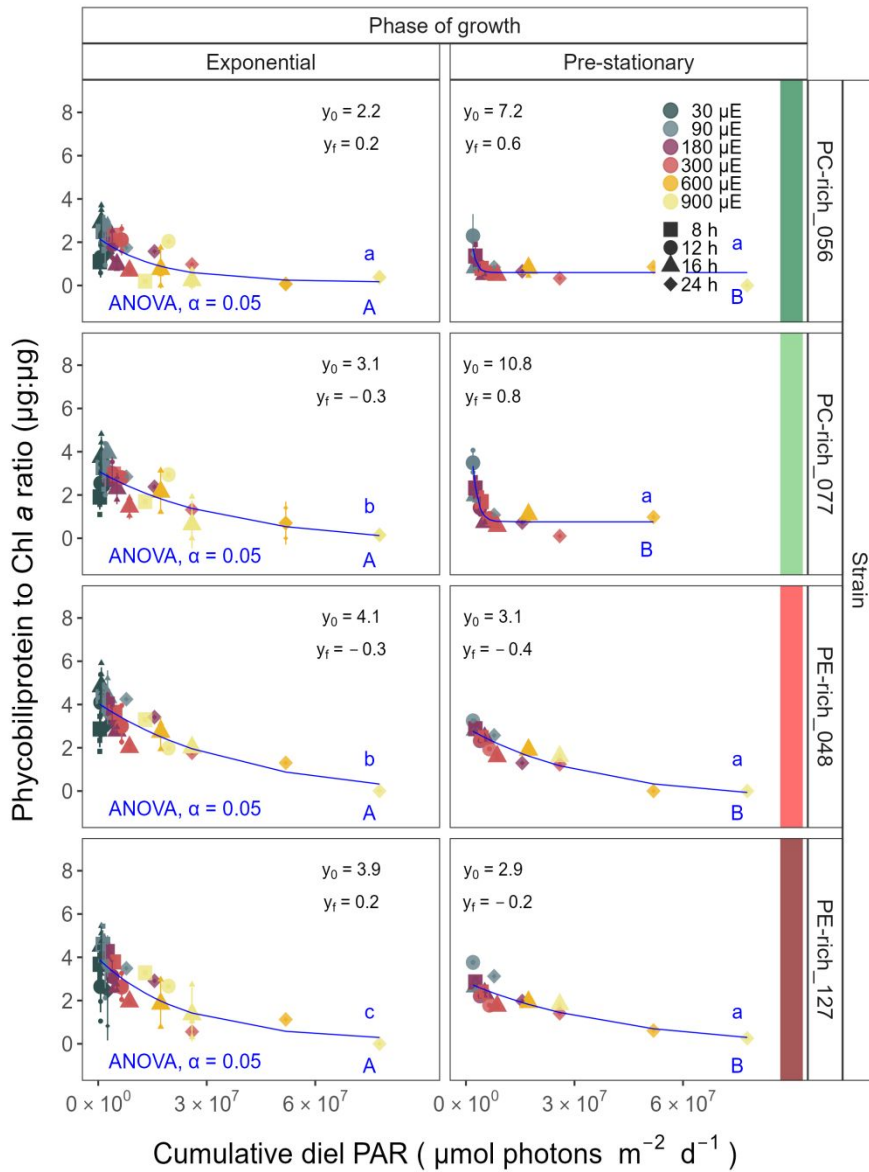
258



259

260 **Fig. S6. (A)** Chlorophyll-specific exponential growth rates ( $d^{-1}$ ) vs. cumulative diel PAR ( $\mu\text{mol photons m}^{-2} \text{d}^{-1}$ ).  
 261 Growth rates ( $\pm \text{SE}$  falling within symbols) were estimated from logistic fits of chlorophyll proxy OD<sub>680</sub> – OD<sub>720</sub>  
 262 ( $\Delta\text{OD}$ ) vs. elapsed time (Fig. 1, Fig. S3B), for two PC-rich cultures (056; dark green, 077; light green) and two PE-  
 263 rich cultures (048; light red, 127; dark red) of *Synechococcus* sp. grown at 30 (dark gray), 90 (light gray), 180  
 264 (purple), 300 (red), 600 (orange), or 900 (yellow) peak PAR  $\mu\text{mol photons m}^{-2} \text{s}^{-1}$  ( $\mu\text{E}$ ); and photoperiods of 8  
 265 (square), 12 (circle), 16 (triangle), or 24 (diamond) h. Solid blue line shows a fit of the pooled growth rates through  
 266 peak PAR for each strain, with a three parameter model (Harrison and Platt, 1986). We also fit the same model  
 267 separately for 30 (dark gray), 90 (light gray), 180 (purple), 300 (red), 600 together with 900 (orange) peak PAR  
 268  $\mu\text{mol photons m}^{-2} \text{s}^{-1}$ , only when they were each significantly different (ANOVA,  $p < 0.05$ ) from the fit of pooled  
 269 data. **(B)** Alpha parameters of the initial rise of growth rate ( $\alpha$ ) vs. cumulative diel PAR, estimated from data pooled  
 270 for each peak PAR (points ( $\pm \text{SE}$ ) connected by dashed lines), and estimated for all data across all peak PAR, for  
 271 each strain (solid blue horizontal line  $\pm \text{SE}$ ).

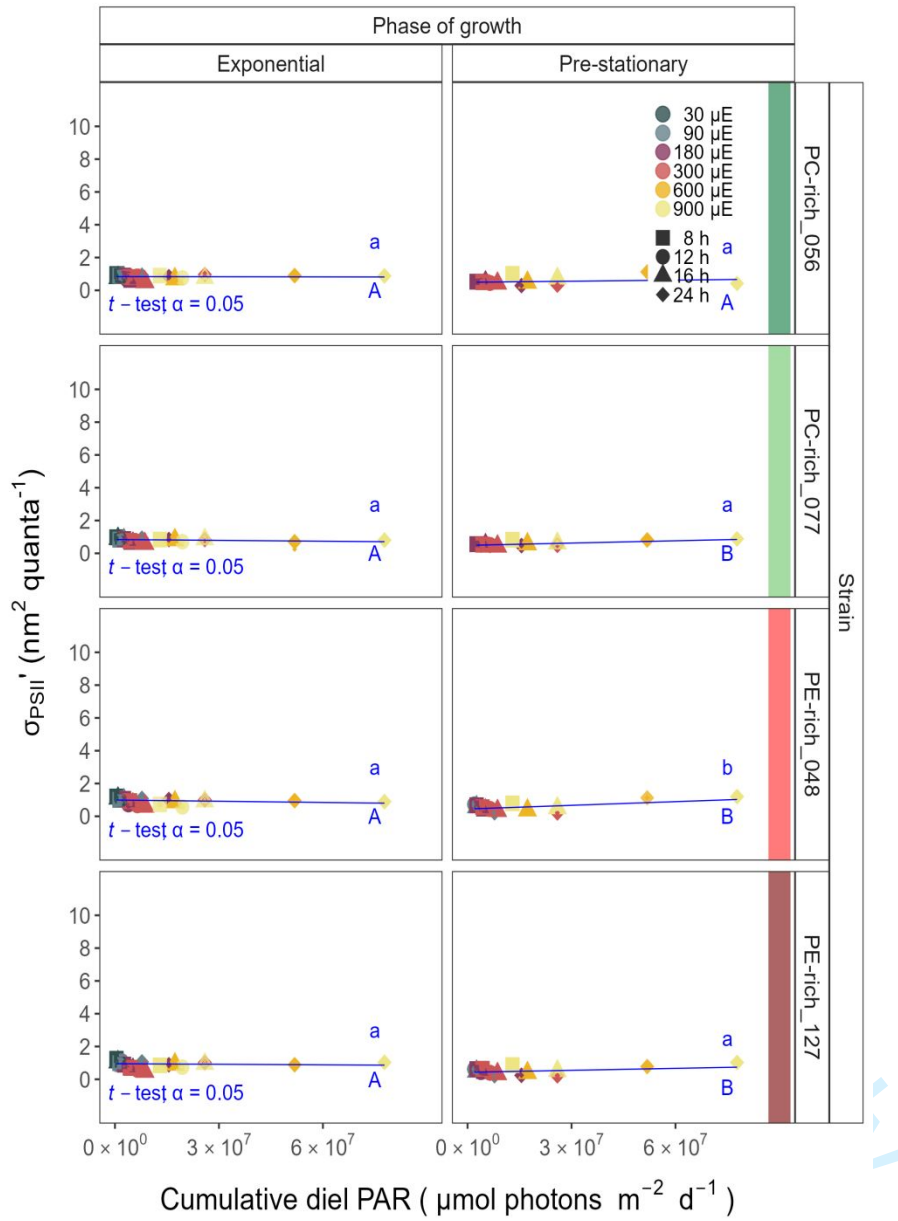
272



273

Fig. S7. Changes of Phycobiliprotein to Chl *a* ratio ( $\mu\text{g}:\mu\text{g}$ ) vs. cumulative diel PAR ( $\mu\text{mol photons m}^{-2}\text{d}^{-1}$ ). Phycobiliprotein to Chl *a* ratio was estimated for two PC-rich cultures (056; dark green, 077; light green) and two PE-rich cultures (048; light red, 127; dark red) of *Synechococcus* sp. grown at 30 (dark gray), 90 (light gray), 180 (purple), 300 (red), 600 (orange), or 900 (yellow) peak PAR  $\mu\text{mol photons m}^{-2}\text{s}^{-1}$  ( $\mu\text{E}$ ); and photoperiods of 8 (square), 12 (circle), 16 (triangle), or 24 (diamond) h. Figure presents data (smaller symbols) and means (bigger symbols) from exponential or pre-stationary phase of growth. Blue solid line shows single phase exponential decay fit for data from each strain and growth phase, fit parameters are presented. Different lowercase letters indicate statistically significant differences between the fit models for different strains within a given phase of growth. Different uppercase letters indicate statistically significant differences between the fit models for different phases of growth within a given strain (ANOVA;  $p < 0.05$ ).

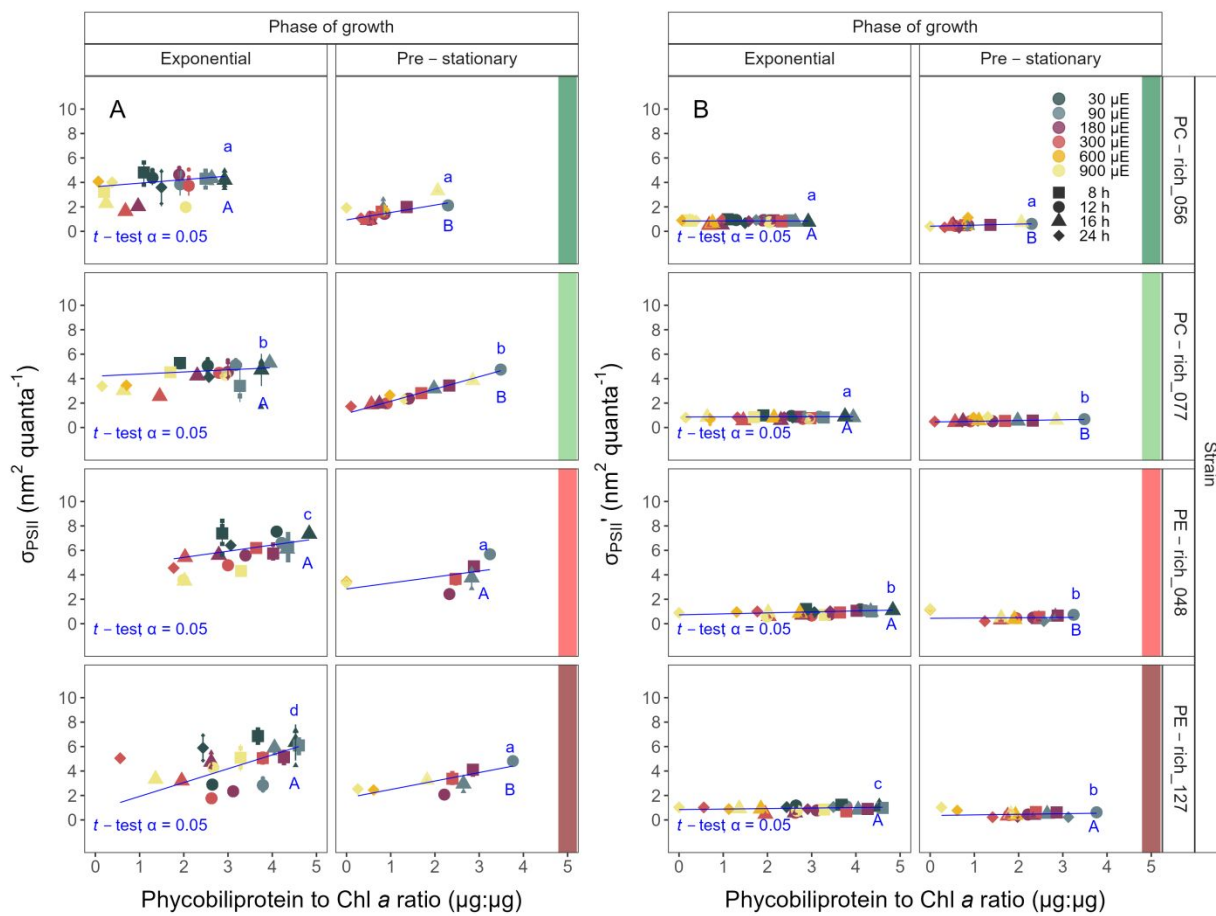
284



285

286 **Fig. S8.** Effective absorption cross section of PSII ( $\sigma_{\text{PSII}'}$ ;  $\text{nm}^2 \text{ quanta}^{-1}$ ) measured under diel peak PAR growth light  
 287 under blue ( $\text{Ex}_{445\text{nm}}$ ) excitation vs. cumulative diel PAR ( $\mu\text{mol photons m}^{-2} \text{ d}^{-1}$ ).  $\sigma_{\text{PSII}'}$  was estimated for two PC-rich  
 288 cultures (056; dark green, 077; light green) and two PE-rich cultures (048; light red, 127; dark red) of  
 289 *Synechococcus* sp. grown at 30 (dark gray), 90 (light gray), 180 (purple), 300 (red), 600 (orange), or 900 (yellow)  
 290 peak PAR  $\mu\text{mol photons m}^{-2} \text{ s}^{-1}$  ( $\mu\text{E}$ ); and photoperiods of 8 (square), 12 (circle), 16 (triangle), or 24 (diamond) h.  
 291 Figure presents data (smaller symbols) and means (bigger symbols) from exponential or pre-stationary phase of  
 292 growth. Blue solid line shows linear model fit for data from each strain and growth phase. Different lowercase  
 293 letters indicate statistically significant differences between the fit models for different strains within a given phase of  
 294 growth. Different uppercase letters indicate statistically significant differences between the fit models for different  
 295 phases of growth within a given strain ( $t$ -test;  $p < 0.05$ ).

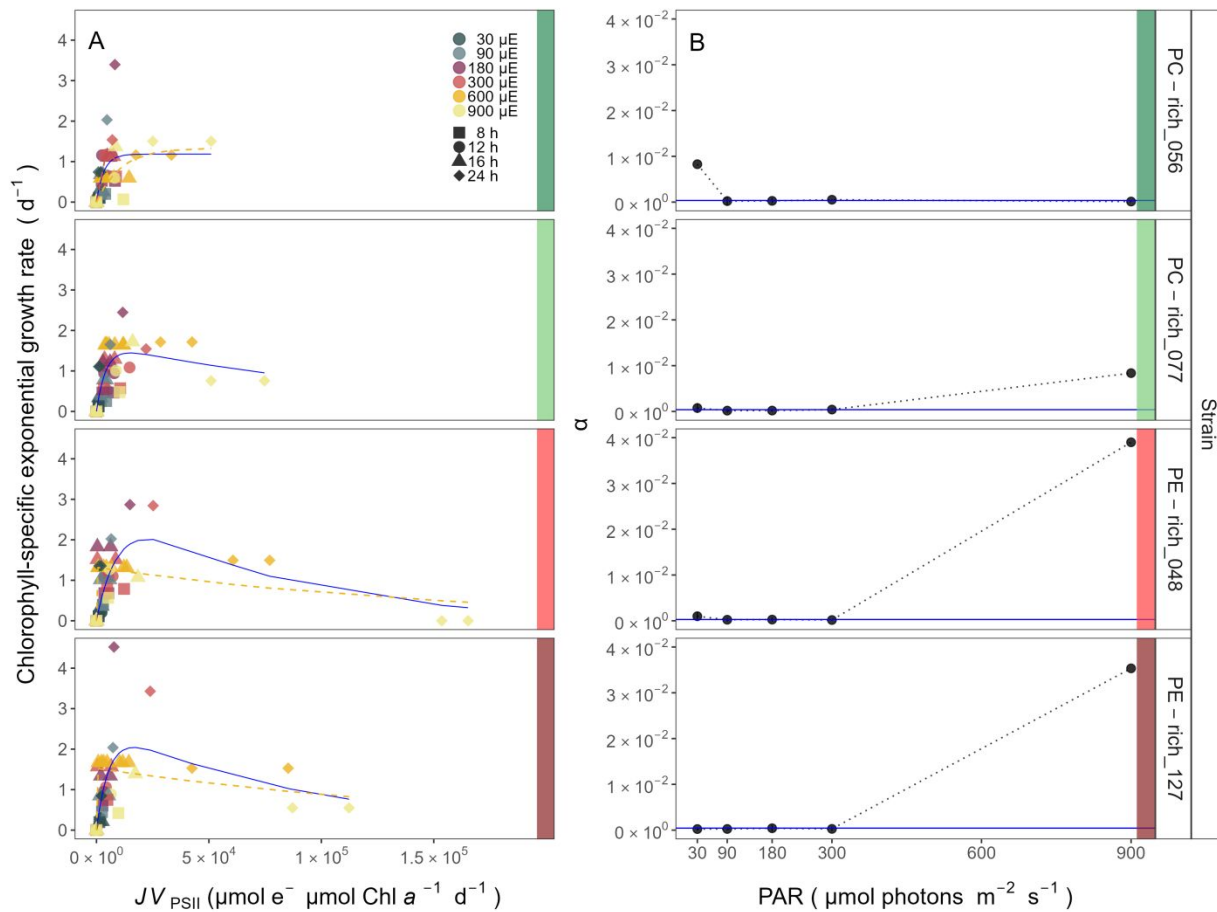
296



297

**Fig. S9. (A)** Changes of effective absorption cross section of PSII ( $\sigma_{PSII}$ ;  $\text{nm}^2 \text{ quanta}^{-1}$ ) measured at the dark period under orange ( $\text{Ex}_{590\text{nm}}$ ) excitation vs. the ratio of sum of  $\mu\text{g}$  phycobilins (PE, PC, APC protein, Phycobiliprotein) to  $\mu\text{g}$  Chl a. **(B)** Changes of effective absorption cross section of PSII ( $\sigma_{PSII}'$ ;  $\text{nm}^2 \text{ quanta}^{-1}$ ) measured under diel peak PAR growth light under blue ( $\text{Ex}_{445\text{nm}}$ ) excitation vs. the ratio of sum of  $\mu\text{g}$  phycobilins (PE, PC, APC protein, Phycobiliprotein) to  $\mu\text{g}$  Chl a.  $\sigma_{PSII}'$  was estimated for two PC-rich cultures (056; dark green, 077; light green) and two PE-rich cultures (048; light red, 127; dark red) of *Synechococcus* sp. grown at 30 (dark gray), 90 (light gray), 180 (purple), 300 (red), 600 (orange), or 900 (yellow) peak PAR  $\mu\text{mol photons m}^{-2}\text{s}^{-1}$  ( $\mu\text{E}$ ); and photoperiods of 8 (square), 12 (circle), 16 (triangle), or 24 (diamond) h. Figure presents data (smaller symbols) and means (bigger symbols) from exponential or pre-stationary phase of growth. Blue solid line shows linear model fit for data from each strain and growth phase. Different lowercase letters indicate statistically significant differences between the fit models for different strains within a given phase of growth. Different uppercase letters indicate statistically significant differences between the fit models for different phases of growth within a given strain (*t*-test;  $p < 0.05$ ).

310



311

**Fig. S10.** (A) Chlorophyll specific exponential growth rates ( $d^{-1}$ ) vs. cumulative diel PSII electron flux ( $JV_{PSII}$ ;  $\mu\text{mol e}^- \mu\text{mol Chl } a^{-1} d^{-1}$ ) measured under diel peak PAR growth light. Growth rates ( $\pm$  SE falling within symbols) were estimated from logistic fits of chlorophyll proxy  $OD_{680} - OD_{720}$  ( $\Delta OD$ ) vs. elapsed time (Fig. S3). PSII flux was estimated using FRRf induction curves with excitation of chlorophyll ( $Ex_{445\text{nm}}$ , blue), for two PC-rich cultures (056; dark green, 077; light green) and two PE-rich cultures (048; light red, 127; dark red) of *Synechococcus* sp. grown at 30 (dark gray), 90 (light gray), 180 (purple), 300 (red), 600 (orange), or 900 (yellow) peak PAR  $\mu\text{mol photons m}^{-2} s^{-1}$ ; and photoperiods of 8 (square), 12 (circle), 16 (triangle), or 24 (diamond) h. Solid blue line shows a fit of the pooled growth rates for each strain, with a three parameter model (Harrison and Platt 1986). We also fit the same model separately for 600 together with 900 (orange) peak PAR  $\mu\text{mol photons m}^{-2} s^{-1}$ , when they were significantly different (ANOVA,  $p < 0.05$ ) from the fit of pooled data. (B) Alpha parameters of the initial rise of growth rate ( $\alpha$ ) vs. cumulative diel  $JV_{PSII}$ , estimated from data pooled for each peak PAR (points ( $\pm$  SE) connected by dashed lines), and estimated for all data across all peak PAR, for each strain (solid blue horizontal line  $\pm$  SE).

324

## 325 **References**

- 326 Harrison, W. G., and T. Platt. 1986. Photosynthesis-irradiance relationships in polar and  
327 temperate phytoplankton populations. *Polar biology* **5**: 153–164.